BUCKLING RESTRAINED BRACES FOR THE SEISMIC STRENGTHENING OF A FIVE-STOREY REINFORCED CONCRETE FRAME STRUCTURE

DIAGONALES DUCTILES CONFINÉES POUR LE RENFORCEMENT PARASISMIQUE D'UN BÂTIMENT DE CINQ ÉTAGES À OSSATURE EN BÉTON ARMÉ

A Thesis Submitted to the Division of Graduate Studies
of the Royal Military College of Canada
by

Robie Michael Gourd, P.Eng.
Major

In Partial Fulfillment of the Requirements for the Degree of
Master of Applied Science in Civil Engineering

23 March 2015

This is to certify that the thesis prepared by

Ceci certifie que le mémoire/la thèse rédigé(e) par

Robie Michael Gourd

Entitled

Buckling Restrained Braces for the Seismic Strengthening of a Five-Storey Reinforced Concrete Frame Structure

complies with the Royal Military College of Canada regulations and that it meets the accepted standards of the Graduate School with respect to quality and originality for the degree of

Master of Applied Science (M.A.Sc.)
Civil Engineering (Structures)

The original sheet was signed on the 23th day of March, 2015 by the members of the Oral Defence Thesis Examination Committee.

Intitulée

Diagonales ductiles confinées pour le renforcement parasismique d'un bâtiment de cinq étages à ossature en béton armé

satisfait aux règlements du Collège militaire royal du Canada et qu'il (elle) respecte les normes acceptées par la Division des études supérieures quant à la qualité et l'originalité pour le grade universitaire de

Maîtrise ès sciences appliquées
(M.Sc.A.)
Génie Civil (Structures)

La feuille originale a été signée le 23e jour de Mars, 2015 par les membres du Comité de l'examen oral du mémoire/de thèse.

Dr. Valérie Langlois, Ph.D.
Chair / Président

Dr. Mark Green, Ph.D., P.Eng.
Examiner External to RMC / Examinateur externe au CMR

Dr. Eugene Boros, Ph.D., P.Eng.
Examiner External to the department and internal to RMC / Examinateur externe au département et interne au CMR

Dr. Pat Heffernan, Ph.D., P.Eng.
Examiner Internal to the department / Examinateur interne au département

Dr. Gordon Wight, Ph.D., P.Eng.
Supervisor / Directeur du mémoire/de thèse

Dr. Michel Tétreault, Ph.D., P.Eng.
Thesis is approved by the Head of Department / Le mémoire/la thèse est approuvé(e) par le directeur du département

To the Librarian: This thesis is not to be regarded as classified.
Au/À la bibliothécaire:
Ce mémoire/cette thèse n'est pas considéré(e) comme publication restreinte

Dr. Gordon Wight, Ph.D.,P.Eng.
Main Supervisor of thesis / Directeur principal de these/du mémoire

Acknowledgements

I would like to first and foremost thank my supervisor, Dr. Gordon Wight for his continuous support and guidance throughout the course of my post-graduate studies. I would like to thank Defence Construction Canada for their support throughout the project. Furthermore I would like to thank our industry partners: J.L. Richards in the development of an appropriate testing program, Ellis-Don Limited and Quest Steel for their technical support and contribution of resources throughout this research. I would especially like to acknowledge ADM (IE) both for the support and funding provided through the Military Engineering Research Group.

The efforts of Mr. Dexter Gaskin were vital to the completion of the experimental testing. He has also imparted a great deal of workshop etiquette to me through his methodical work ethic. I will take these lessons with me wherever I go. Mr. Steve VanVolkinburgh provided outstanding support for the setup and testing of the BRB specimens as well as material and coupon testing. To Dexter and Steve: I sincerely thank you.

I would like to thank the faculty of the Carleton University Civil Engineering Department: to Dr. David Lau for introducing me to the world of structural dynamics and to Dr. Jeffrey Erochko for providing guidance and resources on BRB modelling and dynamic analysis options. Many thanks go out to the Carleton University civil engineering graduate students, with whom I have spent many a late evening in the depths of the Minto CASE building. Your friendship and support throughout my graduate studies in Ottawa cannot be overstated. Thank you to Dr. Hassan Aoude of the University of Ottawa for his thorough and in-depth interpretation of the NBCC.

Finally, to my wife Lindsay, this thesis represents the culmination of over three years of evenings and weekends. The balance of fitting in a part-time master's program into our family's life would not have been possible without your tireless support and encouragement. The completion of this program is as much your accomplishment as it is mine.

Abstract

In 2008, construction commenced on a project to renovate a five storey reinforced concrete structure on the grounds of the Royal Military College of Canada. One of the elements of this renovation was a seismic retrofit, which included the use of 28 unique Buckling Restrained Braces (BRBs) that were designed and installed as a seismic strengthening and dampening system. This research involved the testing of three full-scale 9 m long BRB specimens in an individual uniaxial subassemblage. During the qualification testing, it was apparent that the as-built BRBs were constructed of material which greatly exceeded the specified 248 MPa yield-strength, resulting in braces that exceeded the intended design capacity. Following the qualification testing, one module of the concrete-frame building was modelled using a commercial finite element analysis program and was subjected to both static and dynamic forces. The dynamic analysis applied a Fast Non-Linear Analysis (FNA) using a series of five synthetic time-history functions that are compliant with the 2010 National Building Code of Canada (NBCC). It was concluded that both the designed and as-built braces remain elastic and will only perform plastically in the event of a seismic ground motion between two and five times larger than the Uniform Hazard Spectrum of the NBCC with a probability of exceedance of 2% in 50 years. Although this Seismic Force Resisting System (SFRS) remains chiefly elastic, this seismic upgrade has nevertheless achieved a rigid and effective SFRS. While this over strengthened seismic upgrade will not perform as originally intended, the now robust bracing system will provide effective lateral support and adequate stiffness to the reinforced concrete frame. The as-built BRBs will also greatly reduce the inter-storey drifts during a seismic event.

Résumé

Des travaux de construction ont été entrepris en 2008 dans le cadre d'un projet visant à moderniser un bâtiment de cinq étages en béton armé sur les terrains du Collège militaire royal du Canada. L'un des éléments de cette modernisation était une amélioration parasismique qui incluait l'emploi de 28 éléments de diagonales ductiles confinées (DDC). Ces éléments ont été conçus et installés pour servir de système de renforcement et d'amortissement parasismique. La recherche faisant l'objet du présent rapport incluait l'essai de trois spécimens en vraie grandeur de DDC de 9 m de longueur dans un sous-ensemble uniaxial individuel. Au cours des essais de qualification, il s'est avéré que les DDC étaient fabriquées d'un matériau qui dépassait de loin la limite d'élasticité de 248 MPa prescrite, ce qui leur conférait une résistance supérieure à la valeur prévue. Suite aux essais de qualification, un module du bâtiment à ossature de béton a été modélisé à l'aide d'un programme commercial d'analyse aux éléments finis et a été soumis à des forces statiques et dynamiques. L'analyse dynamique appliquée utilise une approche non-linéaire rapide (ANLR) à l'aide d'une série de cinq fonctions synthétiques de variation en fonction du temps qui sont conformes au Code national du bâtiment – Canada 2010 (CNB). Il fût conclu que les contreventements conçus et ceux construits demeureront élastiques et ne se comporteront de façon plastique qu'en présence d'un mouvement sismique du sol se situant entre deux et cinq fois la valeur de calcul ayant une probabilité de dépassement de 2 % en 50 ans selon le spectre de risque uniforme (SRU). Bien que ce système de résistance aux forces sismiques (SRFS) demeure principalement élastique, cette amélioration parasismique a permis de réaliser un SFRS rigide et efficace. Bien que cette ossature parasismique sur-résistante ne se comporte pas selon l'objectif initial, le système de contreventement robuste offrira un soutien latéral efficace et une rigidité adéquate à l'ossature de béton armé. Les DDC tels que construits réduiront aussi grandement les glissements entre étages lors d'un événement sismique.

Table of Contents

Acknowledgements ii

Abstract iii

Résumé iii

List of Figures vi

List of Tables viii

List of Symbols and Acronyms ix

English Symbols and Acronyms ix
Greek Symbols x
Chapter 1: Introduction and Objectives 1

1.1. Introduction 1
1.2. Objectives 4
1.3. Scope 5
1.4 Content 5
Chapter 2: Literature Review 6

2.1. Literature Review 6
2.1.1. Early BRBs 6
2.1.2. BRBs in North American Codes 6
2.1.3. Contemporary Research 8
2.2. Qualification Testing 10
2.3. BRB Analysis Options 11
2.4 Summary 12
Chapter 3: Buckling Restrained Brace Testing 13

3.1. Testing Overview 13
3.2. Design Philosophy 13
3.3. Subassemblage 14
3.4. BR4 Preliminary Testing 18
3.5. Brace BR6 and BR30 20
3.6. Loading Protocol 21
3.7. Material Testing, Instrumentation and Assembly 22
3.7.1. Material Testing 22
3.7.2. Brace Modification 26
3.7.3. Instrumentation 28
3.7.4. Assembly 30
3.7.5. Preloading 33
3.8. Test Results 33
3.8.1. Test objectives 33
3.8.2. BR30m Results 34
3.8.3. BR6m Results 35
3.9. Discussion 38
3.9.1. Hysteresis Loop Error 38
3.9.2. Overall Brace Performance 38
3.9.3. Load Sharing 39
3.9.4. Un-Bonding and the Effects of Grout 42
3.10 Summary of Qualification Testing 44
Chapter 4: Modelling 46

4.1. Modelling Overview 46
4.2. Equivalent Static Force Procedure (ESFP) 47
4.2.1. Design Spectra 47
4.2.2. Fundamental Period 48
4.2.3. Seismic Weight and Base Shear 49
4.2.4. 3D and 2D model 49
4.2.6. Brace Forces 54
4.3. Dynamic Analysis 56
4.3.1. Non-Linear (NL) Modelling 56
4.3.2. Matching ground motion to a UHS 59
4.3.3. FNA Results 61
4.4. Summary of Modelling 75
Chapter 5: Conclusions 76
5.1 Summary 76
5.2 Conclusions and Recommendations 76
5.2.1. Material Properties 76
5.2.2. Load Sharing 77
5.2.3. Implementation of ω and β Factors 77
5.2.4. Connections 77
5.2.5. Ductility and Over strength 78
5.2.6. Analysis Options 78
5.3. References 79

List of Figures

Figure 1.1 – Sawyer and Girouard buildings prior renovations (Structural tender drawings, 2010) 1
Figure 1.2 – Plan view of modules 1&2 with BRBs highlighted (Structural Drawings, 2010) 2
Figure 1.3 – Typical module with BRB frame and shear wall 3
Figure 1.4 – BRB anatomy 4
Figure 2.1 – BRB mechanics 7
Figure 2.2 – Out of plane buckling (Della Corte et al., 2011) 7
Figure 2.3 – Pinned connection reinforcement detail (Della Corte et al., 2011) 8
Figure 2.4 – Pinned connection detail (Junxian et al., 2014) 10
Figure 3.1 – BRB anatomy 14
Figure 3.2 – Overview of subassemblage 15
Figure 3.3 – Complete subassemblage actuator end 15
Figure 3.4 – Complete subassemblage profile 15
Figure 3.5 – Detail at fixed end 16
Figure 3.6 – Detail at actuator end 17
Figure 3.7 – BRB free body diagram 17
Figure 3.8 – Detail at sliding support collar and roller support 18
Figure 3.9 – BRB dimensions 20
Figure 3.10 – Steel coupon tension test results 23
Figure 3.11 – BR6 weld at mid-span 24
Figure 3.12 – BR6 full penetration view of coupon 24
Figure 3.13 – Tension test result for welded coupon 25
Figure 3.14 – Cyclic loading coupon hysteresis 26
Figure 3.15 – Plasma cutting detail 26
Figure 3.16 –Trimming detail for BR6m 27
Figure 3.17 – Trimming detail for BR30m 28
Figure 3.18 – LVDT Placement 29
Figure 3.19 – Instrumentation location 30
Figure 3.20 – Internal stain gauge and fibre board detail 31
Figure 3.21 – BRB wrapped in un-bonding membrane 31
Figure 3.22 – Damage to the un-bonding membrane during the assembly 32
Figure 3.23 – Brace elevation for grouting 33
Figure 3.24 – BR30m load Vs. displacement hysteresis curve 35
Figure 3.25 – BR6m load Vs. displacement hysteresis loop 37
Figure 3.26 – Coupon test steel yield envelopes 39
Figure 3.27 – BR30m applied load vs. time 40
Figure 3.28 – BR6m applied load vs. time 41
Figure 3.29 – BR6m and BR30m cut away 42
Figure 3.30 – Un-bonding membrane grout interface 43
Figure 3.31 – Un-bonding membrane adhesive failure 43
Figure 3.32 –Yield section taper detail 44
Figure 3.33 –Yield section taper bearing face grout failure 44
Figure 4.1 – Normalized hysteresis backbone curve overlay 47
Figure 4.2 – NBCC response spectra – Kingston, On 48
Figure 4.3 – 3D FE model 48
Figure 4.4 – 3D FE model application of static loads 50
Figure 4.5 – 2D FE model application of static loads 50
Figure 4.6 – 3D and 2D storey drift4.2.5. Deflections and Drift Limits 52
Figure 4.7 – 2D FE model un-braced moment resisting frame 53
Figure 4.8 – ESFP storey drifts 55

Figure 4.9 – Backbone Curves for Fy=450 Steel 57
Figure 4.10 – Backbone Curves for Fy=350 Steel 58
Figure 4.11 – Backbone Curves for Fy=248 MPa Steel 58
Figure 4.12 – 2D FE lumped mass model with NL link elements 59
Figure 4.13 – Kingston Target UHS match east7c2.psa 60
Figure 4.14 – Scaled ground motion overlay east7c2.acc 61
Figure 4.15 – Top storey displacement TH 3 63
Figure 4.16 – Top storey displacement TH 5 63
Figure 4.17 – Top storey displacement TH 10 64
Figure 4.18 – Top storey displacement TH 11 64
Figure 4.19 – Top storey displacement TH 16 65
Figure 4.20 – FNA and ESFP Storey Drift 66
Figure 4.21 – BR6 20xTH11 Link Hysteresis 68
Figure 4.22 – 6 Bolt Connection Factored Resistance 72
Figure 4.23 – 8 Bolt Connection Factored Resistance 72
Figure 4.24 – Upper connection detail (Structural tender drawings, 2010) 73
Figure 4.25 – Lower connection detail (Structural tender drawings, 2010) 74
Figure 4.26 – Upper connection installed 74
Figure 4.27 – Lower connection installed 75
Figure C.5.1 – Column Detail (711m x 711mm) C-1
Figure C.5.2 – Column Detail (610m x 610mm) C-2
Figure C.5.3 – Factored column moment and axial load diagrams C-2
Figure C.5.4 – Moment Resistance Formulation (711 mm x 711 mm) C-3
Figure C.5.5 – Moment axial load interaction (711 mm x 711 mm) C-4
Figure C.5.6 – Moment Resistance Formulation (610 mm x 610 mm) C-4
Figure C.5.7 – Moment axial load interaction (711 mm x 711 mm) C-5
Figure D.5.8 – Kingston, On. Design Response Spectrum D-1
Figure D.5.9 – 3D FE model D-2

List of Tables

Table 3.1 – Brace testing summary 13
Table 3.2 – BRB dimensions 20
Table 3.3 – Values of Δ_{by} 21
Table 3.4 – Load program 22
Table 3.5 – BR6m brace modification calculations 27
Table 3.6 – BR30m brace modification calculations 27
Table 3.7 – Instrumentation dimensions 30
Table 3.8 – BR30m cyclic loading results 34
Table 3.9 – Tabulated strain hardening and friction adjustment factors 36
Table 3.10 – BR6m cyclic loading results 36
Table 3.11 – Adjustment factor relationships 39
Table 3.12 – Percent load sharing per cycle 41
Table 4.1 – BRB cross-sectional dimensions for static analysis 49
Table 4.2 – 2D Frame dimensions 51
Table 4.3 – Seismic Weight confirmation 51
Table 4.4 – 3D and 2D storey drift 51
Table 4.5 – Deflections and inter-storey drifts 53
Table 4.6 – ESFP brace axial forces 54
Table 4.7 – ESFP inter-storey drifts 55
Table 4.8 – Brace axial loads for ductile and over strengthened braces 56
Table 4.9 – PGA for scaled ground motions 61
Table 4.10 – ESFP and FNA absolute top storey displacements 62
Table 4.11 – ESFP and FNA TH5 inter-storey drifts for an un-braced frame 66
Table 4.12 – BRB Forces 67
Table 4.13 – Brace NL response to TH 11 68
Table 4.14 – BRB iterative analyses for 248, 350 and 450 MPa steel 69
Table 4.15 – Bolted connection capacity 71
Table C.5.1 – Factored load and resistance for column moment and axial forces C-5
Table C.5.2 – Moment-axial interaction balanced nominal values C-6
Table D.5.3 – FE model details D-1
Table D.5.4 – Dead, superimposed dead and snow loads D-3
Table D.5.5 – Seismic weight by storey D-3
Table D.5.6 – Equivalent static force D-4

List of Symbols and Acronyms

English Symbols and Acronyms

ADM (IE) ..... Assistant Deputy Minister (Infrastructure and Environment)
AISC ..... American Institute of Steel Construction
A_{sc} ..... Cross-sectional area of the yielding steel
ASTM ..... American Standard Testing Methods
BRB ..... Buckling Restrained Brace
BRBF ..... Buckling Restrained Brace Frame
CBF ..... Concentrically Brace Frame
CISC ..... Canadian Institute of Steel Construction
CSA ..... Canadian Standards Association
Cr ..... Factored axial compressive resistance
C_{ysc} ..... Probable axial compressive resistance
DCC ..... Defence Construction Canada
DND ..... Department of National Defence
E ..... Young's Modulus of elasticity
ESFP ..... Equivalent Static Force Procedure
F_a ..... Acceleration based site coefficient
FE ..... Finite element
FEA ..... Finite element analysis
FNA ..... Fast non-linear analysis
F_y ..... Yield stress in steel
F_{ysc} ..... Specified yield strength or actual yield strength of the steel core, determined by a coupon test in accordance with CSA G40.21
F_u ..... Ultimate stress in steel
H ..... Storey height
HSS ..... Hollow Steel Section
I_E ..... Importance factor
J ..... Overturning moment reduction
LVDT ..... Linear Variable Differential Transformer
L ..... BRB length
L_y ..... Length of yield section
M_v ..... Higher mode effects applied to top storey
NL ..... Non-linear
PGA ..... Peak ground acceleration
P-δ ..... P delta is the effect of eccentric axial loading due to a lateral displacement
PSA ..... Pseudo spectral acceleration
RC ..... Reinforced concrete
R_d ..... Ductility factor
R_o ..... Over strength factor
RMCC ..... Royal Military College of Canada
R_y ..... Steel yield strength adjustment factor, taken as 1.0 when steel strength has been validated by a coupon test in accordance with CSA G40.21
$S_a(0.2)$ ..... Spectral acceleration at 0.2 s
S_a(target) ..... Target spectral acceleration
S_a(Sim) ..... Simulated spectral acceleration
SFRS ..... Seismic force resisting system
T_a ..... Fundamental building period
TH ..... Time history

T_r ..... Factored axial tensile resistance
T_{ysc} ..... Probable axial tensile resistance
U ..... Lateral drift
UHS ..... Uniform hazard spectrum
W ..... Seismic weight
W_b ..... Bay Width
2D ..... Two dimensional
3D ..... Three dimensional

Greek Symbols

β ..... Friction Adjustment factor
Δ_{by} ..... Value of deformation quantity corresponding to the first significant yield of the test specimen
Δ_y ..... Value of deformation quantity corresponding to the first significant yield of the test specimen, in the yield section only
Δ_{out} ..... Value of deformation quantity corresponding to the first significant yield of the test specimen, in the outer cruciform region only
Δ_{bm} ..... Value of deformation quantity corresponding to the design storey drift
$\Delta_{bm1\%st}$ ..... Value of deformation quantity corresponding to the design storey drift at 1%storey height
ΔL ..... BRB elongation
ε_y ..... Yield strain in steel
θ ..... BRB end connection rotation angle
Φ ..... Resistance Factor, taken as 0.90 for structural Steel
ω ..... Strain hardening adjustment factor

Chapter 1: Introduction and Objectives

1.1. Introduction

In 2008, the Department of National Defence (DND) began a project to renovate the Sawyer and Girouard buildings at the Royal Military College of Canada (RMCC). A photo of the original structures is presented in Figure 1.1, with each of the five modules clearly visible and the Sawyer module numbers labeled in red.

Figure 1.1 – Sawyer and Girouard buildings prior renovations (Structural tender drawings, 2010)

One of the elements of this renovation was a seismic retrofit, adding a total of 28 unique Buckling Restrained Braces (BRBs) that were designed and installed as a seismic dampening system, with each BRB built to absorb the effects of earthquake forces and limit the inter-storey lateral drift. Figure 1.2 presents a plan view of modules 1 and 2 with the BRBs numbers with a dotted outline and highlighted in blue. The column stack of BRBs analysed in this research: BR 4, BR5, BR6, and BR7 have a solid outline and are highlighted in orange.

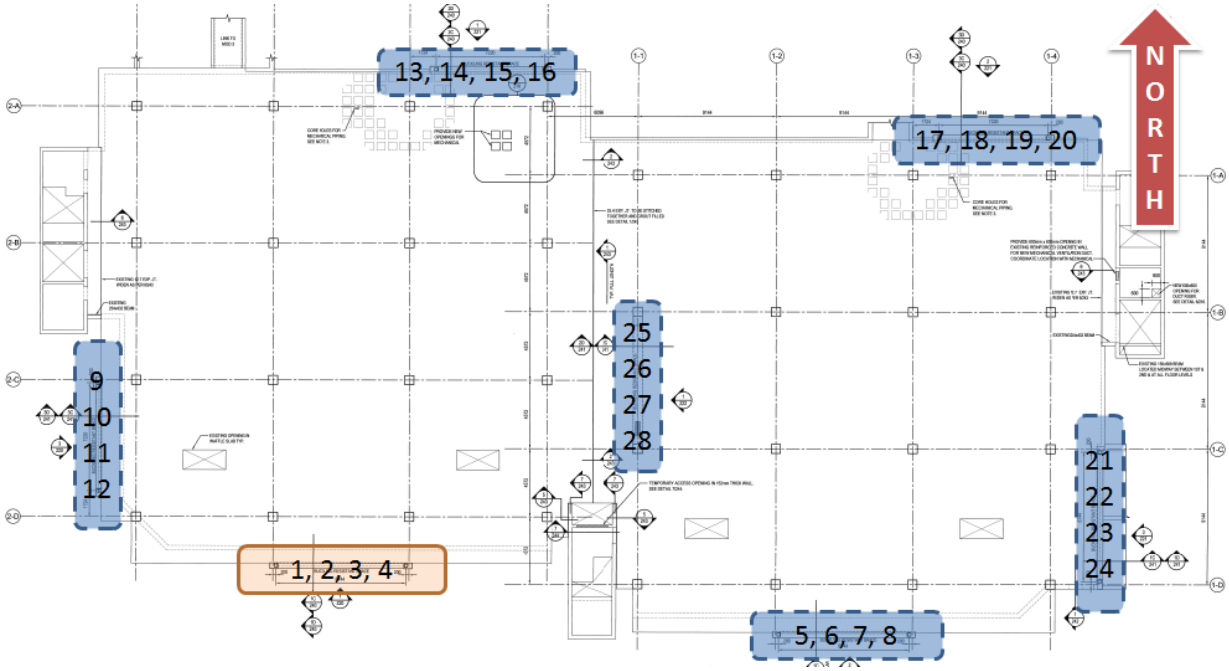

Figure 1.2 – Plan view of modules 1&2 with BRBs highlighted (Structural Drawings, 2010)

Exemplified in a photo of module 3, Figure 1.3 clearly illustrates how the exterior modules were strengthened with BRB frames that braced all five floors with the bottom floor being a rigid shear wall anchored to rock or secured using deep piles. The BRBs are the inclined elements in the frame.

Figure 1.3 – Typical module with BRB frame and shear wall

In the instance of a seismic event, the ground will be subjected to horizontal vibrations. These vibrations will cause the structure to move laterally. With these lateral displacements, the columns and floors will be subjected to large moments that may cause local or global structural failure. Older structures that have limited lateral resistance may require additional lateral support in the form of lateral bracing. While there is a wide range of bracing options available to address the issue of lateral displacements, the seismic upgrade in this particular structure uses BRBs as the seismic lateral force resisting system. A modern BRB is typically comprised of four components: the steel core, un-bonding layer, grout, and casing as presented in Figure 1.4. The steel core can be characterized in two sections: the inner and outer yield section. The outer section consists of a robust outer yield section, with the inner section acting as the structural fuse of the system and is designed to expand and contract along its length; thus providing an axial dampening system that absorbs the kinetic energy from a seismic event. Lateral storey drifts are controlled by the system and energy is absorbed by hysteretic strain hardening until failure. The bond preventing layer is a thin layer encapsulating the yield sections and is intended to un-bond the steel core from the grout. Once the bond preventing layer begins to un-bond, the grout is then able to perform its primary function which is to provide proper lateral support against flexural buckling of the steel core. The function of the casing is to ensure that the composite action of the steel outer casing

and grout provide adequate buckling resistance for the slender inner steel core. Figure 1.4 displays an overview of a typical BRB used in this research.

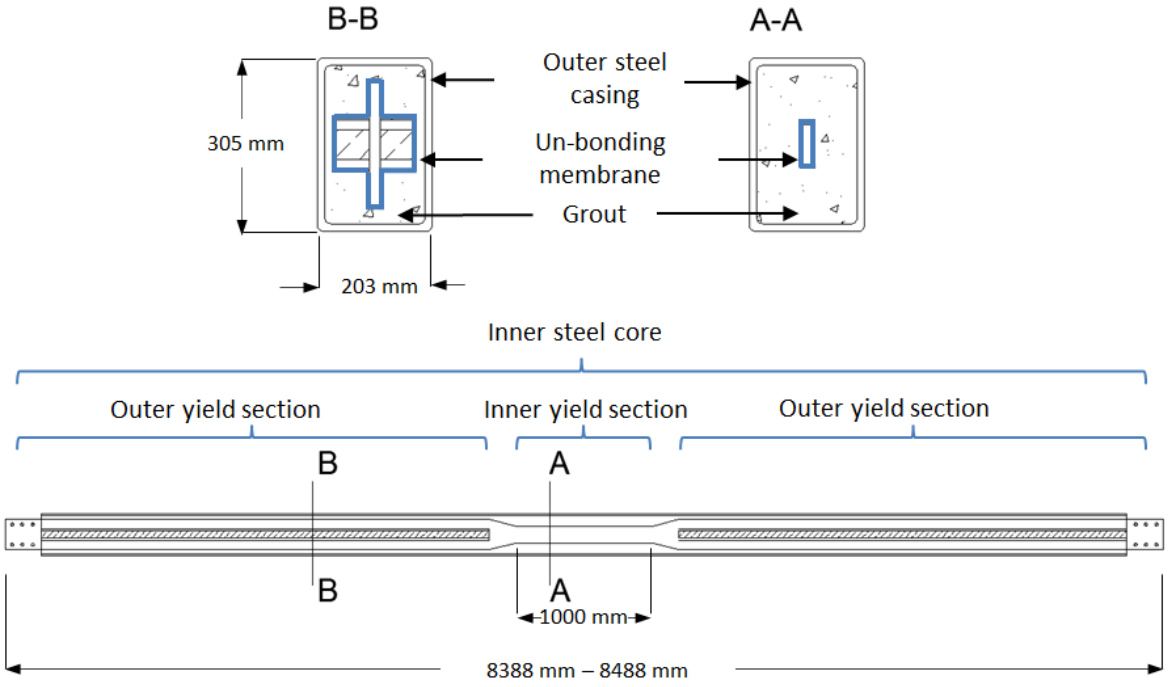

Figure 1.4 – BRB anatomy

The behaviour of three full-scale nine-meter-long BRBs, representative of braces for the seismic upgrade of the Sawyer Buildings, were investigated experimentally. The three BRB specimens were tested in an individual uniaxial subassemblage in accordance with recommendations from CSA S16-09 Design of Steel Structures [1] and the American Institute of Steel Construction (AISC) Seismic Provisions for Structural Steel Buildings [2]. Each brace was designed to withstand a specific axial load in both tension and compression with the ultimate strength being achieved once the brace has undergone extensive plastic deformations and strain hardening. The design of the BRBs was based on using a single type of low grade steel with a yield strength of 248 MPa and varying cross sectional area of internal yield section to resist predicted loads using the Equivalent Static Force Procedure (ESFP).

1.2. Objectives

The objectives of this research are summarized below:

1. Determine the behaviour of the three BRBs under the effects of increasing axial load;
2. Determine suitable friction (β) and Strain-Hardening (ω) factors for use in the structural analysis of the building system;
3. Determine the material properties of the as-built BRBs;
4. Perform a static and dynamic analysis to determine the holistic structural response of a five storey concrete frame building when strengthened by the as-designed BRBs and as-built, over-strengthened BRBs; and
5. Assess the overall effectiveness of the as-built SFRS as a part of the building seismic structural upgrade.

1.3. Scope

The scope of this research was to conduct qualification testing that would provide an understanding of the behaviour of the as-designed and as-built BRBs as applied to a specific structure. The effects of these braces on the design structure are limited to a five storey reinforced concrete frame representative of a single module of the Sawyer Building. The analysis options covered the spectrum of static and dynamic analysis with the focus being FNA. The time histories used in this research were limited to the use of scaled synthetic ground motions that corresponded to NBCC design spectra. The moment connection capacity and out of plane bending of these BRBs were not directly assessed, allowing the design of the subassemblage and the testing of the BRBs to focus on behaviour when subjected to axial loads.

1.4 Content

This research is presented in five chapters with this first chapter being an introduction to BRBs, the Sawyer building seismic structural upgrade and an overview of the investigation outlined in this document. An overview of each of the subsequent chapters is presented below:

Chapter 2 focuses on reviewing contemporary research and relevant literature. The details and objectives of the qualification testing are presented along with analysis options for both static and dynamic analyses.

Chapter 3 presents the brace assembly, set up, and instrumentation, material testing and details of brace modification. The findings of the qualification testing are presented, with the friction and strain hardening factors (β and ω, respectively) being the culminating product of this testing. The qualification testing also highlighted several areas of concern which are identified in this chapter.

Chapter 4 focuses on the modelling of a single five-storey module using un-strengthened, as-designed and as-built models. The Equivalent Static Force Procedure (ESFP) was conducted along with a dynamic Fast Non-Linear Analysis (FNA). The FNA used a series of synthetic ground motion time histories which are also derived in this chapter. An iterative analysis is performed using FNA to determine the ultimate limits of the SFRS. These results of the ESFP and FNA are compared and summarized in this chapter.

Chapter 5 is the conclusion of this research which summarizes each of the key findings, while providing a recommendation for each issue.

Chapter 2: Literature Review

2.1. Literature Review

2.1.1. Early BRBs

Modern construction techniques very often implement lateral bracing in the form of either tension only or rigid tension-compression steel bracing as a method of increasing structural stiffness. While conventional lateral cross-bracing can be used for both wind and seismic applications, the cyclic compressive force applied to steel braces in a seismic event has led to the relatively recent development of the Buckling-Restrained Bracing (BRB) system. One of the earliest documented designs of BRB systems was first published in 1973 by Wakabayashi et al. This initial research on what would later be called a BRB involved a flat steel plate pressed between 2 precast concrete panels, effectively restraining the compressive buckling of the slender internal steel section [3]. In 1976, Kimura et al. began to explore the first mortar encased BRBs [4]. Kimura's design left a void between the steel brace and mortar which allowed for free cyclic motion inside the brace, allowing localized buckling. Both of these early BRB designs were reliant on the void or clearance between the steel core and the concrete. Three years later, Mochizuki et al. [5] introduced a shock absorbing layer between the steel yield section and mortar. This interfacing layer permitted expansion due to Poisson's effects and reduced abrasion during cyclic loading. This shock-absorbing layer was the first of its kind and since that time, a wide range of material has been used, including epoxy and silicon resins, vinyl tapes, plastics, and lubricants. [6]

From the 1980's onward, the use of both types of BRB systems were developed and further researched. The all-steel BRB system is a continuation of the early works of Wakabayashi with the exception of the pre-cast sandwich panels. The all-steel brace restrains the inner yield section by a small void and are much simpler to build without having to grout or facilitate un-bonding. The added benefit of the all-steel brace is the ability to disassemble and inspect; however, the void in the all-steel BRB presents a region of continual localized failure of the inner yield section. Iwata et al. conducted a study in 2000 [7], in which a series of all-steel BRBs were tested against one another. Both braces had a nominal clearance; the all-steel brace had a void, and the second series of BRBs had an un-bonding layer. The results showed the all-steel BRB with the un-bonding layer displayed a better hysteretic performance than the BRB with the void which failed prematurely because of localized plastic strain concentration [7].

2.1.2. BRBs in North American Codes

While the BRB was pioneered in Japan in the mid 1970's, it was not until the 1990's that the first prototypes were commercialized and approved for use. The BRB made its debut in North America in 1999 at the University of California Davis Plant and Environmental Sciences Building [6]. In 2005, following the introduction of the BRB system to the North American market, the American Institute of Steel Construction (AISC) introduced a new qualification standard for BRBs into the U.S. design practice [2]. The additions to the American code permit the installation of a BRB system once it has successfully completed qualification testing and has been proven experimentally [2]. While the AISC code remains the standard for proving a BRB for use in Canada, the Canadian Standards Association (CSA), has added significant provisions to the CSA S16, since the sixth edition in 2001 and the interim edition of 2005. In the seventh edition, adopted in the 2009, clause 27.8 was added to cover buckling restrained braced frames under seismic loading and makes reference to the 2005 AISC document for qualifying BRB performance. This research applies the NBCC 2010 as well as CSA S16-09 and the CSA A23.3-14 codes to the analyses while commenting on variance between the current codes and the applicable codes at the time of initial design.

It is understood that the mechanics of the inner yield section of a BRB are critical to ensuring proper hysteretic behaviour; however, the connection design of each BRB is equally important. As a

brace is subjected to lateral drift, the inner yield section begins to expand and contract. As this occurs, the brace connections begin to exhibit increasing moments as the rotation angle grows during each successive cycle. An illustration of this behavior is presented in Figure 2.1.

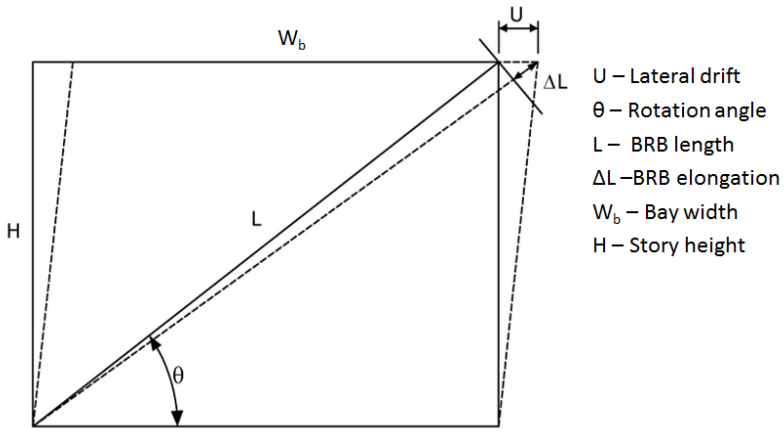

Figure 2.1 – BRB mechanics

It is for this reason that the American Institute of Steel Construction (AISC) guidelines recommend that a single storey be assessed to allow for these moments to develop and to test the out of plane capacity of the connections. In 2002, early tests by Aiken et al. [8] on a single storey, single bay subassemblage were tested with gusset plates and bolted connections. This research found that significant in and out-of-plane deformations occurred in the gusset plates as a result of the rigid bolted connections. The research performed by Tsai and Hsiao [9] in 2008 examined the rotational demands placed on a full-scale bolted BRB frame. Similar out of plane buckling bending was observed as shown in Figure 2.2. The local buckling of the bolted connection was mitigated with the addition of edge stiffener to the gusset plates.

Figure 2.2 – Out of plane buckling (Della Corte et al., 2011)

The concept of a perfectly pinned connection proposed by Fahnestock et al. [10] effectively eliminates the moments created by a rigid bolted connection. The pinned connection requires more flexural stiffness from the brace itself as well as adequate restraints for the casing member of the BRB. Pinned braces tend to have more robust transition zones including reinforced end collars to account for

the stiffness requirements at the inner yield section and outer brace interface [6], an image of this effect is presented in Figure 2.3.

Figure 2.3 – Pinned connection reinforcement detail (Della Corte et al., 2011)

2.1.3. Contemporary Research

Tremblay`s 2004 [11] paper on the testing and design of BRBs confirmed that the soon to be published NBCC 2009 provisions, a Buckling Restrained Braced Frame (BRBF) with a ductility factor, Rd = 4.0, can exhibit satisfactory seismic performance. However, the nonlinear dynamic analysis of low-rise BRB frames designed according to satisfactory seismic performance inelastic demand tends to concentrate seismically generated internal forces at the bottom floor, resulting in core strain demand exceeding the design values. It was also noticed that these design values were constantly exceeded when braces with short yield cores are specified, requiring that provisions must be made at the design stage for such cases of higher demand [11]. In 2006, Tremblay et al. conducted a similar study using a series of all-steel BRB with a void and a series of grout filled BRB with a polyethylene un-bonding layer. The results of this research confirmed the requirement to control localized buckling in order to improve the overall hysteretic performance and development of a uniform strain along the length of the entire yield section. It was noted that at large deformation levels, both long core and short core braces exhibited tension, and to a greater extent; compression forces that exceeded the core yield capacity. This observation was credited to strain hardening and the effects of frictional load sharing between the yield section and outer steel casing. The recommendation is that the design of brace connections must account for these increased brace capacities in both tension and compression [12]. These recommendations are echoed in CSA S16-09 with the introduction of the BRB qualification testing and the strain hardening adjustment factor, ω, and friction adjustment factor, β.

The use of BRBs as seismic dampeners is not only limited to use in low and high-rise buildings but may also be suitable for any structure that may be subjected to a seismic ground motion. The overarching principle of designing an effective BRB system is to ensure that the yield displacement of the BRB is less than the yield displacement of the structure or frame. This principle was applied by El-Bahey and Bruneau in their 2011 research in which a parametric study was conducted to develop a BRB design procedure for reinforced concrete bridges [13]. Their proposed design methodology is a concise approach for the specific application of designing BRBs for reinforced concrete bridge bents. It is based on the assumption that both the BRB "fuse" and the column's lateral systems are un-coupled, assuming that the axial forces from the fuses have a negligible impact on the column capacity. The parametric study concluded that the proposed design process was effective at determining a range of admissible solutions; however as the frame strength increased, the region of admissible solutions decreased, requiring larger BRB fuse elements, ultimately trending towards a rigid, non-plastic brace.

While the performance of both the BRB and principal un-strengthened structure is important, an understanding of the combined global structural behaviour is required in order to predict the actual strengthened structural response. Di Sarno and Manfredi's 2010 [14] research explored a two storey reinforced concrete frame with limited translation ductility and modelled a seismic retrofit using BRBs placed along the perimeter frames. The adopted design approach in this instance assumes that the global response of the inelastic framed structure is the sum of the elastic frame and the plastic BRB system. Non-linear static pushover and dynamic time-history analyses were carried out for both the as-built and retrofitted structures to investigate the efficiency of the adopted intervention strategy. This research used a set of seven code-compliant earthquake records to excite the structures and concluded that, under moderate and high magnitude earthquakes, the damage in the retrofitted structure was concentrated in the BRB dampers and the response of the existing RC framed structure remained elastic. The benefits of conducting a dynamic time history can be illustrated in Jinkoo and Hyunhoon's comparison of the static pushover analysis and time-history analyses for low and medium-rise moment resisting frames strengthened using BRB's [15]. This study observed that the maximum displacements generated by both the static and dynamic analyses of 10 and 20-storey structures were represented closely by the target displacements. However, those of 5-storey structure underestimate the target displacement as much as 25–35%. This discrepancy stems from the fact that the response spectrum is highly irregular in the region of short natural periods, which causes inaccuracy in the process.

The research presented in this thesis is focused on the testing and analyses of pre-designed and installed BRB's. It is valuable to review other seismic bracing systems and bracing configurations. Di Sarno and Elnashai conducted a comparative analysis for BRBs and rigid tension-compression braces installed in concentric arrangements as well as in an exterior mega-brace format. Concentric bracing configurations link storeys together, where a mega-bracing format is applied to the building's exterior not necessarily linked to each story [16]. The different configurations were modelled and excited using six natural earthquake ground motions in a non-linear time history analysis. The reductions in global deformations are dependent on the specific characteristics of each earthquake ground motion, especially frequency content. For near-field records, the benefits in using mega-bracing formats are generally lower than for far-field records. Using the un-braced steel moment resisting frame as the reference point, concentric bracing configurations provided 30% reduction in maximum inter-storey drifts while the mega bracing configuration provides a 50-60% reduction. When comparing the effects of inelastic BRBs versus the elastic tension-compression braces, the inelastic BRBs are found to only be marginally superior in performance despite their greater weight and complexity. The total amount of steel required in the mega-bracing format was found to be 20% less than concentric bracing arrangements, lending mega-braces to have a smaller construction cost. This study also concludes that the preference of mega bracing formats be installed without interruption within the building thus preventing loss of use caused by the structural retrofitting strategy. [17]

While this thesis does not directly test the BRB connection, the connection design and behaviour of the connection are relevant to and impact the behaviour and effectiveness of the BRB. Throughout the qualification testing, the BRB designed end connections required temporary stiffening modifications, enabling the braces to be inserted into the testing set up without bending under the effects of their own resistance. These temporary external modifications were required since the BRB's end connections provided inadequate out-of-plane stiffness when tested in isolation from the structural frame of the SFRS. A review of end connections issues and solutions are addressed in Della Corte's 2011 review of buckling restrained braces [6], however a more recent, 2014 publication by Junxian et al.[18] presents a unified design approach to the pinned connection where several failure modes are examined. Traditional pinned and fixed connections are typically strengthened with an end transition stiffening portion; however, the persistence of out-of-plane bending in pinned connections continued to be problematic for this connection configuration. The authors of this study qualified and tested a pinned connection using a collar and focusing on the out-of-plane stability design of connections and core extension. A diagram of the pin-and-collar connection detail is proposed in Figure 2.4 [18]. This research does not directly assess the moment resistance or stiffness of the end connections, however there exist several, and relatively low-tech methods of providing increased out of plane stiffness to a traditional end connection

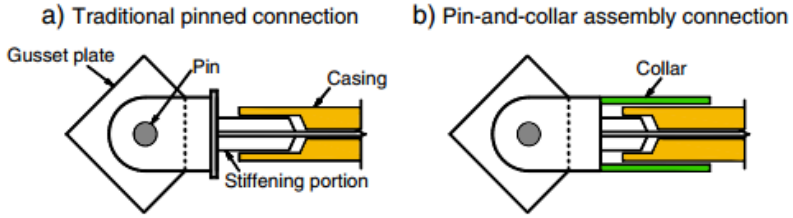

Figure 2.4 – Pinned connection detail (Junxian et al., 2014)

2.2. Qualification Testing

The qualification testing of BRBs is governed by CSA S16-09, Design of Steel Structures, which added significant provisions to the interim 2005 version of this code, CSA S16-05. Clause 27.8 was added in 2009 to cover buckling restrained braces under seismic loading [19]. As a part of this new clause CSA S16-09, a formula for design of the steel core is provided. The factored tension and compression resistance of the steel core is presented in Equation 2.1; were T_r is the factored axial tensile resistance, C_r is the factored axial compressive resistance, $\emptyset$ is the structural steel resistance factor, A_{sc} is the cross sectional area of the yielding steel, and F_{ysc} is the specified yield strength or actual yield strength of the inner steel core.

:

$$T_r = C_r = \emptyset A_{sc} F_{ysc} \qquad \text{Equation 2.1}$$

The requirement for a full-scale qualifying BRB test was a new addition to the S16-09. This testing is critical to confirm the predicted response of the designed BRB. While Equation 2.1 provides the simplified approximation for preliminary design, the performance of a BRB varies between tension and

compression strokes. The qualification testing provides the strain hardening adjustment factor, ω, and friction adjustment factor, β, which can be applied to all braces of similar design. This empirical data obtained from the qualifying test specimens can be applied to Equation 2.1 to estimate the probable tensile and compressive resistances, respectively T_{ysc} and C_{ysc}. Equation 2.2 and Equation 2.3 present the application of the strain hardening and friction adjustment factors. R_y is the steel yield adjustment factor, taken as 1.0 when steel strength has been validated by coupon testing.

$$T_{ysc} = \omega A_{sc} R_y F_{ysc} \quad \text{Equation 2.2}$$

$$C_{ysc} = \beta \omega A_{sc} R_y F_{ysc} \quad \text{Equation 2.3}$$

The immediate objective of this testing is to satisfy the requirements of the CSA S16-09 seismic design clause 27.8, and produce values for ω and β. The acceptance criteria outlined in annex T of the 2005 AICS Seismic Provisions for Structural Steel Buildings will also be validated. Additional material tests were performed in order to better understand the material properties. There were also modifications made to the braces to ensure that the BRB specimens performed as required, given the constraints of the subassemblage.

2.3. BRB Analysis Options

Following the qualification testing, the BRBs were modelled using commercial finite element analysis software using the predetermined material properties and a five storey reinforced concrete frame was analysed using both static and dynamic approaches.

The two methods of seismic analysis prescribed by clause 4.1.8.7 of the 2010 NBCC are the Equivalent Static Force Procedure (ESFP) and dynamic analysis. The code dictates that all analysis for design earthquake actions shall be carried out by the dynamic analysis procedure except that the ESFP may be used for structures that meet any of the following criteria: the structure must be in an area of low seismicity, be a low rise structure less than 60m in height with a fundamental building period of less than 2 s and not be torsionally sensitive [20].

While the seismic analysis of a reinforced concrete frame of the type considered in this project can be completed using the ESFP and the static axial loads in the Seismic Force Resisting System (SFRS) can be used in the verification of BRB design, the nonlinear dynamic time history is an essential step in understanding the complete brace performance. In order to conduct a dynamic analysis, the SFRS must be subjected to an appropriate ground motion that matches the 2010 NBCC Uniform Hazard Spectrum (UHS) for a 2% in 50 year return period. The specific UHS depends on location and site condition, where site condition is described by a classification scheme based on the time-averaged shear wave velocity in the top 30 m of the soil deposit. While the UHS is the driving data set for the ESFP, the FNA method requires an appropriate ground motion in order to generate a time history analysis. Atkinson [21] presents the stochastic finite-fault method used to generate earthquake time histories that may be used to match the 2005 NBCC UHS for a range of Canadian sites. The earthquake records presented by Atkinson include pseudo-spectral accelerations as well as associated ground motions for the full range of site conditions in both Eastern and Western Canada. All data is available, open source at www.seismotoolbox.ca. [22]

Contemporary BRB research is substantial; however, there are several bodies of work that provide unique parallels and insight to this thesis. Tremblay 2006 explores the effects of short and long core BRBs under dynamic and slow speed time histories [12] while also focusing further research on low rise steel braced frames. This 2010 research explored and modelled a seismic retrofit using BRBs placed along the perimeter frames of a two-storey reinforced concrete frame [14]. Di Sarno and Manfredi's research also used a set of synthetic code-compliant earthquake records under moderate and high magnitude earthquakes to generate dynamic time histories. The focus of Jinkoo and Hyunhoon's research was the correlation between the accuracy of static and dynamic analysis methods and storey heights, using BRBs applied to 5, 10 and 20 storey moment resisting frame structures [15]. While recent papers have published in similar fields, the investigation outlined in this document is unique in that it expands the field of knowledge for BRBs by investigating the experimental behaviour of short core, grout-filled BRBs and analyzing the effectiveness of these BRBs when used in a low-rise reinforced concrete frame seismic structural upgrade.

2.4 Summary

Research into BRB behaviour began in the early 1970s in Japan and the technology has developed rapidly across Europe and North America in the early part of the 21st century. It was not until 2005 that North American codes began to publish guidelines and standards for the design and testing of BRBs. With this relatively new technology in service, research has focused on determining appropriate code factors such as ductility and over strength factors (R_d and R_o) as well as procedures to approximate friction and strain hardening factors (β and ω) for use in design. Recent BRB research has examined alternative bracing configurations, analysis options and brace connection designs. The finding of contemporary researchers in the field of BRBs has greatly contributed to the experimental investigation and analyses outlined in the following chapters.

Chapter 3: Buckling Restrained Brace Testing

3.1. Testing Overview

As a part of this research, three full scale braces were tested in a uniaxial subassemblage. The first brace that was tested was the brace titled BR4. This brace was instrumental in highlighting a number of modifications and additions to the testing protocol, which will be discussed further in this chapter. The subsequent two braces were named BR6 and BR30. Both of these braces were disassembled with their inner yield sections being modified in order to perform plastically within the testing frame. These braces were renamed BR6m and BR30m to denote modified cross sections. Both brace BR6m and BR30m were subjected to a cyclic loading protocol and achieved significant strain hardening before reaching ultimate capacity within the limits of the subassemblage. The yield and ultimate capacities of the BRBs are tabulated in Table 3.1. The design and setup of the qualification testing of the BRBs was focused on the axial application of tension and compressive forces. The components of this subassemblage were designed around the limiting capacity of a 1,000 kN actuator.

Table 3.1 – Brace testing summary

BRB	Configuration	Yield	Ultimate	Performance
		kN	kN	
BR4	Unmodified	>1,000	>1,000	Purely elastic did not yield
BR6m	Modified yield section	625	970	Plastic strain hardening to failure
BR30m	Modified yield section with butt weld at mid-span	525	957	Plastic strain hardening to failure

From the qualification testing, the friction and strain hardening values were calculated and a number of observations were made regarding the grout and un-bonding membrane interface which may have led to additional load-sharing that would increase the overall capacity of the braces. The results of each qualification test are summarized with a number of conclusions presented; including the overall brace design and construction as well as load sharing and un-bonding issues. The qualification and material testing set the conditions for understating the issues of over strengthened BRBs in Chapter 4, along with a review of maximum allowable compression stroke and bolted connection capacity.

3.2. Design Philosophy

As discussed in the introduction, a BRB is the structural fuse of the system that relies on the inner yield section to absorb the kinetic energy in the structural system generated by inter-storey drifts. The mechanics of this system are facilitated by the bond preventing layer, in this case, a 1.5 mm Blueskin® self-adhesive waterproofing membrane, further referred to in this document as the un-bonding membrane. This un-bonding membrane is intended to un-bond the steel core from the grout and confine the inner yield section, preventing buckling in compression. The mechanism of bond prevention relies on the smooth surface of the un-bonding membrane to minimise the bonding action of the grout as well as to reduce the friction at the un-bonding membrane to grout interface during cyclic loading. Appendix A Appendix A outlines the specific dimensions for each brace while Figure 3.1 displays an overview of a typical BRB anatomy in this seismic upgrade.

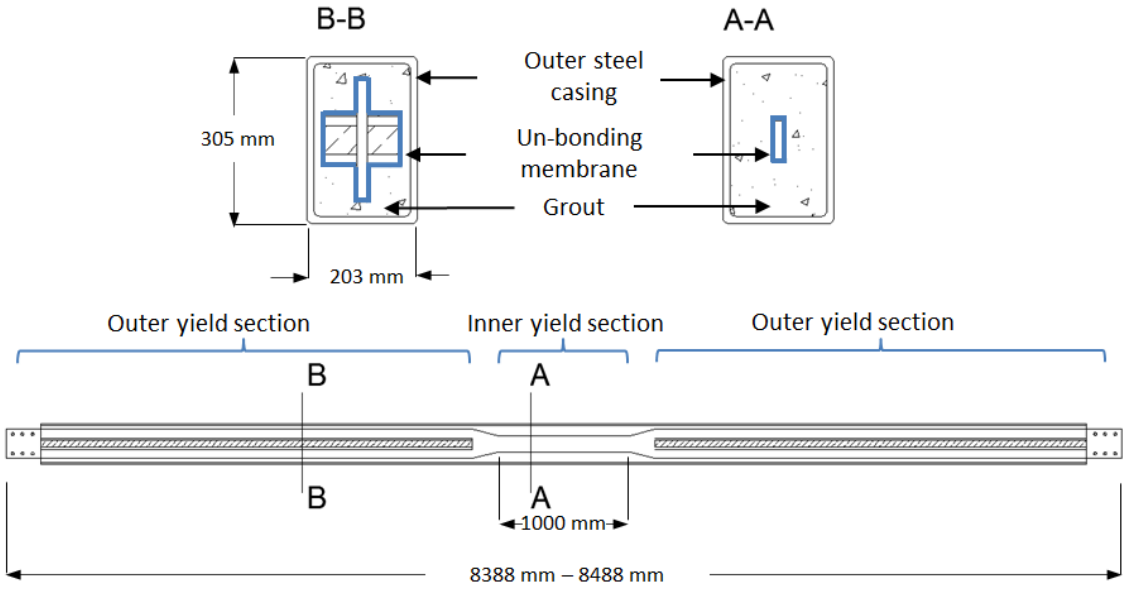

Figure 3.1 – BRB anatomy

The area of primary interest within the BRB is the inner steel core. The length of the core can be divided into two sections: yielding and non-yielding. The yielding or middle section is the centre and most slender portion of the brace. The length and cross-section of the yield section are the controlling design dimensions of the brace. The non-yield or cruciform section has a much more robust and rigid cross-section, ensuring that the remainder of the brace remains elastic, forcing the plastic deformations to occur in the yield section. This configuration of both the yield and non-yield sections of the inner steel core ensures the predictability of the braces entire behaviour and failure.

While the inner steel core remains the critical yield section of the brace, the transition zone between the outer to inner section is also of interest. The taper from the yield to non-yield sections is a 1:4 slope. This design slope was chosen to reduce the stress concentrations at the yield section interface. The wings on the reinforced outer cruciform section share the same 1:4 taper as the yield section interface, and also share the addition of a 13 mm thick asphalt saturated fibre board. The fibre board creates a compressible layer that enables the brace to undergo axial deformations without compressing the grout. This allows the yield section to exhibit similar strain hardening in both tension and compression cycles.

3.3. Subassemblage

The AISC publication titled Seismic Provisions for Structural Steel Buildings specifies that a test be conducted of the brace in a one storey subassemblage test frame resembling a single storey [2]. The purpose of testing the complete storey subassemblage is to confirm that the brace design can accommodate the deformations and rotational demands of the design of one storey. This provision of the AISC was not adhered to because the focus of this research was the performance and response of the brace itself. The brace is the principal element of the SFRS frame and it was anticipated that the deformations of the brace and frame would be small. One of the factors in the design of the subassemblage is the limit of the actuator capacity. The maximum applied load was limited by the 1,000 kN actuator that was available in the RMCC Structural Laboratory. The constraint of 1,000 kN also governed the selection and modification of the BRBs in order to facilitate yielding, cyclical loading, strain hardening and ultimate failure.

A frame was designed and erected to accommodate a BRB measuring between 8 m and 9 m in length. Due to the extreme loads applied to the testing frame, the vertical supporting columns were laterally braced with a diagonal 102 mm x 102 mm x 12 mm HSS. All bolts used in the construction of this test frame were ASTM A490, grade 9 structural bolts including floor anchor bolts. A truncated overview of the entire subassemblage can be seen in Figure 3.2.

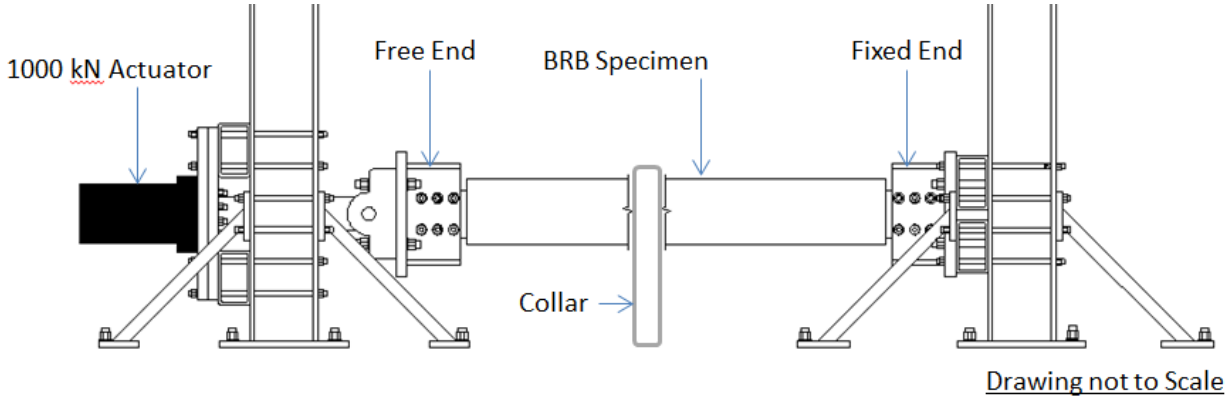

Figure 3.2 – Overview of subassemblage

Figure 3.3 and Figure 3.4 show the complete subassemblage for Brace BR4 in full detail with basic dimensions annotated on the figure for reference. Each test required minor modifications to the apparatus in order to accommodate braces of different lengths.

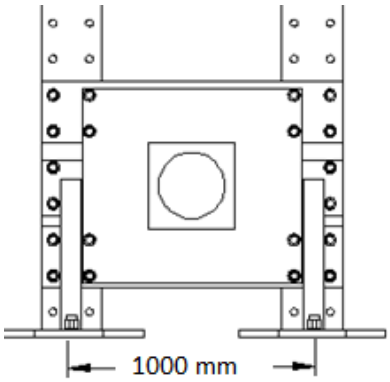

Figure 3.3 – Complete subassemblage actuator end

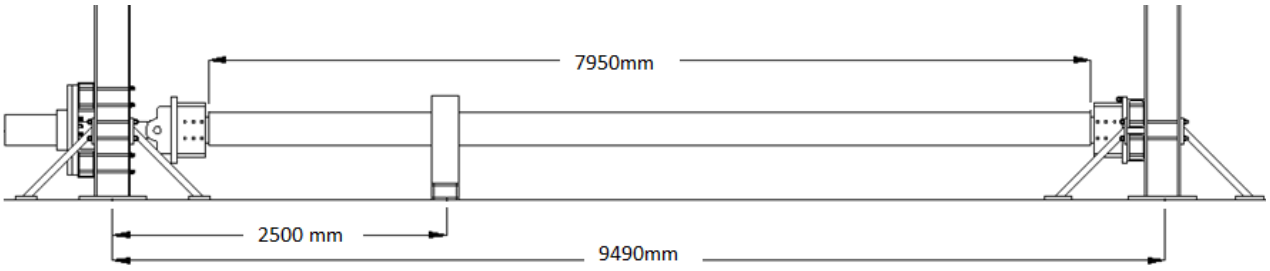

Figure 3.4 – Complete subassemblage profile

In the subassemblage, the fixed end of the test frame is seen in Figure 3.5. This conn**e**ction uses six 19mm A490 bolts to connect the BRB to the test frame and provides a completely fixed and rigid connection. Since the single storey, single bay subassemblage is simplified to a straight axial test, the detail of the as-built bolted connection and gusset plates were not reproduced. While the exact performance of the brace connection due to the connection end moments were not tested, the actuator foot on the moving end of the BRB permitted bending at the connection which was apparent during the start of the BR4 testing. The actuator foot is mounted to an omnidirectional ball joint that, when loaded, would cause buckling of the BRB at the steel core-grout interface under the compression cycle. The rotation at the actuator foot end was mitigated by the addition of two 25 mm steel support props that stabilized the foot in the compression cycle by transferring load to the cruciform supports of the outer yield section. This modification was essential in order to make the subassemblage mimic the constraints of the installed BRB. A photo of the modification to the connection at the actuator foot can be seen in Figure 3.6. The capping plate was also removed from the BRB at the actuator end of the specimen to facilitate this stiffening and to ensure the full range of compression stroke. The effects of capping of the BRB and limiting the compression stroke are discussed in chapter 4.

Figure 3.5 – Detail at fixed end

Figure 3.6 – Detail at actuator end

Another design feature in the subassemblage was the addition of roller supports at two thirds of the length from the fixed end. All of the components of the subassemblage and test frame components are illustrated in the free body diagram included in Figure 3.7.

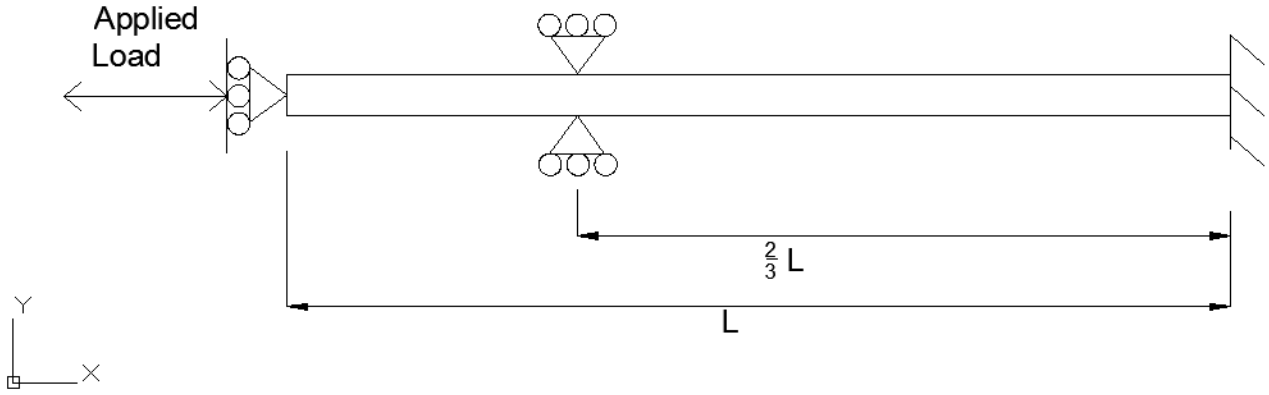

Figure 3.7 – BRB free body diagram

The AISC qualification testing does not call for a collar support as a part of the subassemblage, however given the actuator connection, this roller support restricted movement in the lateral directions and facilitated smooth uniaxial loading in the longitudinal direction of the brace. This support also helped to reduce the effects of localised buckling at the end of the brace which was unrestrained by the ball joint at the actuator foot. In the subassemblage, two short columns were bolted to the strong floor and adjustable Teflon® sliders were aligned to provide a collar of support to the sides and top of the outer case. A photo of the sliding support collar can be seen in Figure 3.8.

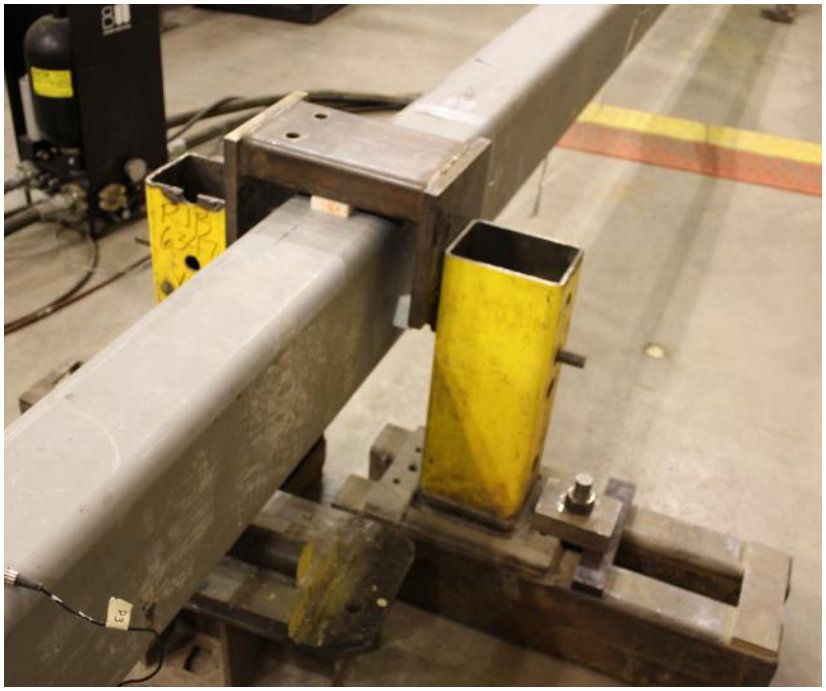

Figure 3.8 – Detail at sliding support collar and roller support

3.4. BR4 Preliminary Testing

This research was conducted using three BRBs from the Sawyer Building project. Two braces were labeled BR4 and BR6 while the third brace that was used in the testing did not correspond to any of the braces listed in Appendix A and is referred to in the text as BR30. Brace BR4 was used in the preliminary stages of the research and helped to determine underlining issues with the brace configuration and design. BR4 was assembled, set up and instrumented as per the procedure outlined in section 3.7. Given the design specifications of cross-sectional area, 2,413 mm^2 and yield strength of 248 MPa, the brace BR4 was estimated to commence plastic deformation at an axial load of 663 kN; however the brace did not perform as expected and did not exhibit any plastic deformations, even under the maximum applied load of 1,000 kN. From this preliminary testing it was confirmed that the grade of steel was greater than the 248 MPa steel specified in the structural drawings in Appendix A. This irregularity required further testing in order to confirm the strength of steel in braces. A copy of the initial mill report was reviewed and specific yield tests revealed that three samples of steel were tested and the yield strength was found to be between 373 MPa and 476 MPa, however it was impossible to correlate the data in the mill report to the plate steel in any specific brace. For this reason, coupon tests were required to confirm the steel properties of each brace in further testing.

After reviewing the test data for BR4, it was noticed that the strain gauges on the outer core registered substantial strains, and at times during the loading program carried upwards of 30% of the load. The identification of load sharing between the brace inner steel core and the outer casing identified the issue of slow or incomplete un-bonding of the inner steel core from the grout and helped define the modifications required for the testing protocols of the remaining braces. The issue of load sharing was further investigated in subsequent brace testing and it was found that capacity increase due to load transfer between the inner steel core and outer steel casing was present in both BR6m and BR30m. While full scale dynamic testing was not conducted, it is predicted that the effects of loads sharing will increase under a dynamic ground motion. Similar observations regarding load sharing effects were published by Tremblay in 2006 where a slow rate loading was compared with a dynamic load program, resulting in a 5% increase in brace yield resistance under a dynamic load [12].

While the preliminary BR4 testing did not provide empirical results that directly contributed to this research, it provided valuable insight into the composition and performance of the BRB system. The over strength characteristics of brace BR4 helped lay out the testing framework and protocol to better understand the material and gather information to better understand the actual brace capacity.

3.5. Brace BR6 and BR30

With the completion of the preliminary findings on brace BR4, further testing was conducted on braces BR6 and BR30. These additional braces were selected based on availability and accessibility from the Sawyer renovation project and were in need of further refinement in order to ensure yield within the constraints of the testing apparatus. The dimensions for both braces are presented in Figure 3.9 and Table 3.2. The highlighted braces represent the brace tested during this research. BR6m and BR30m are the modified versions of the brace corresponding to the BR numbering prefix. This modification process is further described in section 3.5.2.

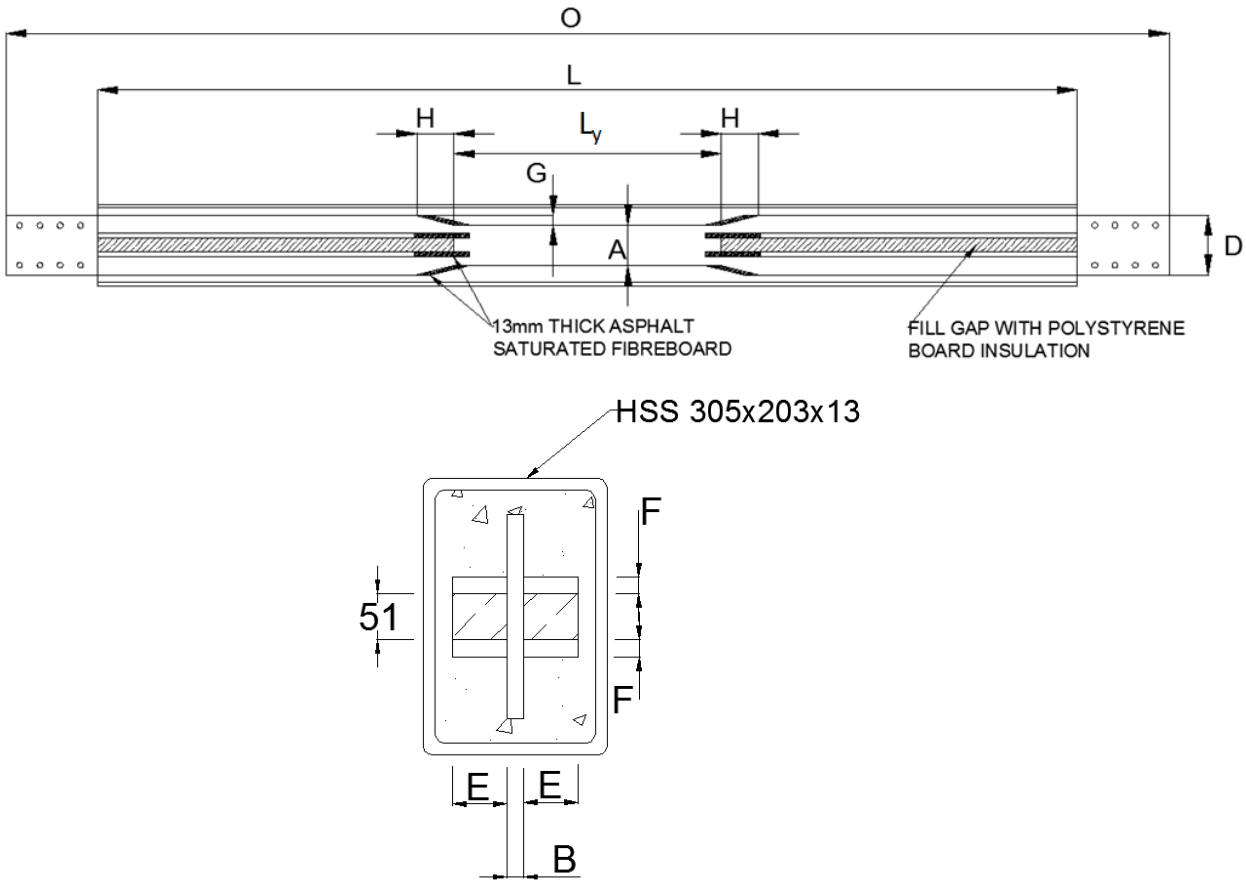

Figure 3.9 – BRB dimensions

Table 3.2 – BRB dimensions

BRB	A	B	D	E	F	G	H	O	L	L_y
	Mm	mm	mm	mm	mm	mm	mm	mm	mm	mm
BR4	127	19	225	60	19	49	196	8,482	7,948	1,000
BR6	178	22	225	60	22	24	92	8,388	7,728	1,000
BR6m	70	22	225	60	22	78	313	8,388	7,728	900
BR30	203	19	250	60	19	24	41	8,488	7,802	1,000
BR30m	80	19	250	60	19	85	290	8,488	7,802	900

3.6. Loading Protocol

The requirements for qualifying cyclic tests of buckling restrained braces are outlined by the AISC Seismic Provisions for Structural Steel Buildings [1]. This document defines the minimum design storey drift to be no less than 1% of the storey height. In the design of the RMCC Sawyer building, the storey height is 3,810mm and therefore $\Delta_{bm1\%st}$ is equal to 3.81mm. The second value to be calculated was the Δ_{by} or the displacement at first sign of yielding [2]. In order to determine Δ_{by} the strain at the point of yield was calculated using Equation 3.1 and the displacement of the inner yield section was calculated using Equation 3.2; where E refers to the modulus of elasticity, ε_y is the yield strain, Δ_y is the yield deformation and L_y is the length of the inner yield section.

$$\varepsilon_y = \frac{f_y}{E} \qquad \textbf{Equation 3.1}$$

$$\Delta_y = \varepsilon_y Ly \qquad \textbf{Equation 3.2}$$

Until the brace achieves inelastic deformations, the entire brace performs elastically; however, the relative stiffness will be used to account for the increase in cross sectional stiffness and reduced deformations of the outer cruciform. The effects due to the elastic deformations of the outer cruciform, Δ_{out}, are accounted for in total deformation at the point of yield. Since there were only subtle differences in the values of Δ_{by} of the modified braces, and it is intended to be a start state for the loading program, a rounded average of 4 mm for Δ_{by} was chosen as start state for the loading program as it captures the total inelastic deformations of the complete brace. The values for the three braces to be tested are presented in Table 3.3.

Table 3.3 – Values of Δ_{by}

BRB	E	f_y	ε_y	Δ_y	$Area_y$	$Area_{out}$	Δ_{out}	Δ_{by}
	MPa	MPa	μm/mm	mm	mm^2	mm^2	mm	mm
BR4	200000	275	1.37	1.38	2413	8835	2.61	3.98
BR6	200000	450	2.35	2.25	3916	10230	5.79	8.04
BR6m	200000	450	2.35	2.02	1540	10230	2.31	4.34
BR30	200000	350	1.85	1.75	3857	9310	4.93	6.68
BR30m	200000	350	1.85	1.58	1520	9310	1.97	3.55

According to the AISC guidelines, the BRB shall conduct 2 cycles of loading starting at the first sign of significant yield and continuing in increments of 0.5 $\Delta_{bm1\%st}$ until the brace has reached 2.0 Δ_{bm}. Following this linear progression of loading, the load program reduces to one complete cycle at an increased rate of 1.5 $\Delta_{bm1\%st}$ as required until the brace reaches a cumulative inelastic deformation of 200 times the yield deformation. The load program outlined in the AISC publication is intended to confirm the

design of seismic braces. This load program was used as a guideline in developing a load program for this experimental investigation. The load program developed for this series of tests included more gradual load steps and provided a greater opportunity for the brace to reach the cumulative inelastic deformation of 200 times the yield deformation. The reasoning for more load steps in this program was twofold. Firstly, the relatively short yield section required less aggressive loading progression because the 1,000 mm yield section would not be able to exhibit the required cumulative deformation. Secondly, a more iterative approach with increasing load steps produces more fidelity at the moment of failure and provides more data for analysis. In order to insert incremental load steps, the value Δ_{bm} was added as an intermediary step. Δ_{bm} represents the approximate midpoint between Δ_{by} and $\Delta_{bm1\%st}$. The modified load program can be seen in Table 3.4.

Table 3.4 – Load program

Δ_{by}	4	mm	
Δ_{bm}	13	mm	$\approx 3\ \Delta_{by}$
$\Delta_{bm1\%st}$	38.1	mm	$\approx 9\ \Delta_{by}$

Load Step	Cycles and Amplitudes			Deformations				
	Results			Elastic Def	Inelastic Def		Cumulative Inelastic Def	
	Tension	Compres-sion	Total Def					
	mm	mm	Mm	mm	mm	# of Δ_{by}	mm	# of Δ_{by}
Δ_{by}	4	-4	16	16	0	0	0	0
Δ_{by}	4	-4	16	16	0	0	0	0
$0.5\ \Delta_{bm}$	6.5	-6.5	26	16	10	2.5	10	2.5
$0.5\ \Delta_{bm}$	6.5	-6.5	26	16	10	2.5	20	5
$1.0\ \Delta_{bm}$	13	-13	52	16	36	9	56	14
$1.0\ \Delta_{bm}$	13	-13	52	16	36	9	92	23
$1.5\ \Delta_{bm}$	19.5	-20	78	16	62	15.5	154	38.5
$1.5\ \Delta_{bm}$	19.5	-20	78	16	62	15.5	216	54
$2.0\ \Delta_{bm}$	26	-26	104	16	88	22	304	76
$2.0\ \Delta_{bm}$	26	-26	104	16	88	22	392	98
$2.5\ \Delta_{bm}$	32.5	-33	130	16	114	28.5	506	126.5
$1.0\ \Delta_{bm1\%st}$	38.1	-38	152	16	136.4	34.1	642.4	160.6
$1.5\ \Delta_{bm1\%st}$	57.2	-57	229	0	228.8	57.2	871.2	217.8
$2.0\ \Delta_{bm1\%st}$	76.2	-76	305	0	304.8	76.2	1176	294

3.7. Material Testing, Instrumentation and Assembly

3.7.1. Material Testing

For a BRB, it is the dimension and material properties of the yield section which controls the performance of the overall brace. If proper un-bonding occurs, the cross-sectional area of the yield section multiplied by the ultimate strength of the material will give an accurate estimate of the brace's overall capacity. Because of the unconfirmed material properties, a tension test was conducted on representative coupons in accordance with ASTM 370-11a, Mechanical Testing of Steel Products [22] and CSA G40.21 [23].

3.7.1.1. Tension Test

In order to collect sufficient material from the yield section to machine coupons, while not removing too much so as to render the brace ineffective, a thickness of 25 mm was shaved off the brace. The results of two typical coupon tests are displayed in Figure 3.10. The results of the tension tests

clearly identify both braces are constructed out of two completely different grades of steel. The points of yield seen from the tension tests results indicates that grades of steel are 350 MPa and 450 MPa for braces BR30 and BR6 respectively. The ultimate capacity for both grades of steel was found to be constant between 515-525 MPa across all coupons.

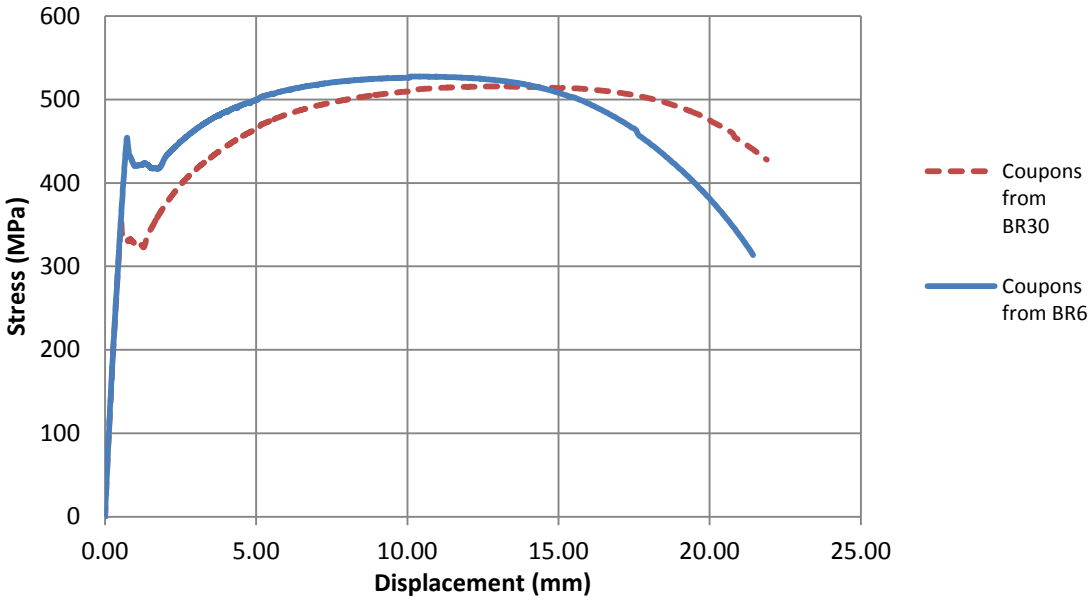

Figure 3.10 – Steel coupon tension test results

While the CSA S16 Clause 27.8.3.2 states that "splices shall not be used in the [BRB] steel core" [19], during the modification of the braces it was noticed that the BR6 was welded with a full penetration butt weld at mid-span of the inner yield section. Figure 3.11 shows the weld at mid-span as it was discovered during the assembly. Figure 3.12 is a profile shot of a BR6 coupon after it has been milled, showing the clear penetration of the weld.

Figure 3.11 – BR6 weld at mid-span

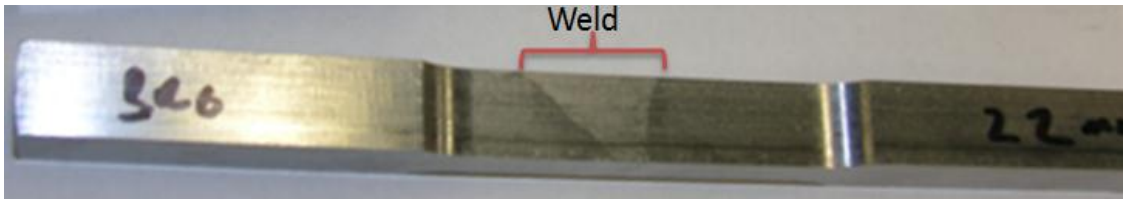

Figure 3.12 – BR6 full penetration view of coupon

It is difficult to provide a definitive assessment as to the effects of the full penetration weld on the overall performance of the BRB given that there is only one welded coupon tested in tension due to the limited material obtained from the shaving of the brace yield section. The comparison of the welded coupon with a typical un-welded coupon of the same material is presented in Figure 3.13. While there is early yielding of the coupon at 400 MPa followed by the gradual yielding into the plastic range, there is little deviation from the yield envelope of the non-welded coupons. Following yield of the steel, the welded coupon loses its residual strength more rapidly than the non-welded coupons.

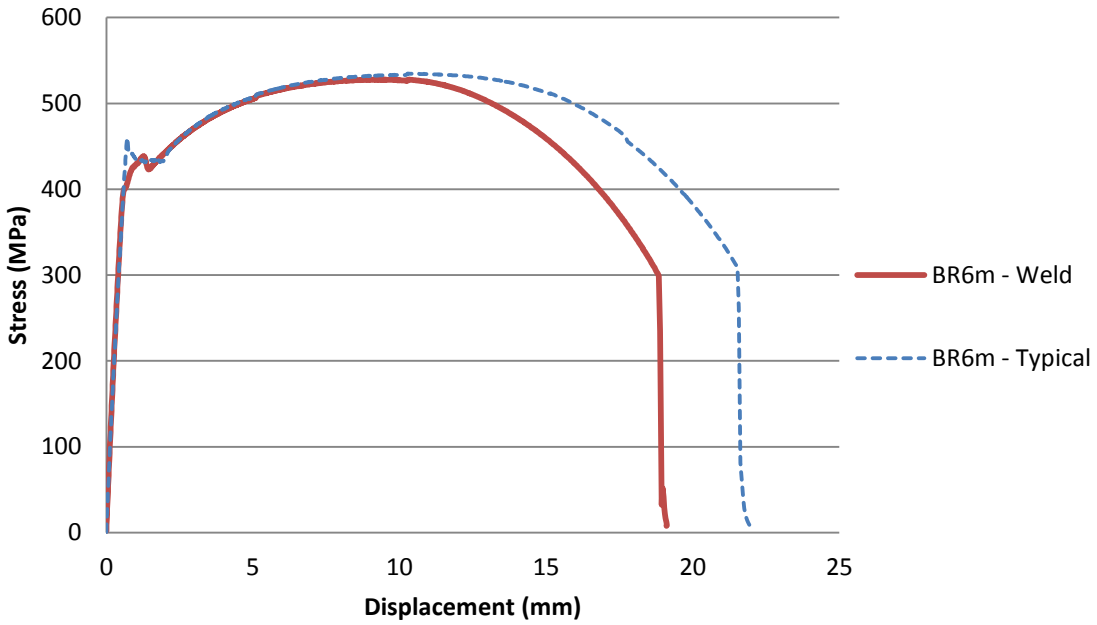

Figure 3.13 – Tension test result for welded coupon

3.7.1.2. Cyclic loading test

To understand the hardening response of the inner yield section material unaffected by the grout or outer core of the full-scale BRBs, steel coupons were subjected to high rate cyclic loading in order to produce hysteresis curves of each brace material. The results of the cyclic coupon test were used in the generation of tangent lines in order to represent the transition zones of the hysteresis loop and were used in the shaping of hysteresis backbone curves in the dynamic modelling as outlined in Section 4.3. The cyclic loading program is a scaled down version of the load program used in the qualification testing of the full-scale braces, in order to visualise the anticipated kinematic hardening shape of the brace. The rate of loading was set at 1 Hz, to match the approximate fundamental building frequency. The hysteretic response of each brace material is presented in Figure 3.14.

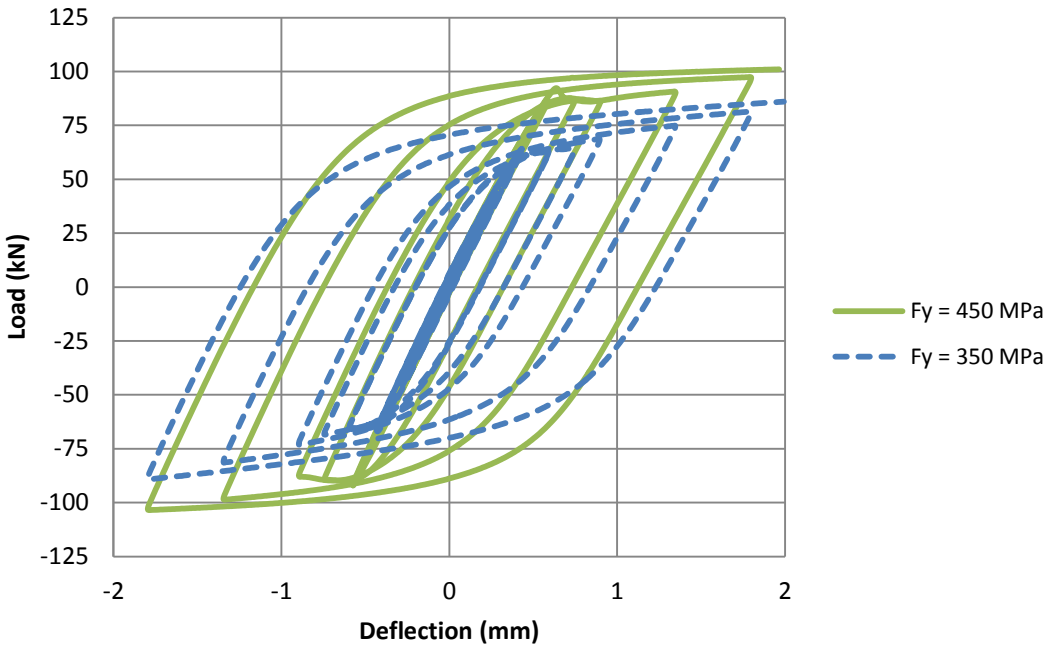

Figure 3.14 – Cyclic loading coupon hysteresis

3.7.2. Brace Modification

With the grade of steel quantified using the coupon tension test, the capacity and performance of the brace were confirmed. From these calculations; modifications could be made to the yield section of the inner steel core so as to achieve yield and failure within the constraints of the subassemblage. The yield sections for both braces were trimmed by hand using a plasma torch. A photo of the plasma cutting process is presented in Figure 3.15. The rough edge seen at the bottom of the brace was the area where the material was removed in order mill the coupons. The top edge of the of the brace shows the finished trimmed edge which was cut to the dimensions outlined in Figure 3.16 and Figure 3.17.

Figure 3.15 – Plasma cutting detail

Given that the grades of steel for BR6 and BR30 are 450 MPa and 350 MPa respectively and the thickness of the inner brace were 22 and 19 mm respectively, the overall depth of each braces yield

section was trimmed to 70 mm and 80 mm respectively. The modified dimensions, presented in Figure 3.16 and Figure 3.17, were derived based on the linear relationship between yield stress and cross-sectional area in order to determine the depth of each yield section, with considerations for ultimate strength and the possible effects of load sharing. Ultimate strength was considered to ensure the brace would fail within the 1,000 kN +/- 10% load limit. Tabulated calculations are presented in Table 3.5 and Table 3.6.

Table 3.5 – BR6m brace modification calculations

BR6	Load Sharing (%)	Inner Yield Section			Steel Capacity		
		Depth (mm)	Width (mm)	Area (mm^2)	Design Yield 248 MPa (kN)	Actual Yield 450 MPa (kN)	Ultimate 515 MPa (kN)
Design Brace	0%	178	22	3,916	971	1,762	2,017
Trimmed Brace	0%	70	22	1,540	382	693	793
Trimmed Brace + Load Sharing	30%	70	22	1,540	496	901	1,031

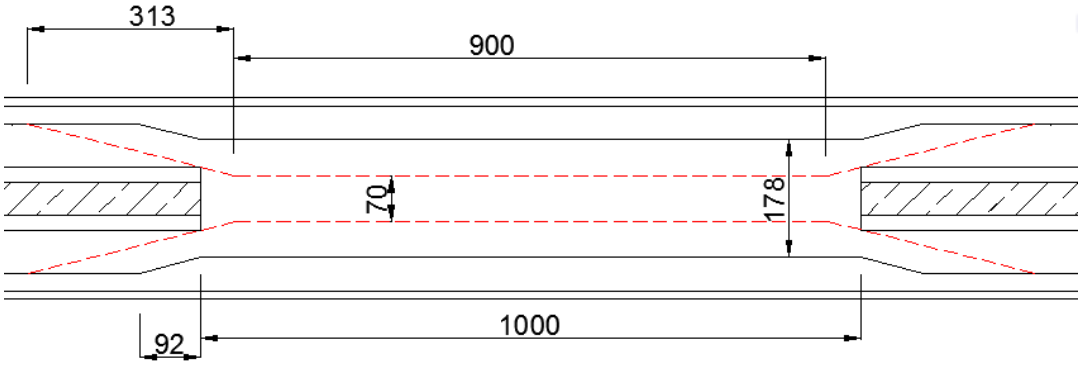

Figure 3.16 –Trimming detail for BR6m

Table 3.6 – BR30m brace modification calculations

BR 30	Load Sharing (%)	Inner Yield Section			Steel Capacity		
		Depth (mm)	Width (mm)	Area (mm^2)	Design Yield 248 MPa (kN)	Actual Yield 450 MPa (kN)	Ultimate 515 MPa (kN)
Design Brace	0%	203	19	3,857	957	1,350	1,986
Trimmed Brace	0%	80	19	1,520	377	532	783
Trimmed Brace + Load Sharing	30%	80	19	1,520	490	692	1,018

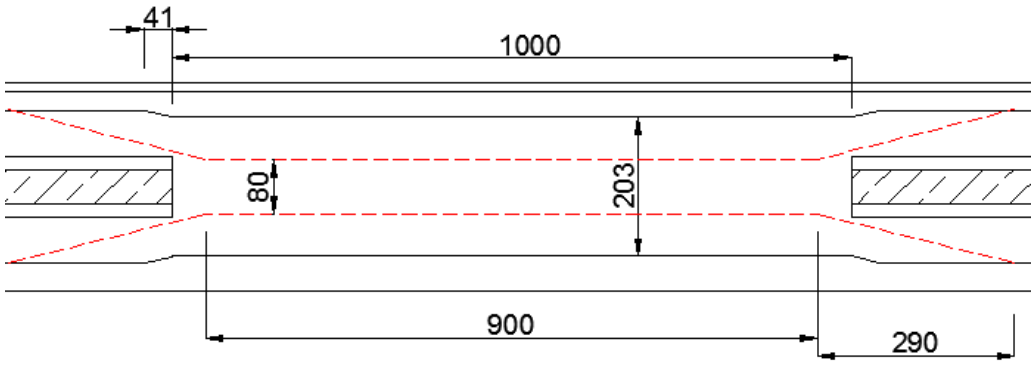

Figure 3.17 – Trimming detail for BR30m

In addition to the depth modification of the yield section, the length was reduced from 1,000 mm to 900 mm in both yield sections. This reduction in length was essential in order to allow the similar 1:4 tapering transition slope between the inner yield section and outer non-yielding sections. This reduction of yield length slightly limits the amount of allowable strain hardening and reduces the overall allowable displacement. With these modifications to each brace, the naming conventions are reflected as BR6m and BR30m to denote the modifications made to each brace's dimensions.

3.7.3. Instrumentation

In order to monitor and record the behaviour of the braces, the entire system was instrumented using sixteen 10 mm, 120Ω foil strain gauges and four 150 mm stroke Linear Variable Differential Transformers (LVDTs). Two LVDTs were placed on the subassemblage so as to measure the true deflection of the inner steel core, relative to the outer casing. The final two LVDTs were positioned to measure deflection of the entire system relative to the test frame. The LVDT placement was intended to isolate the relative displacement of the inner steel core, in the event that the internal strain gauge data was unusable. LVDT placement is presented in Figure 3.18. Each brace was fitted with 16 strain gauges with four of the strain gauges placed directly on the yield section of the internal brace while the remaining 12 strain gauges were placed on the outer steel casing Figure 3.19 and Table 3.7 outline the locations of strain gauges.

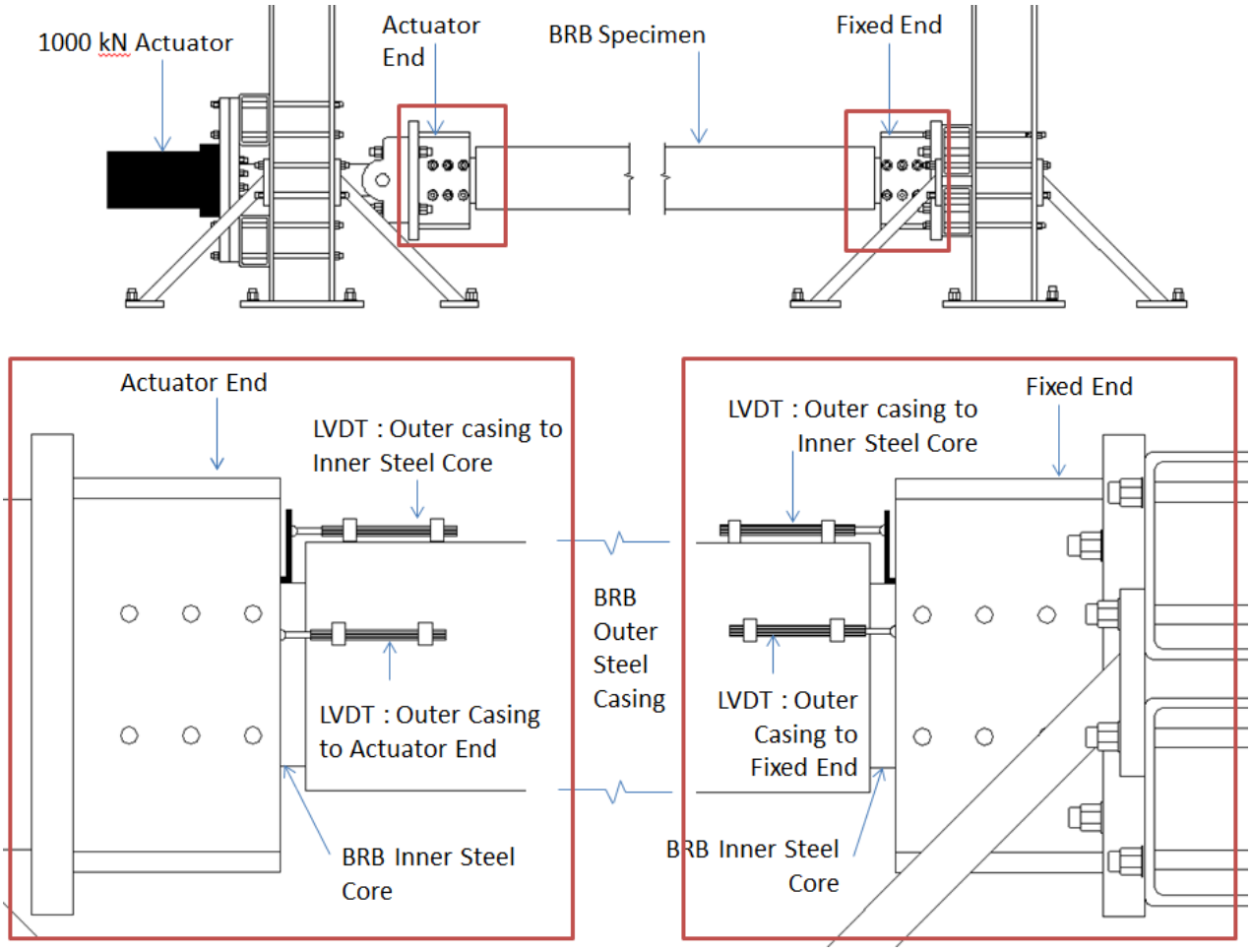

Figure 3.18 – LVDT Placement

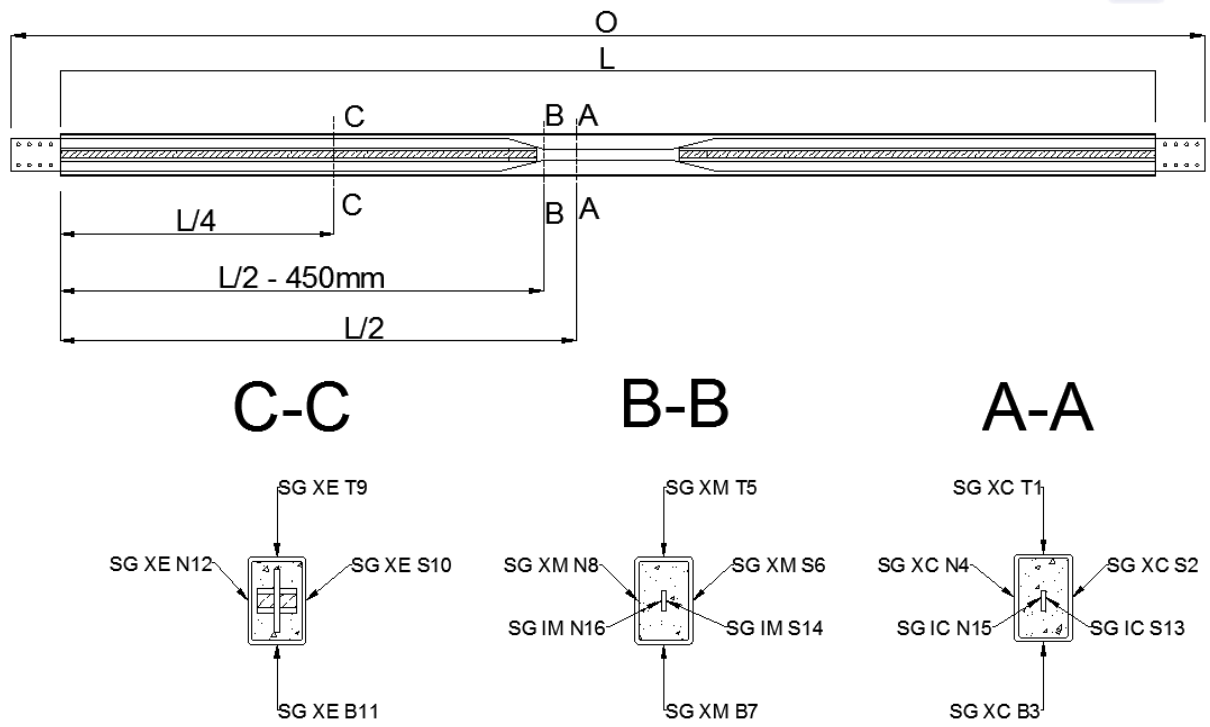

Figure 3.19 – Instrumentation location

Table 3.7 – Instrumentation dimensions

Brace	Dimensions (mm)				
	O	L	A-A (L/4)	B-B (L/2-450)	C-C (L/4)
BR 6m	8,412	7,726	3,638	3,413	1,932
BR 30m	8,488	7,802	3,676	3,451	1,949

3.7.4. Assembly

With the yield section of the inner core trimmed to the prescribed dimension, the brace was reassembled. First, the strain gages on the yield section were covered with a 5 mm thick layer of modelling clay to provide additional standoff and protection from the grout. The compression edges of the inner brace were padded with 13 mm asphalt saturated fibre board. This fibre board is designed to enable the brace to cycle through the early stages of the load protocol with little interaction between the grout and steel. This detail can be seen in Figure 3.20, along with the addition of polystyrene foam that was inserted between the supporting wings of the outer non yield cruciform section. The filling of this void reduced the overall contact surface area of the inner steel brace inside the grout, while providing a void to run the internal strain gauge cabling to the data acquisition module.

Figure 3.20 – Internal stain gauge and fibre board detail

Following the padding and protection of the instrumentation, the brace was completely wrapped in a 1.5 mm un-bonding membrane to separate the grout and inner core during loading. A photo of this can be seen at Figure 3.21. Once the wrapping of the inner core was complete, the brace was reassembled and the inner core was winched into the outer casing using the same assembly techniques used on the construction site. While every effort was made to cover the steel with the un-bonding membrane, Figure 3.22 shows considerable tearing to the membrane at the edges of the inner yield section during assembly. The potential consequences of this tearing due to this assembly technique will be referenced later in the discussion of load sharing.

Figure 3.21 – BRB wrapped in un-bonding membrane

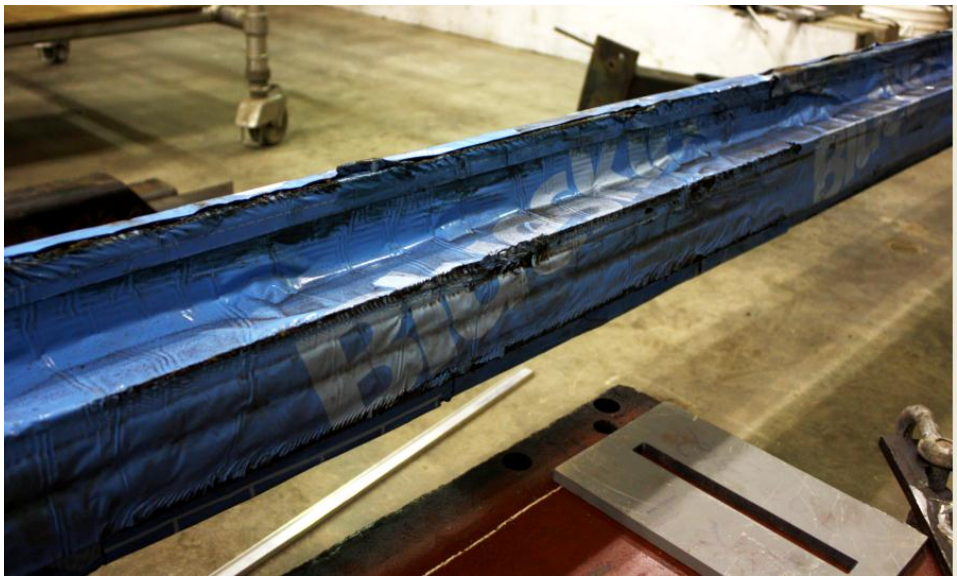

Figure 3.22 – Damage to the un-bonding membrane during the assembly

With the brace completely assembled, the entire system was elevated, shimmed and prepped for grouting. The braces were elevated to mirror the in-situ grouting technique used in the project. Once the braces were filled with grout they were allowed to cure for 48 hours before being lowered and the outer casing instrumentation mounted. Figure 3.23 shows the scaffolding and pillars used to elevate the BRBs for grouting.

Figure 3.23 – Brace elevation for grouting

Following complete assembly of the BRB and verification of the instrumentation, the braces were installed into the subassemblage as described in Section 3.3. With the installation complete, the braces were ready for testing under the prescribed load program.

3.7.5. Preloading

In preparation for the testing of both braces, the instrumentation was connected, zeroed and the frame was preloaded up to 100kN. This preload confirmed the bolt tolerance, slack in the system and allowed for a complete verification of bolt engagement throughout the subassemblage. This preloading also verified that the brace remained elastic at 100kN, with no indication of yielding. Once the preload was complete, the brace was returned to equilibrium to verify a net zero displacement, confirming the instrumentation was calibrated and that no yielding occurred.

3.8. Test Results

3.8.1. Test objectives

The immediate quantifiable result for this experiment was the analysis of the cumulative inelastic deformations. The actual results of the load program produced a load vs. displacement hysteresis curve allowing for the ω and β values to be extrapolated. This cumulative inelastic deformation count is the

major acceptance criteria outlined in the Annex T of the 2005 AISC Seismic Provisions for Structural Steel Buildings [2]. Upon further analysis of the data and test results, there were a number of observations and deductions made that are presented in Section 3.9.

3.8.2. BR30m Results

BR30m was subjected to a continuous cyclic loading test in accordance with the loading program outlined in Section 3.6. The maximum elongation of the brace was 37 mm with the total cumulative inelastic deformations of the brace being 635 mm or 159 times Δb_y. The results of the loading protocol are displayed in Table 3.8. The brace began to experience yield at between 500 kN and 525 kN in tension and compression. The maximum applied load to the brace was 895 kN in tension and 957 kN in compression with ultimate failure achieved at 725 kN in tension. The load vs. displacement hysteresis loop is presented in Figure 3.24. For analysis of these results, forces in compression are negative.

Given that the maximum force applied to the BRB did not develop displacements which were greater than or equal to 2.0 times the design storey drift, the maximum applied tension load of 895 kN was used to calculate ω. Rearranging Equation 2.2, the strain hardening adjustment factor, ω for BR30m was calculated to be 1.68. With ω now determined, Equation 2.3 was rearranged to solve for β, using the maximum applied load in compression of 957 kN, and a ω of 1.68. The compression adjustment factor for BR30m was calculated to be 1.07. These adjustment factors are summarized in Table 3.9.

Table 3.8 – BR30m cyclic loading results

Δ_{by}	4	mm	
Δ_{bm}	13	mm	$\approx 3\,\Delta_{by}$
$\Delta_{bm1\%st}$	38.1	mm	$\approx 9\,\Delta_{by}$

Load Step	Cycles and Amplitudes					Deformations			
	Testing Protocol		Results			Elastic Def	Inelastic Def	Cumulative Inelastic Def	
	Tension	Compression	Tension	Compression	Total Def				
	mm	mm	mm	mm	mm	mm	# of Δ_{by}	mm	# of Δ_{by}
Δ_{by}	**4**	**4**	4.3	-3.8	16.2	16	0.05	0.2	0
Δ_{by}	**4**	**4**	4.3	-4	16.6	16	0.15	0.8	0.15
$0.5\,\Delta_{bm}$	**6.5**	**6.5**	6.8	-6.1	25.8	16	2.45	10.6	2.6
$0.5\,\Delta_{bm}$	**6.5**	**6.5**	6.5	-6.5	26	16	2.5	20.6	5.1
$1.0\,\Delta_{bm}$	**13**	**13**	12.1	-8.6	41.4	16	6.35	46	11.45
$1.0\,\Delta_{bm}$	**13**	**13**	12.2	-10	44.4	16	7.1	74.4	18.55
$1.5\,\Delta_{bm}$	**19.5**	**19.5**	20	-18.3	76.6	16	15.15	135	33.7
$1.5\,\Delta_{bm}$	**19.5**	**19.5**	20.6	-20.1	81.4	16	16.35	200.4	50.05
$2.0\,\Delta_{bm}$	**26**	**26**	26	-24	100	16	21	284.4	71.05
$2.0\,\Delta_{bm}$	**26**	**26**	27.1	-26.1	106.4	16	22.6	374.8	93.65
$2.5\,\Delta_{bm}$	**32.5**	**32.5**	38.7	-33.6	144.6	16	32.15	503.4	125.8
$1.0\,\Delta_{bm1\%st}$	**38.1**	**38.1**	37	-36.8	147.6	16	32.9	635	158.7
$1.5\,\Delta_{bm1\%st}$	**57.2**	**57.2**	0	0	0	0	0	0	0
$2.0\,\Delta_{bm1\%st}$	**76.2**	**76.2**	0	0	0	0	0	0	0

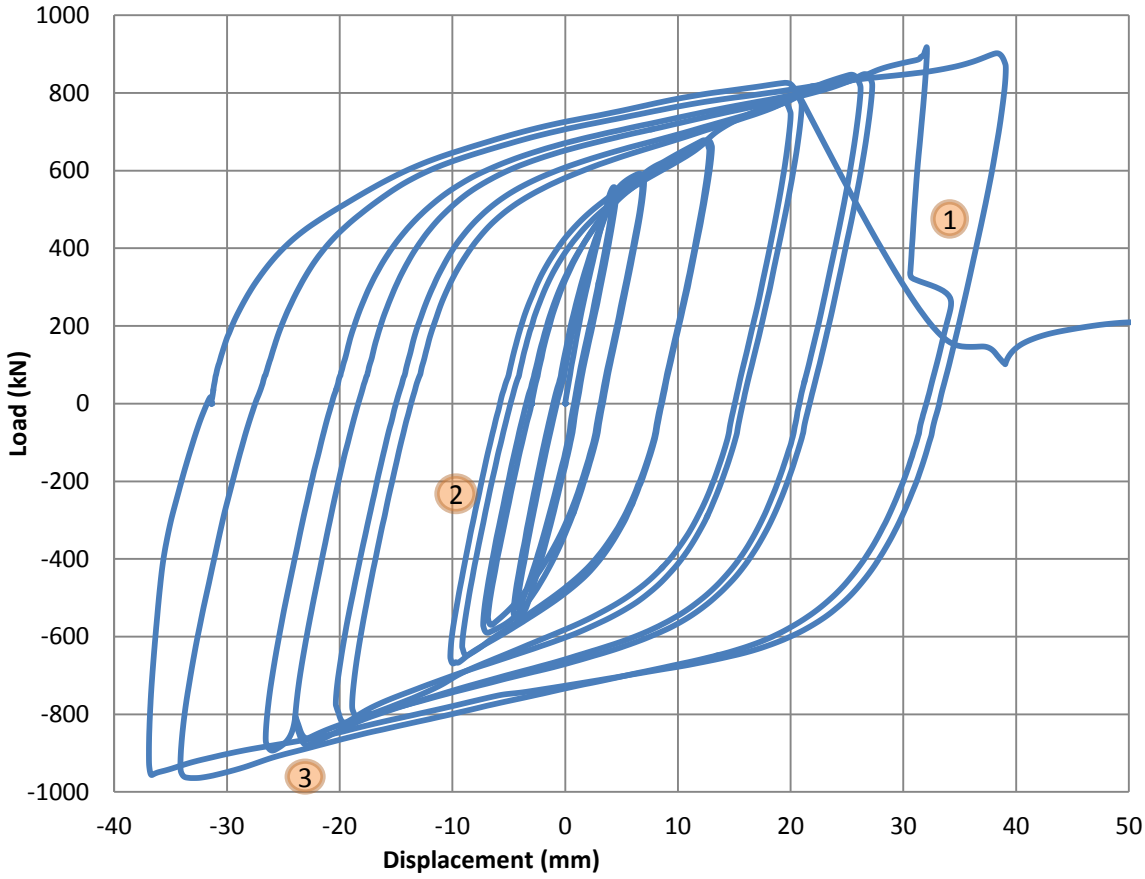

Figure 3.24 – BR30m load Vs. displacement hysteresis curve

- Note 1: Maximum range of LVDT in mid cycle stroke.
- Note 2: Cautious run up to the first round of testing
- Note 3: Pressure safety lock on hydraulic pumps

3.8.3. BR6m Results

The maximum elongation of BR6m brace was 37 mm with the total cumulative inelastic deformations of the brace were 551 mm or 138 times Δb_y. The results of the loading protocol are displayed in Table 3.10. The brace began to experience yield between approximately 600 kN and 625 kN in both tension and compression. The maximum applied load to the brace was 875 kN in tension and 970 kN in compression with the ultimate failure achieved at 864 kN in tension. The load vs. displacement hysteresis loop is presented in Figure 3.25. Notes depicted in the hysteresis loop graph are discussed in Section 3.9.

BR6m also did not achieve the recommended deformation of 2.0 times the design storey drift; therefore, the maximum applied tension load of 875 kN was used to calculate ω. Using the same procedure as with BR30m, the maximum applied load in compression of 970 kN and a ω of 1.26 was determined. The factor, β for BR6m was calculated to be 1.11. These adjustment factors are tabulated in Table 3.9.

Table 3.9 – Tabulated strain hardening and friction adjustment factors

Brace	Fy	A	Maximum Tension Force	Maximum Compressive Force	ω	β
	MPa	mm^2	kN	kN		
BR30m	350	1,520	895	957	1.68	1.07
BR6m	450	1,540	875	970	1.26	1.11

Table 3.10 – BR6m cyclic loading results

Δ_{by}	4	mm
Δ_{bm}	13	mm
$\Delta_{bm1\%st}$	38	mm

Load Step	Cycles and Amplitudes					Deformations			
	Testing Protocol		Results			Elastic Def	Inelastic Def	Cumulative Inelastic Def	
	Tension	Compres-sion	Tension	Compres-sion	Total Def				
	mm	mm	mm	mm	mm	mm	# of Δ_{by}	mm	# of Δ_{by}
Δ_{by}	**4**	**4**	4.1	-3.9	16	16	0	0	0
Δ_{by}	**4**	**4**	4	-3.9	15.8	16	-0.05	-0.2	-0.05
0.5 Δ_{bm}	**6.5**	**6.5**	9.3	-7.3	33.2	16	4.3	17	4.25
0.5 Δ_{bm}	**6.5**	**6.5**	7.6	-7.3	29.8	16	3.45	30.8	7.7
1.0 Δ_{bm}	**13**	**13**	14.4	-13.9	56.6	16	10.15	71.4	17.85
1.0 Δ_{bm}	**13**	**13**	13.6	-13.5	54.2	16	9.55	109.6	27.4
1.5 Δ_{bm}	**19.5**	**19.5**	19.9	-19.6	79	16	15.75	172.6	43.15
1.5 Δ_{bm}	**19.5**	**19.5**	19.4	-20.2	79.2	16	15.8	235.8	58.95
2.0 Δ_{bm}	**26**	**26**	26.3	-26.2	105	16	22.25	324.8	81.2
2.0 Δ_{bm}	**26**	**26**	26.3	-29.3	111.2	16	23.8	420	105
2.5 Δ_{bm}	**32.5**	**32.5**	32	32.5	129	16	28.25	533	133.25
1.0 $\Delta_{bm1\%st}$	**38.1**	**38.1**	20	0	40	16	6	557	139.25
1.5 $\Delta_{bm1\%st}$	**57.2**	**57.2**	0	0	0	0	0	0	0
2.0 $\Delta_{bm1\%st}$	**76.2**	**76.2**	0	0	0	0	0	0	0

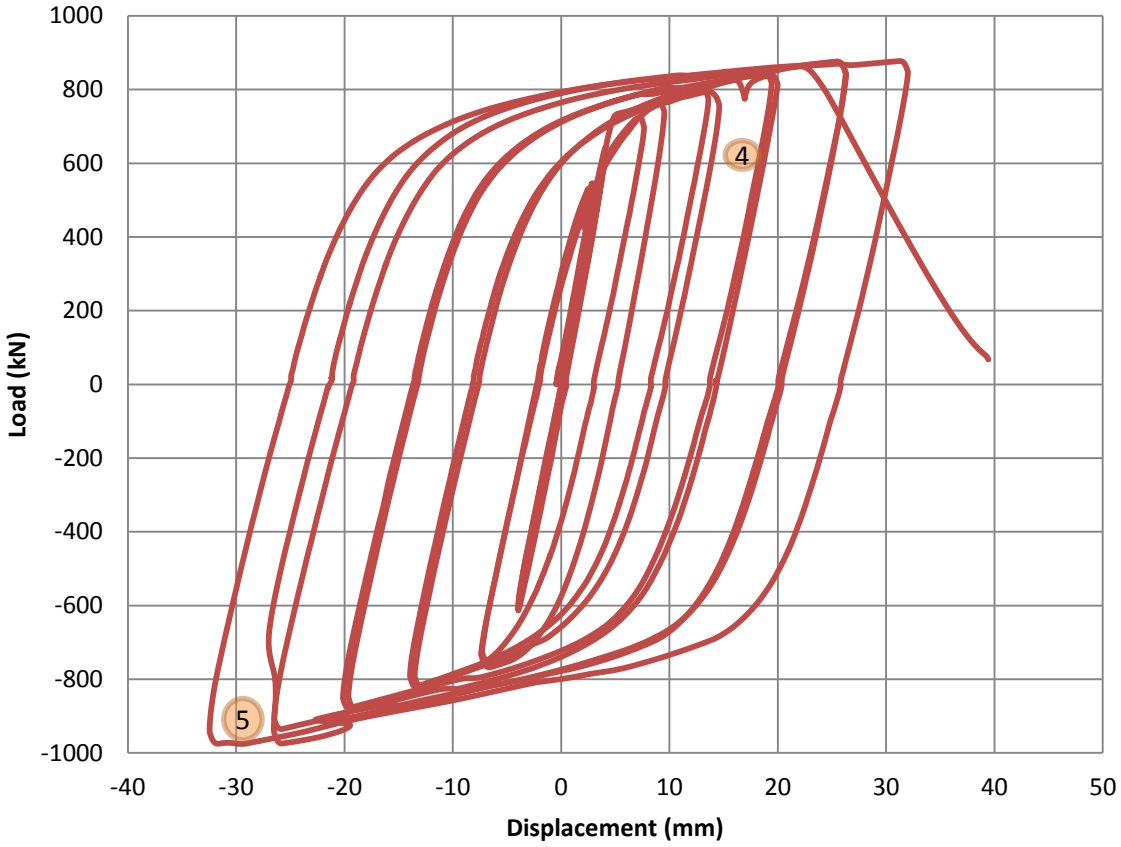

Figure 3.25 – BR6m load Vs. displacement hysteresis loop

- Note 4: Maximum range of LVDT in mid cycle stroke.
- Note 5: Pressure safety lock on hydraulic pumps

3.9. Discussion

3.9.1. Hysteresis Loop Error

From the hysteresis curves presented in Figure 3.24 and Figure 3.25, there are some inconsistencies when compared to a pure stress-strain curve. Since the internal strain gauges did not survive the cyclic loading, the actuator load was plotted against internal yield section displacement. The overall stroke of the actuator could not be used due to the amount of overall displacement in the entire subassemblage, hence the specific placement of the LVDTs to isolate the relative displacement of the inner yield section. Relying on the LVDTs for displacement measurements were the source of minor errors in the data collection. Looking back at Figure 3.24 and Figure 3.25, notes 1and 4 denotes the flattening of the curve when the LVDT maxed out in stroke during mid-cycle. The test was paused, and the LVDTs were reset prior to continuing with the tests.

In addition to the LVDT error there are both human and mechanical errors present in data collection. Note 2 in Figure 3.24 represents a cautious run up to the first round of testing. This error was eliminated in further testing, once the full capacity of the brace and subassemblage was determined. Note 3 and note 5 attempts to highlight a small dip in capacity as a result of a manual override to a pressure safety lock on the hydraulic pumps. This pressure safety element was inherent to the setup of the actuator and did not adversely affect the overall performance of the test.

3.9.2. Overall Brace Performance

Even with the addition of intermediate load steps to the AISC guidelines, both BRBs were unable to achieve 200 Δ_{by} of cumulative inelastic deformations. While factors such as the BRB yield section dimensions are directly linked to the brace's capacity, the performance of the brace in cyclical loading is governed by the material properties. Table 3.5 and Table 3.6 present the variations between design yield strength, actual yield strength and ultimate strength. While the Ultimate strength for both BR6m and BR30m are similar, the points of yield are 450 MPa and 350 MPa respectively. This difference in yield strengths allows for a larger strain hardening envelope between the point of first yield and ultimate strength. This increased envelope will enable the BRB to cycle and accumulate more inelastic deformations prior to ultimate failure. Figure 3.26 highlights the differences in the yield envelopes between the three materials.

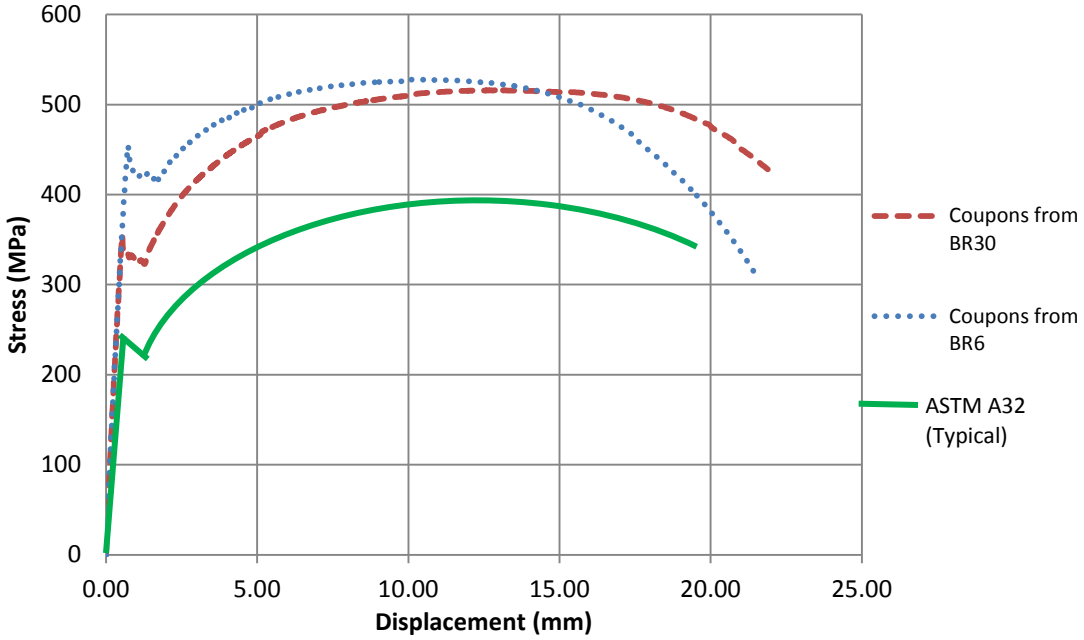

Figure 3.26 – Coupon test steel yield envelopes

With the existence of two distinct materials for each brace, the adjustment factors cannot be combined or averaged as each brace's behaviour is unique based on material properties. Given the simplification of the approximation used in determining the adjustment factors, the magnitude of the strain hardening factor, ω, is inversely proportional to the yield strength of the material and the size of the of the yield envelope. The friction adjustment factor, β, is less dependent on the material properties of the inner yield section as it is on the contact regions between the steel and grout, hence the minor difference in β between the two braces (Table 3.11).

Table 3.11 – Adjustment factor relationships

Brace	Fy (MPa)	difference	ω	difference	β	difference
BR30m	350	22%	1.68	25%	1.07	4%
BR6m	450		1.26		1.11	

3.9.3. Load Sharing

An effect that was identified early on during the BR4 testing was the progressive load sharing between the inner yield section and the outer steel casing. This effect was due to the incomplete un-bonding of the grout from the un-bonding membrane on the inner steel core. The presence of this load sharing was discovered when the BR4 brace, despite its design specifications, was not able to achieve yield within the 1,000 kN loading limit. Prior to the discovery of inconsistency in steel grades during the coupon tests, the data was analysed to identify possible sources of strength inflation. The values of the internal and external strain gauges were reviewed and it was discovered that the force in the outer steel casing was exhibiting substantial strains. For illustration purposes, Figure 3.27 and Figure 3.28 present

the final eight cycles of the load program. The force in the outer steel was calculated by averaging the strain values of the outer core and multiplying the mean by the cross sectional area of the HSS. The values of the force in the steel core was plotted versus time and overlaid atop the applied load versus time. This comparative analysis relates the effects of load sharing to each step of the load program.

Although every effort was made to protect the strain gauges located on the inner yield section, none of the gauges survived the cyclic loading to provide any usable data. For this reason, the plot of force in the yield section versus time was the product of an algebraic formula, simply the difference between the applied load and force in outer steel casing. The resultant curves are is plotted in Figure 3.27 and Figure 3.28.

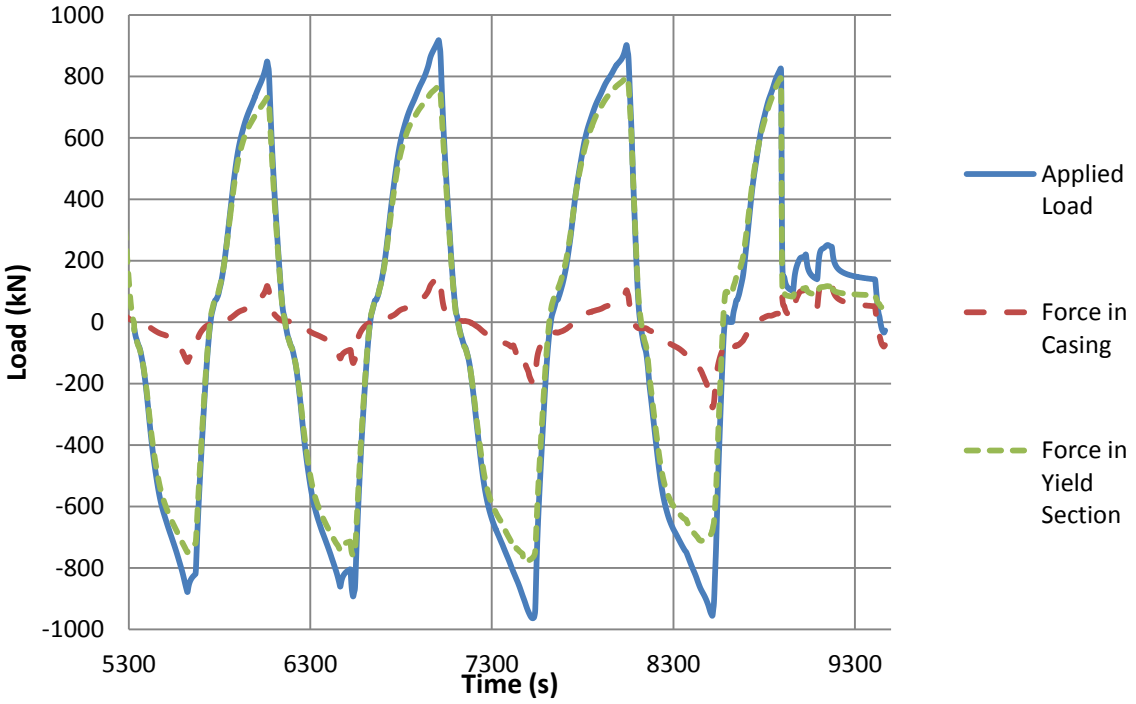

Figure 3.27 – BR30m applied load vs. time

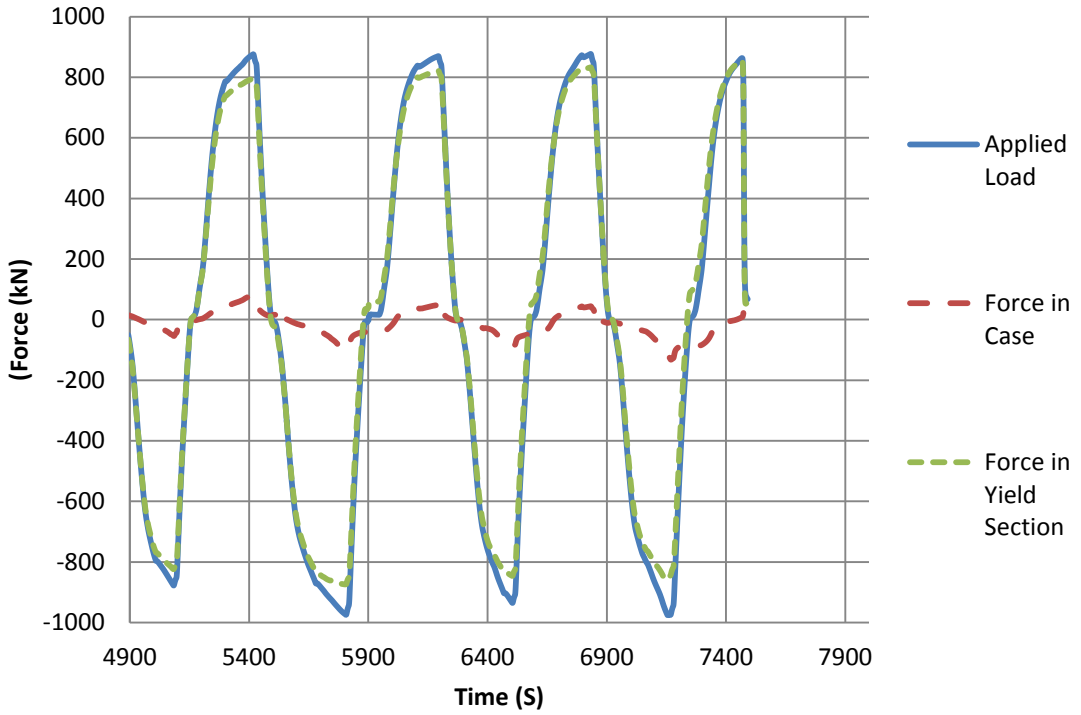

Figure 3.28 – BR6m applied load vs. time

While both braces exhibited similar load sharing curves, BR30m shows more significant signs of load sharing with the larger magnitudes typically occurring on the compression strokes. Increased load sharing during the compression stroke of the load program is likely due to the contact between the tapered edges of the yield section contacting the grout, whereas the load sharing in tension stroke would only be due to transfer of load between the un-bonding membrane and grout. Maximum load sharing values are tabulated in Table 3.12 for the final eight cycles of the load program for both BR6m and BR30m.

Table 3.12 – Percent load sharing per cycle

Brace	Percent Load Sharing per Cycle								
	C	T	C	T	C	T	C	Average	T
BR6m	8%	8%	9%	5%	12%	5%	14%	9%	0% -Fail
BR30m	18%	18%	18%	21%	25%	15%	30%	21%	0% -Fail

C= Compression
T= Tension

It is difficult to definitively identify the sources of the load sharing between the two braces; however, it is certain the grout brace interface is the only medium of transferring load between the inner steel brace and outer steel casing. With this in mind, the assembly of the brace is likely to have significant impact on the bond between the un-bonding membrane and grout. It is also important to note that these results were obtained at a slow rate of loading. A dynamic loading protocol would affect the overall brace performance. In Tremblay, 2006, a slow rate loading was compared with a dynamic load program. It was found that the dynamic loading resulted in a 5% increase in brace yield resistance [12].

3.9.4. Un-Bonding and the Effects of Grout

The effects of load sharing are directly correlated to the increase in overall brace capacity. Similar effects of load sharing have been noted in research using grout filled BRBs. Chen et al. demonstrated significant Poisson's effects on frictional behaviours between the inner steel plate and mortar [24], while Tremblay et al. noticed that axial loads and bending moments could be developed in the outer steel tube of braces that used a polyurethane un-bonding agent between the steel core and mortar [25]. Since the effects of load sharing are not a desirable product of BRB performance and CSA S16 allows for these effects to be captured with qualification testing and factors ω and β, there is limited research in to the specific mechanisms of load sharing.

The mechanisms of load sharing for both BR6m and BR30m can be narrowed to the bond between the un-bonding membrane and the grout. In order to examine the deformations and failure modes, the outer steel casing was opened up to expose the inner yield section. The grout was chipped away and the inner yield section was removed. Figure 3.29 shows the hollowed BRB with the yield section removed.

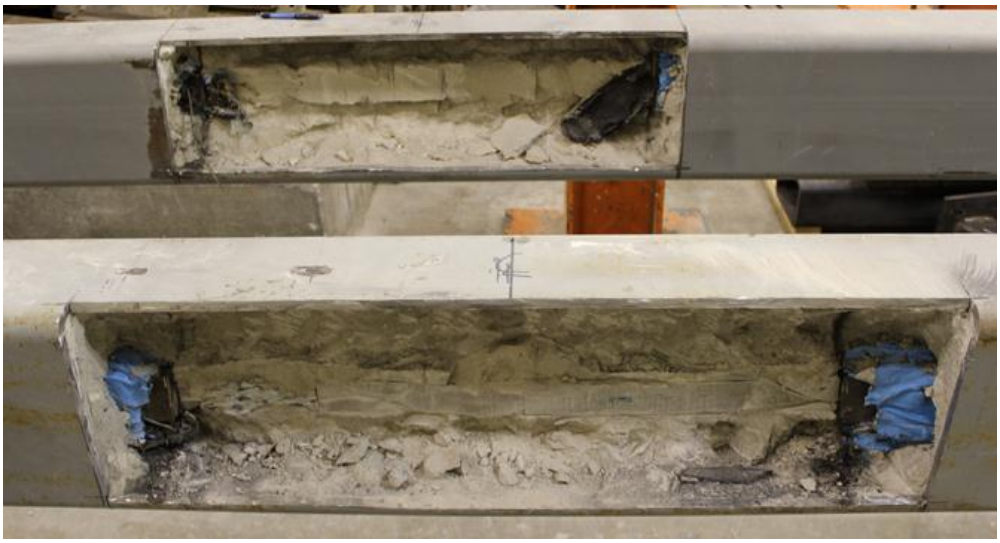

Figure 3.29 – BR6m and BR30m cut away

During the removal of the grout, it became evident that there was only partial un-boning between the un-bonding membrane and grout. The steel is intended to move freely within the un-bonding membrane wrap; however, energy is being absorbed in the grout. When the grout was removed, large pieces of grout were still firmly fastened to the un-bonding membrane. The discovery of extensive shearing of the grout supports the conclusion that the un-bonding membrane transferred loads to the outer steel casing. Figure 3.30 shows the grout failure plane.

Figure 3.30 – Un-bonding membrane grout interface

Further evidence suggests that the bond between the adhesive layer and un-bonding membrane may in fact be weaker than the membrane grout interface. The detail of the brace at the actuator end following the failure of BR30m is shown in Figure 3.31. It depicts the outer cruciform of the inner brace sliding out of the un-bonding membrane wrapping along the adhesive interface. Once BR30m had achieved ultimate capacity, the inner steel core was pulled out of the un-bonding membrane with an applied tension load of 200kN. This residual strength can be seen in the failure leg of the BR30m hysteresis loop in Figure 3.24.

Figure 3.31 – Un-bonding membrane adhesive failure

The load sharing during the compression stroke may share some of the same issues of improper un-bonding as during the tension stroke, with the addition of the bearing force of the tapered face of the yield section making contact with the grout. While the asphalt saturated fibre board is only 13 mm thick, it provides 53 mm of standoff in the horizontal plane, Figure 3.32. Even though the fibre board creates adequate standoff, it requires an application of load in order to compress the material and will still inhibit the full range of motion. During the disassembly of BRB and removal of grout, it was noticed that grout surrounding the compression zone of the tapered yield section bearing face had completely failed and crumbled away easily, as seen in Figure 3.33. This observation supports the conclusion that the load

sharing in the compression stroke is due, in part, to the contact with the grout and bearing face of the tapered yield section.

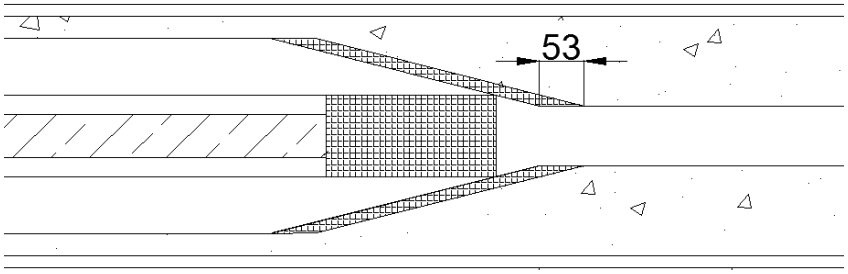

Figure 3.32 –Yield section taper detail

Figure 3.33 –Yield section taper bearing face grout failure

3.10 Summary of Qualification Testing

From the three BRBs subjected to the AISC qualification testing along with the related inspections, testing and subordinate research, the over-arching finding is centred on the specification and fabrication of the inner yield section material. The friction factors for both braces were found to be similar with slight differences largely due to variations in assembly, where as the strain hardening factors correlated directly to the range between yield and ultimate strength of the two materials.

While the specification of the inner yield section material is critical to overall brace performance, the fabrication and assembly techniques can have a marked effect on BRB mechanics. A full penetration weld at the mid span of BR6 was an unexpected discovery given that CSA S16 prohibits any splicing of the inner steel core. While a weld at mid span will likely affect a BRB's performance under a seismic event, this was not further studied as a part of this research. Another, more quantifiable area of brace performance modification due to assembly was the area of the grout at the inner yield section interface. Proportionally large strains (up to 30% of the applied load) were recorded in the BRBs outer steel casing during cyclic testing. These loads could only have been transferred through the grout and un-bonding membrane interface. The standardisation and quality control of BRB assembly would help ensure similar

brace performance across the full series of BRBs, giving more relevance to the ω and β which account for these effects and are applied to all BRBs of similar construction. While these large load sharing values were noticed in slow speed qualification testing, these effects may be reduced under real-time seismic loading.

Chapter 4: Modelling

4.1. Modelling Overview

With the BRB material properties validated and the qualification testing of the BRBs completed, the focus of this research shifted to the modelling of the BRB system for strengthening a five-storey reinforced concrete frame representing the Sawyer Building at RMCC. The mechanics of a BRB system were analysed using the two methods of seismic analysis prescribed by clause 4.1.8.7 of the 2010 NBCC, which are the Equivalent Static Force Procedure (ESFP) and dynamic analysis. The code dictates that all analysis for design earthquake actions shall be carried out by the dynamic analysis procedure except that the ESFP may be used for structures that meet any of the following criteria: [20]

1. In cases where: $I_eF_aS_a(0.2)$ is less than 0.34, where:
    a) F_a = Acceleration based site coefficient
    b) I_e = Importance Factor, 1.0 for regular importance structures.
    c) $S_a(0.2)$ = Spectral acceleration at a natural period of 0.2 s
2. Regular structures that are less than 60m in height and have a fundamental building period, Ta less than 2 s,
3. If there exists a structural irregularity but the structure is not torsionally sensitive, is less than 20m in height and has a Ta less than 0.5 s in each of the two orthogonal directions.

All Finite Element (FE) modelling was carried out using the commercial Finite Element Analysis (FEA) program ETABS. A three dimensional (3D) model was assembled using frame and shell elements. The square shell elements were four-node area objects, used to model membrane and plate-bending behavior. The shell elements represent the waffle slabs and drop panels. The frame objects were used to model beams, columns, and braces in both the 3D and two dimensional (2D) models. The shell elements in the 3D model were modelled by frame elements in the 2D model with the same weight and moment of inertia corresponding to the tributary area of the lumped mass model. The frame elements used in the FEA modes are straight lines which connect two nodes. Biaxial bending, torsion, axial deformation, and biaxial shear are all accounted for in the beam-column formulation. Nonlinear properties can be assigned to both frame and shell elements; however, the dynamic analysis option in this particular case used link elements. A link object connects two joints separated by a length in order to model unique or specific structural behaviors. Link elements have six deformational degrees-of-freedom (DOF) including axial, shear, torsion, and pure bending. There are several link force-deformation relationships that may be specified for each of the 6-DOF. [26] For the case of multi-linear uniaxial plasticity, a non-linear kinematic link element was used to model the hysteretic force deformation properties of the BRBs. The performance of the link elements is based on the hysteresis backbone curves, derived from the ω and β factors obtained from the qualification testing. An example of a hysteresis backbone curve superimposed on the experimental results is presented in Figure 4.1. The figure below shows a normalised point of initial yield located at 1 and -1 on the load or y-axis. The strain hardening factors ω and $-\omega$ are located at the ϵ_{ref} and $-\epsilon_{ref}$ points on the displacement or x-axis. The friction factor β is added to the maximum compression stroke of the hysteresis curve. The friction factor ultimately changes the slope of the compression leg of the hysteresis backbone, making it a unique, asymmetrical curve to represent the hysteretic behaviour of braces with similar construction.

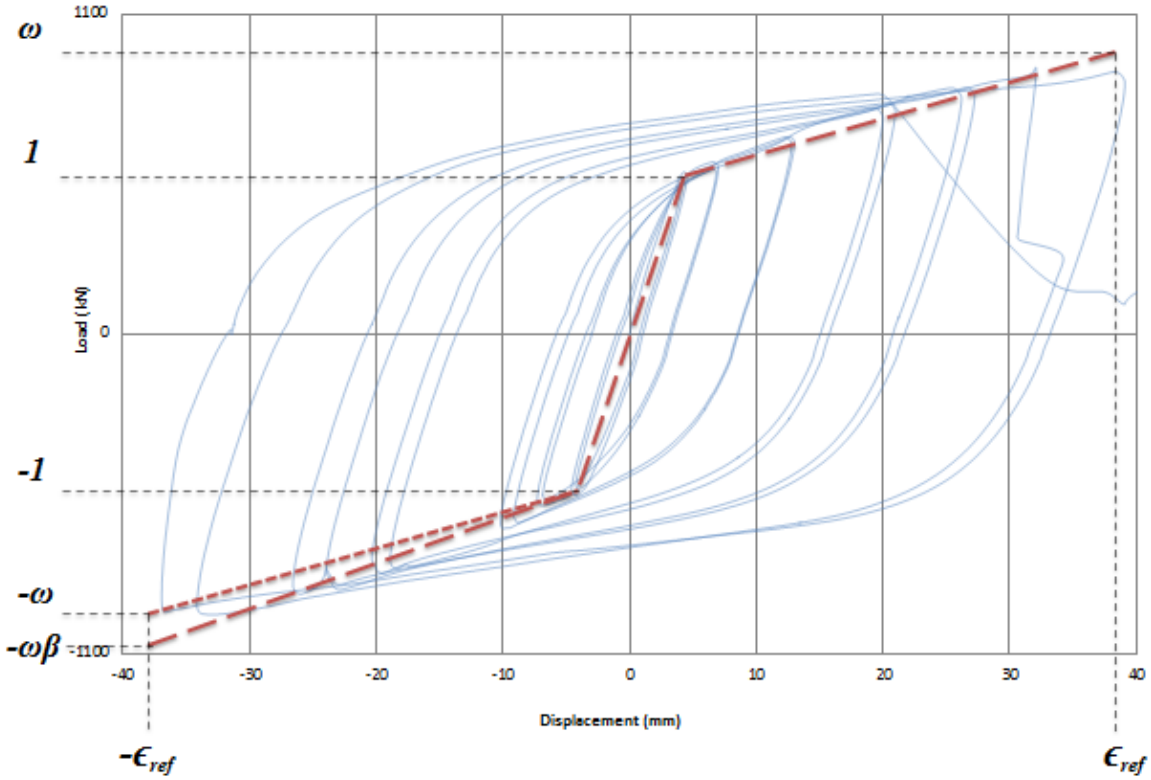

Figure 4.1 – Normalized hysteresis backbone curve overlay

4.2. Equivalent Static Force Procedure (ESFP)

The salient data from the ESFP is presented in this section, covering the design spectra, fundamental building period and the estimation of seismic weight. A full and detailed ESFP for the structure enclosed in Appendix D. While the straight forward ESFP produces static lateral loads, the generation of the 3D and 2D FE models is also used in further modelling analysis. In particular, the 2D lumped mass model is used as a comparison between both static and dynamic analyses.

4.2.1. Design Spectra

The first step in the ESFP was to determine the soil classification for the building site as well as the spectral accelerations for the city of Kingston in accordance with the NBCC geographic seismic data. The five modules of the Sawyer building stretch across two unique soil classifications. Modules 1 and 2 are sighted on original undisturbed rock, while modules 3, 4, and 5 are sited on reclaimed parts of Navy Bay. The soil in this particular location tends to be largely comprised of compacted fill, represented by the NBCC soil classification C. See Figure 4.2 for the NBCC 2010 response spectrum for both soil classifications. Given that acceleration based site coefficient, F_a is a function of soil classification and is set as 1.0 for soil class C and 0.7 for soil class B, the first condition of the ESFP mentioned in the modelling overview is met.

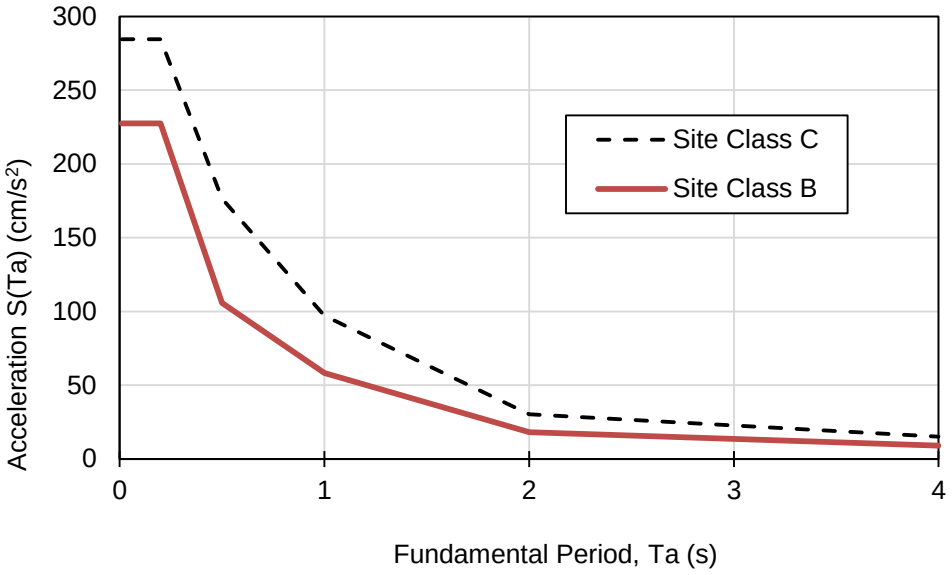

Figure 4.2 – NBCC response spectra – Kingston, On.

4.2.2. Fundamental Period

In order to estimate the fundamental building period of a single module, a full 3D FE model was developed using frame and shell elements. A fully extruded view of the waffle slab and column frame is presented in Figure 4.3.

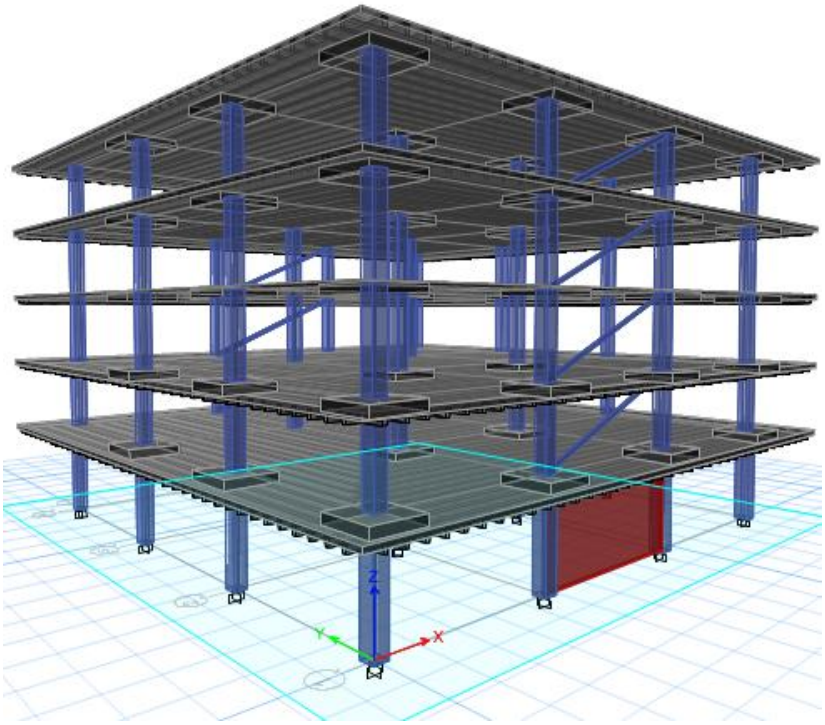

Figure 4.3 – 3D FE model

Once the model was constructed, the FEA program generated the modal periods and frequencies for both directions. Due to symmetry within the model, the fundamental building period, T_a was found to be 0.721 s in both the East-West and North-South directions.

4.2.3. Seismic Weight and Base Shear

With the 3D model developed, the seismic weight was easily calculated by storey. In addition to the dead weight of the building, the superimposed dead weight as well as 25% of the snow load must also be applied to the structure in order to capture an accurate seismic weight. The base shear, the ductility and over strength factors were selected in accordance with table 4.1.8.9 of the NBCC. It is important to note that when the BRBF system was designed, the 2005 NBCC presented R_d and R_o factors for moderate ductility concentrically braced frames tension-compression Braces were 3.0 and 1.3 respectively. In 2010, a provision for BRBF was added, citing R_d and R_o values of 4.0 and 1.2 respectively.

4.2.4. 3D and 2D model

The 3D model used in the estimation of seismic weights was further developed to include the dimensions of the bracing elements. Since the lateral loads will only be applied statically, the BRBs are modelled as tension-only braces with the cross-sectional area corresponding to the dimensions of the BRB yield section. This simplification also assumes complete un-bonding of the inner yield section from the grout at the initial point of loading. While this simplification meant the braces were modelled with the exclusion of composite action and thus lower axial stiffness, the desired effect was to estimate the maximum inter-storey drifts and top storey displacements. These dimensions are presented in Table 4.1. The stiff outer cruciform sections were not modelled separately and as such, the tension-only brace elements were less stiff than the as-designed braces. In order to increase brace stiffness for the analysis, stiffness modifiers were later added to each brace in order to approximate appropriate brace forces. This process is further described in section 4.2.6.

Table 4.1 – BRB cross-sectional dimensions for static analysis

Brace	Depth (mm)	Width (mm)
BR 8	127	19
BR 7	152	19
BR 6	177	22
BR 5	177	22

In addition to defining the BRB properties, the concrete design handbook allows for specific reductions to be made in reinforced concrete elements under the cracked moment reduction factors presents CSA A23.3 [27]. These factors are detailed in clause 21.2.5.2.1 in the special provisions for seismic design. The reduction factors for beams and slabs estimated at 0.4 and 0.2 respectively. Specific reduction factors for each column are related to cross-sectional area and column axil forces due to dead and live loads. These seismic column reduction factors range between 0.6 and 0.75 for this particular model. Member properties for the computation of slenderness effects in beams and columns are presented in clause 10.14.1.2 where the cracked moment of inertia of concrete columns is a reduction to 0.7 while beams and slabs reduction factors are estimated at 0.35 and 0.25 respectively. With a pan-joist system (waffle slab) being an integration of beams and slabs, a value of 0.3 was applied as a cracked moment of inertia and the column reduction factor for all columns was selected as 0.7. For the transfer of in-plane loads, it was assumed that the slabs act as rigid diaphragms. The lateral loads were divided along the four column lines of the 3D model as displayed in Figure 4.4. While a 3D model had proven to be essential in

estimating building periods and seismic weights, it was at this stage in the analysis where computational efficiencies were essential to transition the model into one better suited for dynamic analysis. For this reason, the building was lumped into a 2D frame exhibiting one half of the tributary area while accounting for one half of the building mass, stiffness and lateral loads.

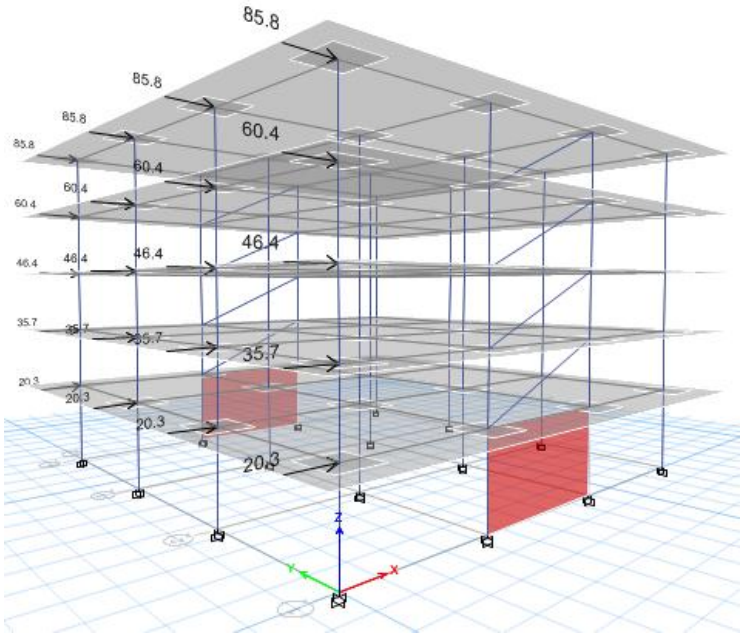

Figure 4.4 – 3D FE model application of static loads

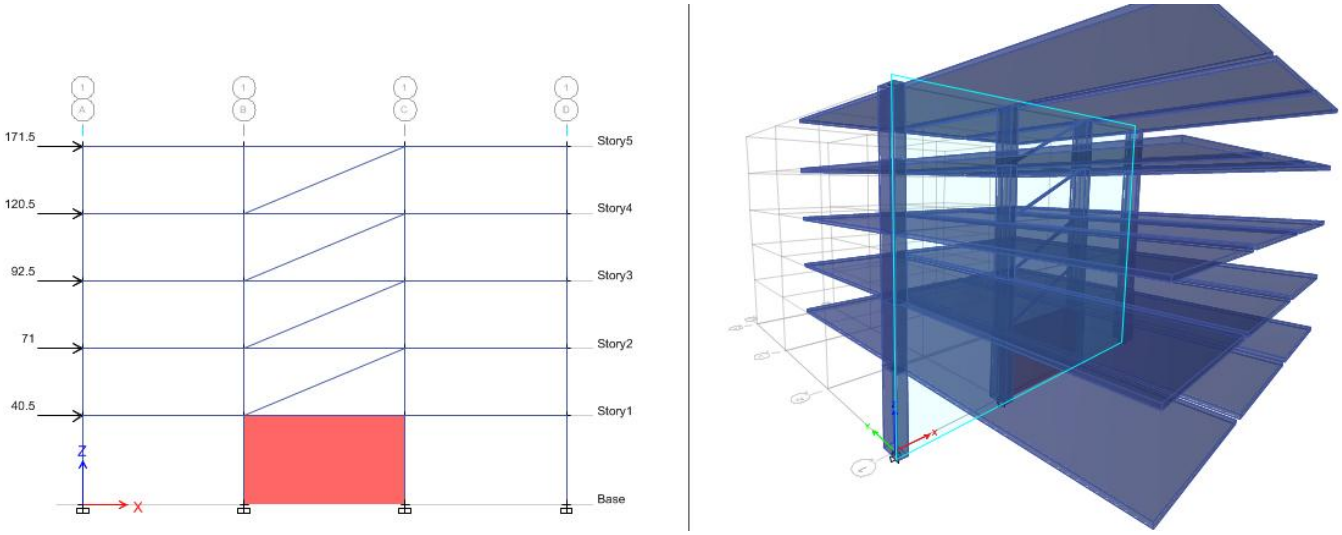

Figure 4.5 – 2D FE model application of static loads

In the 2D lumped mass model, the columns were simply added together in width, while the waffle slab was converted into a beam that represented the same bending moment of inertia while maintaining the same storey weight as one half of the corresponding waffle slab and drop panels. Using symmetry, the BRBs and shear wall respond to one half of the building's tributary area; thus performing similarly to the

3D model. See Table 4.2 for dimensional values and Table 4.3 for comparison of the 2D frames seismic weight with one half of the 3D model.

Table 4.2 – 2D Frame dimensions

2D Frame Component	Depth (mm)	Width (mm)
Beam – Storey 2 & 3	229	24,500
Beam – Storey 4, 5, and roof	208	24500
Column – Ground	711	1,422
Column – Storey 2, 3, 4, & roof	610	1,220
BRB elements	no change	
Shear Wall	no change	

Table 4.3 – Seismic Weight confirmation

½ of 3D Frame Model				2D Frame Model	
Level, i	Height, h	Weight at Level i (kN)		Weight at Level i (kN)	
	m	Floor	Columns	Beam	Column
Roof	20.27	3,239	0	3,290	0
5	16.46	3,239	267	3,290	267
4	12.65	3,239	267	3,290	267
3	8.84	3,593	267	3,632	267
2	5.03	3,593	267	3,596	267
Basement	0	-	448	-	448
Σ Component (kN)=		16,904	1,517	17,099	1,517
Σ Weight (kN)=			18,421		18,616

In order to verify the 2D models performance, both the 3D and 2D models were analysed using the ESFP and the same cracked moment of inertia modifiers outline the 3D model. The storey displacements along the leeward columns are presented in Table 4.4 and graphically in Figure 4.6.

Table 4.4 – 3D and 2D storey drift

Level	3D Storey Displacement	Inter-storey Drift	2D Storey Displacement	Inter-storey drift
	mm	mm	mm	mm
roof	11.5	1.9	12	2.5
5th	9.6	2.9	9.5	2.8
4th	6.7	3.5	6.7	4
3rd	3.2	3	2.7	2.6
2nd	0.2	0.2	0.1	0.1
Ground	0	0	0	0

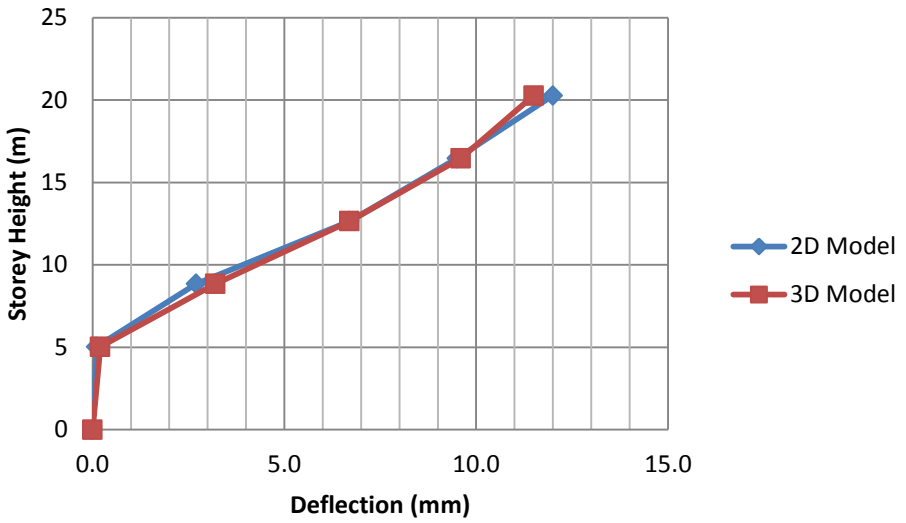

Figure 4.6 – 3D and 2D storey drift4.2.5. Deflections and Drift Limits

With an effective 2D model in place, the lateral deflections and inter-storey drifts were assessed. The defections calculated using the FEA program were multiplied by Rd and Ro in order to give realistic values of the anticipated deflections, as stated in 4.1.8.13 of the NBCC. In order to establish a baseline to compare the effectiveness of the BRBF, the 2D frame was modelled without the BRBs or shear wall. Assessing the unmodified structure meant a recalculation of the ESFP for the concrete moment frame. Using the Ro and Ro values of 1.5 and 1.3 respectively for a conventional moment resistant concrete frame structure, the ESFP produced lateral forces that were twice that of the same frame strengthened by the BRBF. This is not surprising, since the Ro factor is half that used in the previous ESFP (see Appendix D). The lateral loads for the 2D moment resisting frame model are shown in Figure 4.5.

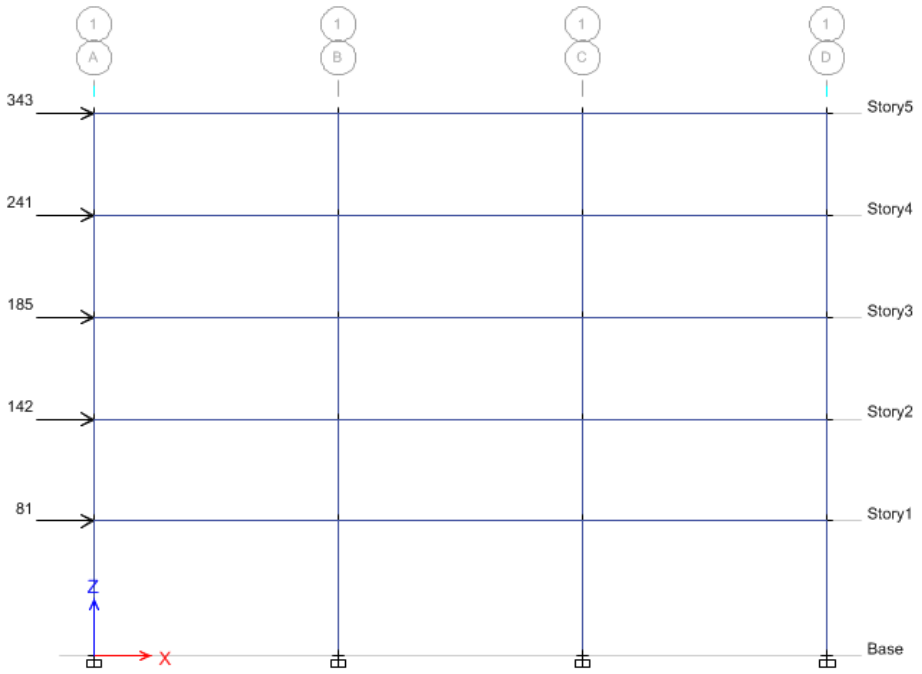

Figure 4.7 – 2D FE model un-braced moment resisting frame

The NBCC section 4.1.8.13 states that the lateral deflections calculated using either the ESFP or dynamic analysis must be multiplied by the R_d and R_o factors and these corresponding inter-storey drifts shall be limited to $0.025h_s$, or 95 mm when referencing a storey height of 3.81 m. The risk associated with significant lateral drifts between storeys is that the existing concrete columns could fail in flexure and lose their capacity to support the buildings gravity loads. While all inter-storey deflections presented in Table 4.5 are well below the limit of 95 mm, the structure was designed in the early 1970's prior to the extensive development of seismic provisions in the NBCC. A moment resistance (M_r) check, along with moment-axial interaction diagrams of the un-braced frame columns identified that all columns have sufficient M_r when compared to the factored moment (M_f) generated by the ESFP, see Appendix C. The designer proposes $1/6^{th}$ of 95 mm or roughly 16 mm limit. This conservative approach is most certainly an effective drift limit, however, with no great moment resistance deficit in the un-braced frame it is very likely that a less complex and more economical rigid lateral bracing system could have been employed.

Table 4.5 – Deflections and inter-storey drifts

Level	2D Steel BRBF (Rd=3, Ro= 1.3)			2D Concrete Moment Frame (Rd=1.5, Ro= 1.3)		
	ETABS Storey Drift	Storey Drift x Rd Ro	Inter-storey Drift	ETABS Storey Drift	Storey Drift x Rd Ro	Inter-storey Drift
	mm	mm	mm	mm	mm	mm
roof	12	46.8	9.8	72	140.4	21.5
5th	9.5	37.1	10.9	61	119	29.3
4th	6.7	26.1	15.6	46	89.7	33.2
3rd	2.7	10.5	10.1	29	56.6	33.2
2nd	0.1	0.4	0.4	12	23.4	23.4
Ground	0	0	-	0	0	-

4.2.6. Brace Forces

The axial forces in the braces, determined at the end of the ESFP, summarised in Table 4.6 are intended to be the basis for the selection of yield area cross-sections for each BRB. These static values are compared against the dynamic results in Section 4.3. The assumption of immediate un-bonding will produce lower brace stiffness and lower brace axial forces, as previously discussed in Section 3.9.4. The process of statically accounting for full composite action of a BRB is intended to assign cross-sectional area modifiers to account for the added stiffness of the composite braces and as such, estimated the upper bound of axial forces. These area modifiers were calculated using the principle of equivalent area, effectively transforming the grout and outer steel casing into an equivalent cross-section of steel. This area modification increases the braces' stiffness and subsequently the axial load carried by each brace. The dimensions, modifiers and axial loads are presented in Table 4.6.

Table 4.6 – ESFP brace axial forces

Brace	Depth (mm)	Width (mm)	Un-bonded Brace Axial Force (kN)	Brace Area Stiffness Modifier	Composite Brace Axial Force (kN)
BR 8	127	19	**105**	4.2	**157**
BR 7	152	19	**174**	3.5	**259**
BR 6	177	22	**254**	2.6	**327**
BR 5	177	22	**188**	2.6	**285**

The qualification testing has established that the material and construction techniques of the as-built BRBs have produced braces that greatly exceed their original design. The NBCC and CSA S16 make an exception for cases where the energy-dissipating elements have been oversized, a limit has been placed on the maximum forces that non-dissipating elements must resist by setting the maximum anticipated seismic load equal to that corresponding to R_d multiplied by R_o equal to 1.3. [19]. The design values for R_d and R_o are 3 and 1.3 respectively. Re-running the ESFP with and Rd multiplied by Ro value of 1.3 produces similar storey drifts as the BRBF, presented in Table 4.7 and graphically in Figure 4.8. The brace axial loads for the over strength braces are, as expected, three times larger than the ductile BRBF with an R_d x R_o three times smaller than the moderately ductile bracing.

Table 4.7 – ESFP inter-storey drifts

Level	Intended Ductile BRBF (R_d=3, R_o= 1.3)			Concrete Moment Frame (R_d=1.5, R_o= 1.3)			Actual Over Strength BRBF (R_d=1, R_o= 1.3)		
	FEA Storey Drift	Storey Drift x R_dR_o	Inter-storey Drift	FEA Storey Drift	Storey Drift x R_dR_o	Inter-storey Drift	FEA Storey Drift	Storey Drift x R_dR_o	Inter-storey Drift
	mm	mm	mm	mm	mm	mm	mm	mm	mm
roof	12	46.8	9.8	72	140.4	21.5	35.8	46.5	9.1
5th	9.5	37.1	10.9	61	119	29.3	28.8	37.4	13.3
4th	6.7	26.1	15.6	46	89.7	33.2	18.6	24.2	13.7
3rd	2.7	10.5	10.1	29	56.6	33.2	8.1	10.5	10.1
2nd	0.1	0.4	0.4	12	23.4	23.4	0.3	0.4	0.4
Ground	0	0	-	0	0	-	0	0	-

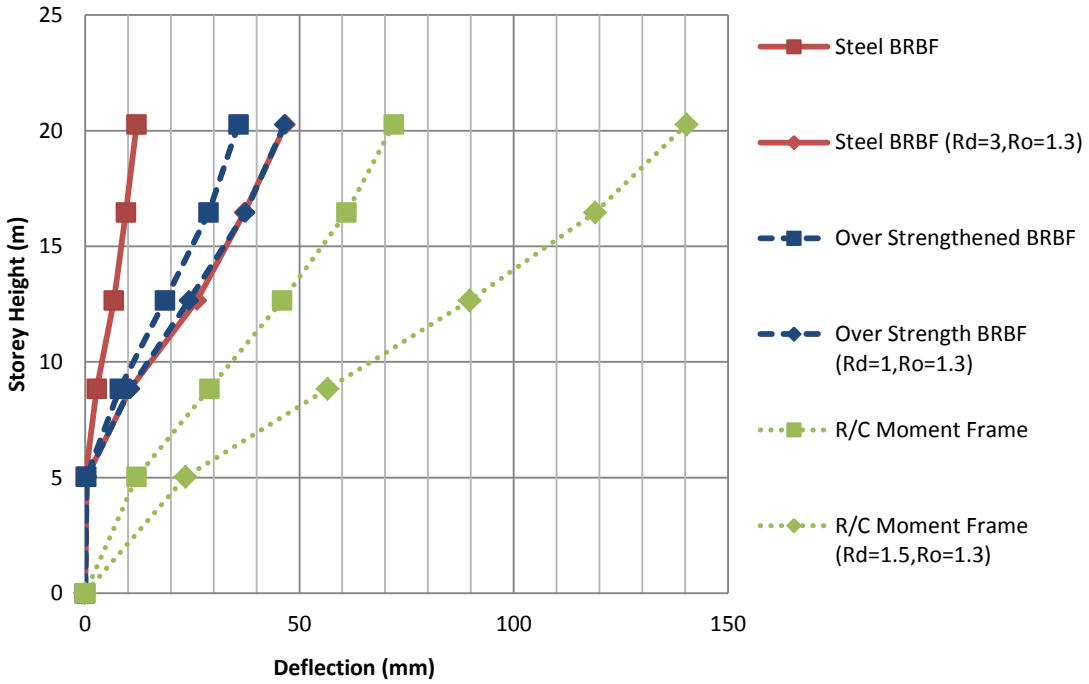

Figure 4.8 – ESFP storey drifts

Table 4.8 – Brace axial loads for ductile and over strengthened braces

Brace	Rd=3, Ro=1.3	Rd=1, Ro=1.3
	Un-bonded Brace Axial Force (kN)	Over Strength Brace Axial Force (kN)
BR 8	105	311
BR 7	174	510
BR 6	254	742
BR 5	188	550

Regardless of the excessive axial loads caused by the reduced R_d and R_o factors in the ESFP, the axial loads are still well within the capacity of the braces and connections while providing comparable lateral support and drift control.

4.3. Dynamic Analysis

Despite the fact that the ESFP is a relevant analysis option given the geographic seismicity and natural period of the structure, the presence of nonlinear or plastic damping elements such as BRBs demands a deeper level of analysis to determine the real time behaviour of the entire structure under an appropriate design earthquake. While the dynamic analysis is not directed as essential by the NBCC, it is recommended as a prudent step in understanding the holistic structural response.

For the dynamic analysis of the BRB system, the Fast Nonlinear Analysis (FNA) methodology was chosen for its computational accuracy and efficiency. FNA is a modal analysis method useful for the dynamic evaluation of nonlinear structural systems mainly for is use of the derived Ritz vectors. The concept of derived Ritz vectors was proposed by Wilson in 1982 where he proposed a method that would drastically reduce computational effort in solving the Eigen solution. The derived Ritz vectors are generated by taking into account the spatial distribution of the dynamic loading, whereas the natural mode shapes neglects this very important information when solving the dynamic problem. The derived Ritz vector algorithm automatically contains the advantages of a number of proven techniques including static condensation, Guyan reduction, and static correction [28]. Due to of its computationally condensed formulation and use of Ritz vectors, FNA is well-suited for time-history analysis and using modern FEA software, FNA is a computationally efficient means of analysing a nonlinear system. The structural model being assessed via the FNA approach should be mostly linear-elastic, have a limited number of nonlinear members and lump nonlinear behavior within link objects. [26]

4.3.1. Non-Linear (NL) Modelling

In generating an FNA model, the 2D lumped mass model used in the ESFP is enhanced by the addition of multi-linear kinematic plastic link elements with non-linear axial properties. The nonlinear mechanics of these link elements are driven by the hysteresis back bone data derived from the BRB qualification testing and respective material testing. The hysteresis curves for the modified braces incorporates the core material yield strength, modulus of elasticity and tangent modulus into consideration, along with the ω and β factors determined during the qualification testing . A hysteresis backbone represents the strain hardening path that a material will follow during cyclic loading. The hysteresis loop is composed of the backbone curve extended along the translated yield surface during kinematic hardening. When the BRB is unloaded and transitioning between tension and compression cycles, the reverse backbone is followed during the compression stroke. Typically, a bi-linear backbone

curve representing the modulus and tangent modulus are all that is required, however in this model, a tri-linear backbone curve was used to better approximate the structure's dynamic response. Figure 4.9, Figure 4.10, and Figure 4.11 present the hysteresis backbone data for each of the material properties found during the qualification testing. The material data is applied to the specific geometry of each brace in a complete modular bracing column, creating a series of representative backbone curves. These overlapped backbone curves defined the strain hardening path for the non-linear behaviour of FEA model. The backbone data for the 248 MPa steel was generated using the ω and β factors from the qualification testing modified by the typical tangent modulus for A320 Steel. Figure 4.12 presents the 2D lumped mass model. This model presents the five-storey frame with a shear wall at the base, modelled by a rigid shell element. The non-linear link elements are represented in this model with the strongest braces, BR5 and BR6 positioned at the bottom. It should be noted that while each module has unique seismic loads, the bottom two braces of each BRB stack share the same geometry. The brace link elements presented in the figure below are labeled for an inner yield steel with F_y=248 MPa.

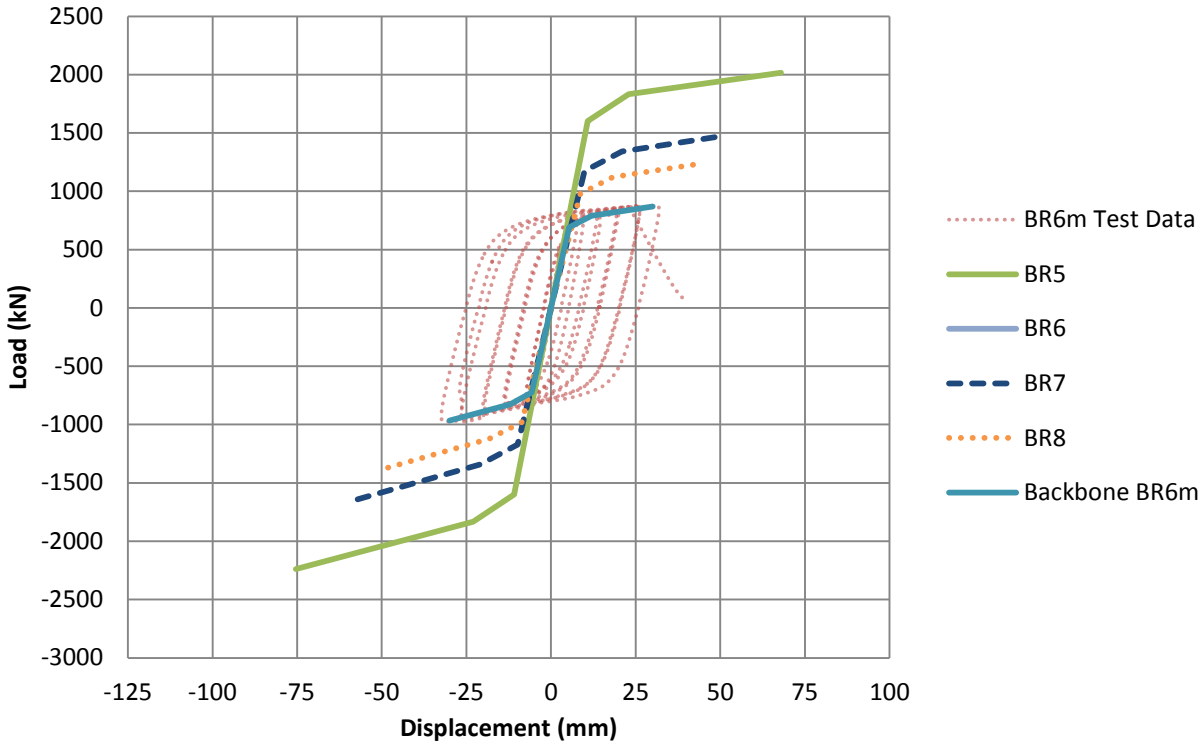

Figure 4.9 – Backbone Curves for Fy=450 Steel

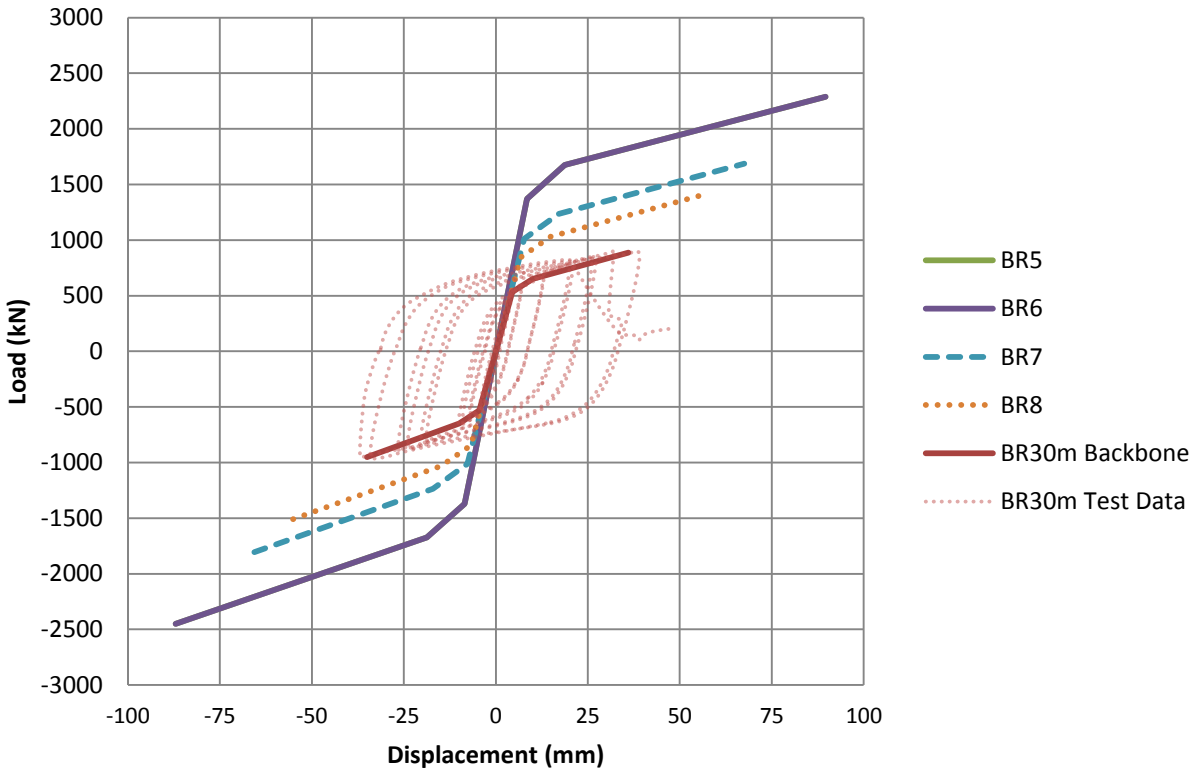

Figure 4.10 – Backbone Curves for Fy=350 Steel

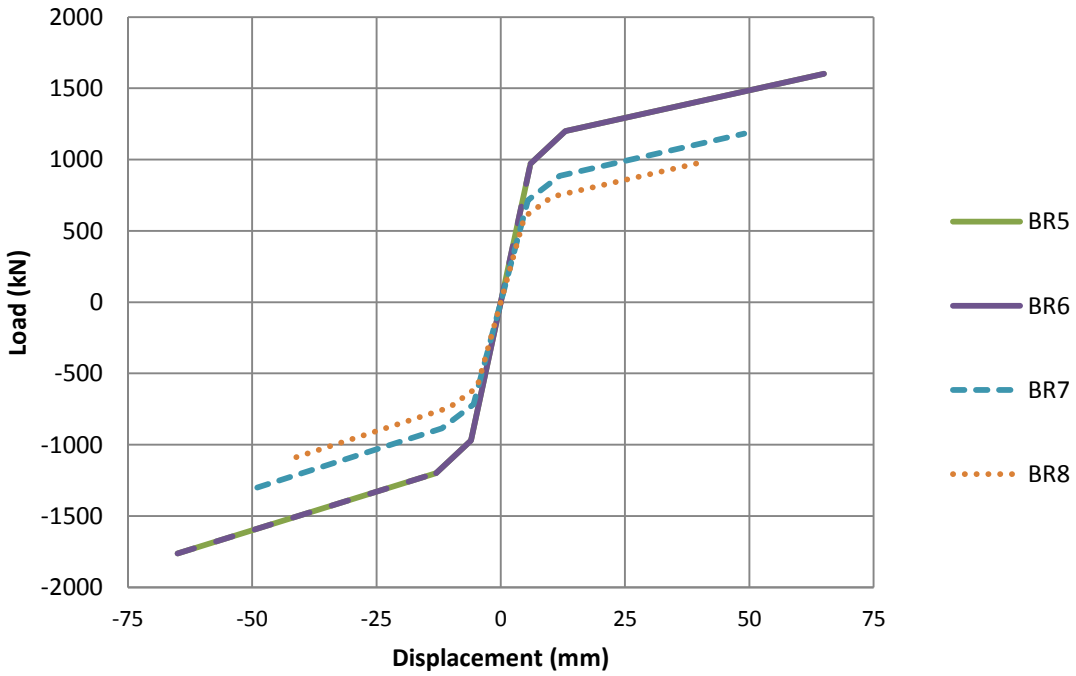

Figure 4.11 – Backbone Curves for Fy=248 MPa Steel

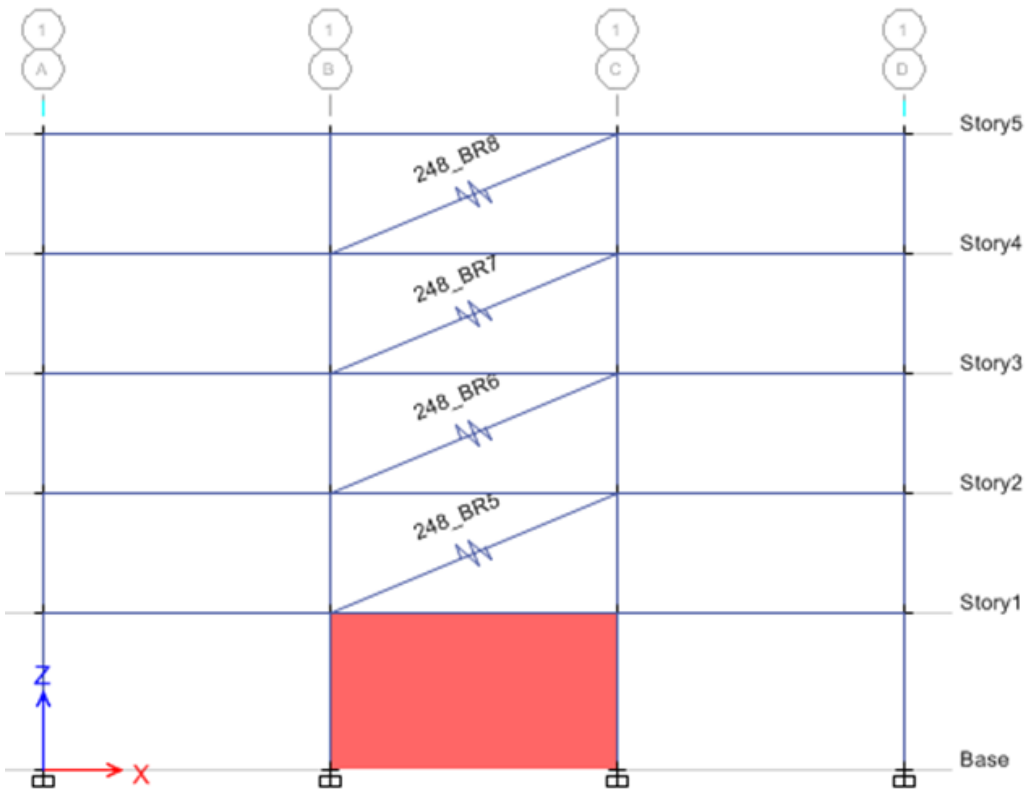

Figure 4.12 – 2D FE lumped mass model with NL link elements

4.3.2. Matching ground motion to a UHS

The seismic design provisions of the NBCC describe earthquake ground motions for which structures are to be designed, in terms of a uniform hazard spectra (UHS) having a 2% chance of being exceeded in 50 years. The specific UHS depends on location and site condition, where site condition is described by a classification scheme based on the time-averaged shear wave velocity in the top 30 m of the deposit. While the UHS is the driving data set for the ESFP, the FNA method requires an appropriate ground motion in order to generate a time-history analysis. Atkinson presents the stochastic finite-fault method used to generate earthquake time histories that may be used to match the 2005 NBCC UHS for a range of Canadian sites [21]. The earthquake records presented by Atkinson include pseudo-spectral accelerations as well as associated ground motions for the full range of site conditions in both eastern and western Canada. All data is available via open source at www.seismotoolbox.ca [21].

Using the target spectral acceleration from the NBCC, presented previously in Figure 4.2, as SA_{Target} and given that the structure has a fundamental period of 0.721 s, the period range of interest can be determined as 0.1 – 1 s in an area greater than 100km from the nearest fault. The second record set for a magnitude 7 earthquake in eastern Canada for soil type C was selected. In this file, there exist 45 distinct simulated spectral accelerations, SA_{sim} available for matching the UHS. For each record within the file, the ratio (SA_{target}/SA_{sim}) was calculated at every period within the period range of interest along with the mean and standard deviation of (SA_{target}/SA_{sim}). Five records were chosen with the lowest standard deviation or best shape but having a mean in the approximate range of 0.5 -1. Each selected

record was scaled by multiplying by the mean. Figure 4.13 presents a summary of the most appropriate simulated spectral accelerations all scaled to match the target UHS between the range of 0.1 – 1 second. For further reading and a detailed ground motion matching protocol, refer to Atkinson's 2009 research regarding NBCC compatible time histories [21].

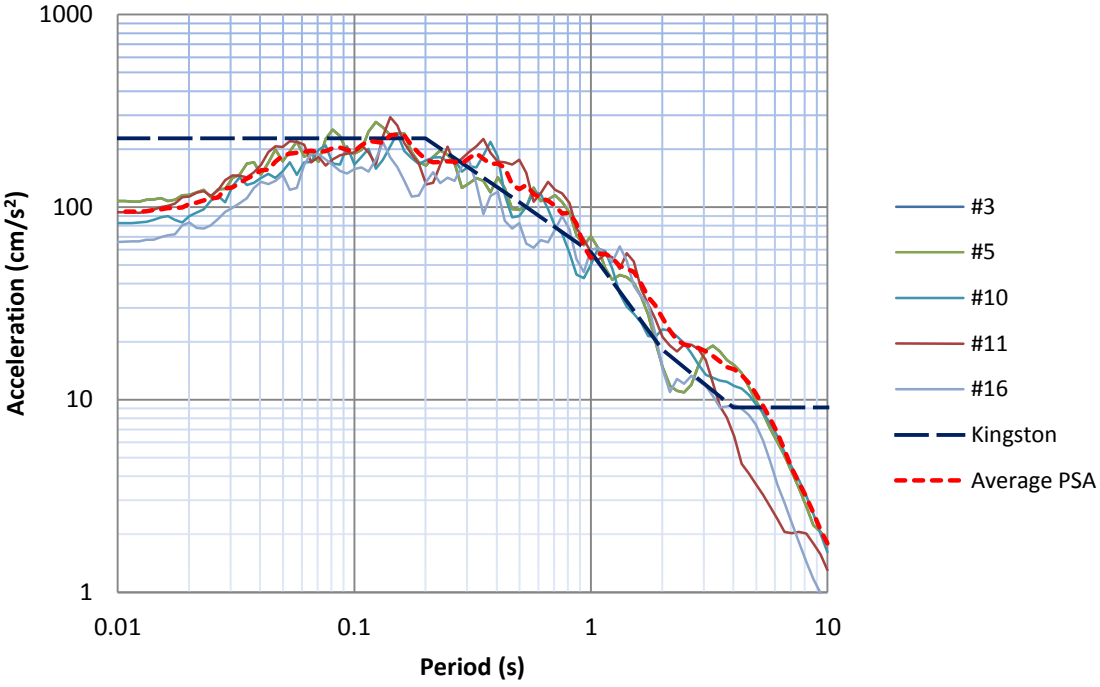

Figure 4.13 – Kingston Target UHS match east7c2.psa

The scaling of specific pseudo spectral acceleration (PSA) data sets confirmed that each of the time histories fit to the UHS for site class B in Kingston. Each PSA has a corresponding ground motion with the same scalar for each PSA being applied to the ground motion time-history (TH). The scaled ground motions are overlaid in Figure 4.14. The scalar value for each TH is listed in in the Figure 4.14 legend. As a verification to confirm Peak Ground Acceleration (PGA), the NBCC PGA value for Kingston is compared to the PGA for each of the five scaled time histories in Table 4.9.

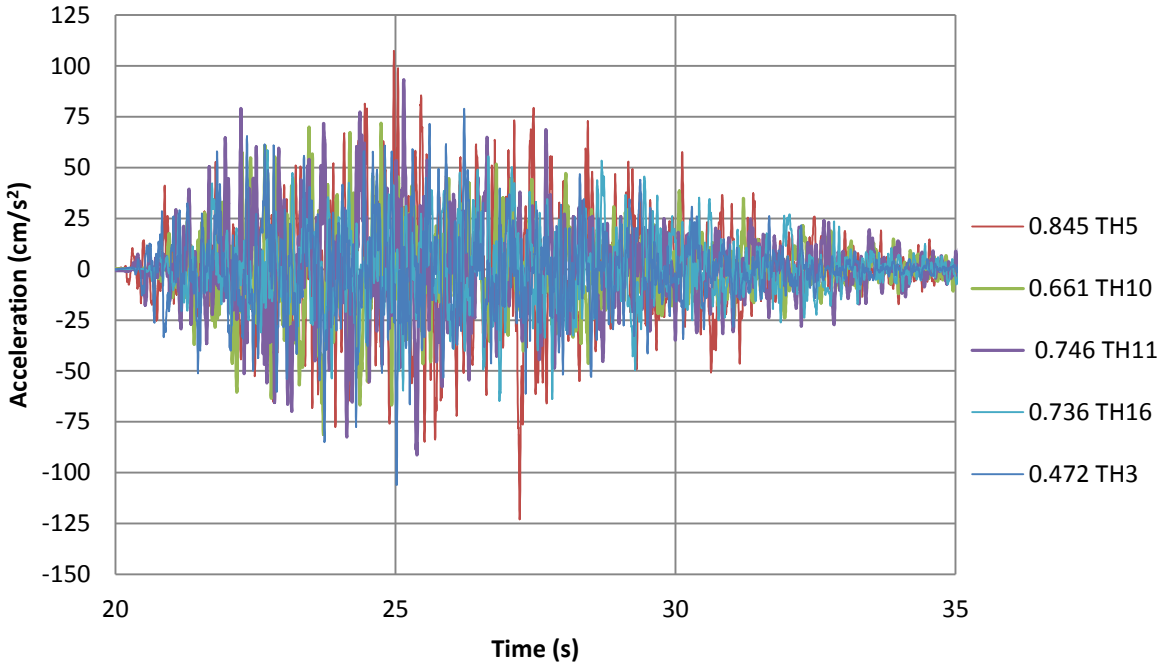

Figure 4.14 – Scaled ground motion overlay east7c2.acc

Table 4.9 – PGA for scaled ground motions

Ground Motion id	Scalar	PGA	Time
		cm/s^2	sec
3	0.472	-106	25.002
5	0.845	-122	21.516
10	0.661	-81	23.716
11	0.746	93	24.122
16	0.736	-65	26.858

NBCC - Kingston PGA = 118 cm/s^2

A minimum of five ground motions is recommended to capture an appropriate range of structural responses [21]. The PGA values in Table 4.9 shows a wide range of values with the maximum value being 122 cm/s^2, confirming that the five selected ground motions will be an appropriate representation of the UHS for Kingston, which is 118 cm/s^2 according to the NBCC 2010 location and climactic data [20].

4.3.3. FNA Results

With the model constructed and time histories generated, running a FNA was possible. A conservative modal load case was defined using 40 Ritz vectors so as to capture the appropriate degrees of freedom. This modal load case accounted for acceleration in the x-direction as well as dead load in the

z-direction. The mass used in analysis was generated by the individual elements and the ground motion accelerations determined in the previous section were applied as an input acceleration in the z-direction. In order to minimise dynamic effects caused by the application of a dead load, the self-weight of the structure was applied in the z-direction as a non-linear time history using a 20 second ramp function with 99% modal damping in order to reduce the dynamic effects of the dead load. The five ground motions were applied as accelerations in the x-direction using the modal-ritz case damped at 5%, which is a typical damping value for the first natural frequency. [29]

4.3.3.1 Storey Displacements and Drifts

The initial FNA was run using all five simulated ground motion records on three separate models of which the first model was an un-braced frame. This model was used as the control model to determine the un-strengthened top storey displacement. The second model in this FNA was a braced frame using the NL link with the multi-linear kinematic plastic link elements with non-linear axial properties for F_y=284 MPa steel. This model generated an estimate of the top storey displacements as well as the link displacements and forces. The third model was the same as was analyzed using the equivalent static force procedure (ESFP), to demonstrate the axial loads generated in a stiff frame by the five ground motions in comparison to the ESFP. The results of the top storey displacements are presented in Table 4.10. The results tabulated below are for two types of bracing under unique analysis options. The un-braced frame and frame braced with tension-only braces were tested using the ESFP. A second set of models were created for the FNA, which included an un-braced frame along with a frame using nonlinear link elements. This FNA used the all five synthetic ground motion time histories to produce an absolute top storey displacement.

Table 4.10 – ESFP and FNA absolute top storey displacements

Model		Absolute Top Storey Displacement (mm)											
		ESFP		TH3		TH5		TH10		TH11		TH16	
SRFS Type	Analysis Type	ETABS	ETABS x R_dR_o	ETABS	ETABS x R_dR_o	ETABS	ETABS x R_dR_o	ETABS	ETABS x R_dR_o	ETABS	ETABS x R_dR_o	ETABS	ETABS x R_dR_o
Un-braced R_dxR_o=1.95	FNA	-	-	28	55.2	49.3	96.1	23.1	45	31	59.7	30.4	59.3
	ESFP	72	140	-	-	-	-	-	-	-	-	-	-
Braced R_dxR_o=3.9	FNA	-	-	10.4	40.6	11	42.9	8.7	33.9	11	41.3	8.3	32.4
	ESFP	12	46.8	-	-	-	-	-	-	-	-	-	-

The results for each of the top storey displacements were obtained from the maximum values for each corresponding ground motion time history. Displacement-time history graphs are presented below in Figure 4.15 through Figure 4.19. The time histories presented below include the linear elastic or tension only brace subjected to the five ground motions using FNA. The use of the nonlinear brace element in FNA is intended for comparison to the results of model with the non-linear link elements.

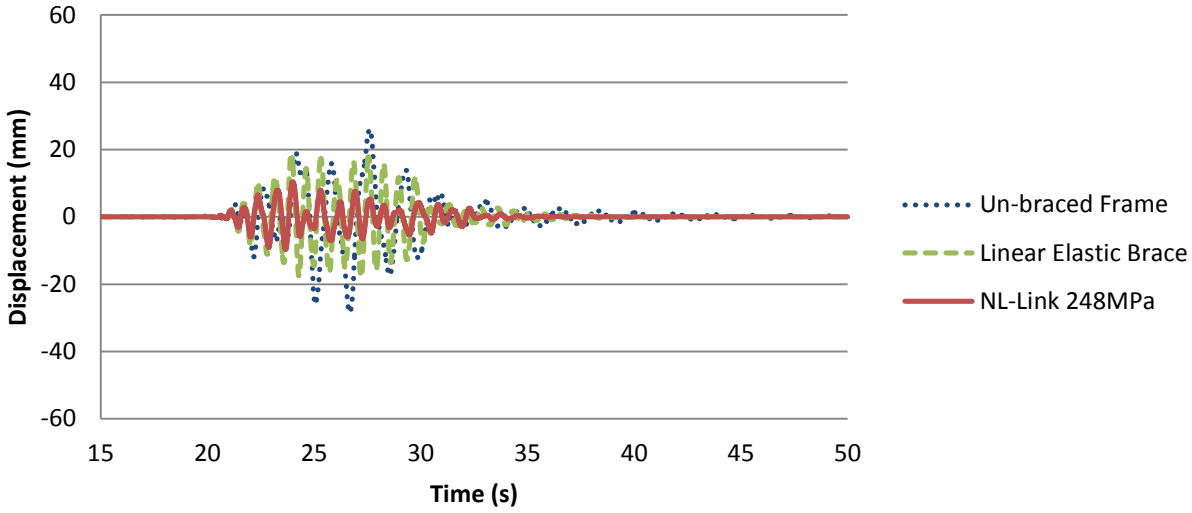

Figure 4.15 – Top storey displacement TH 3

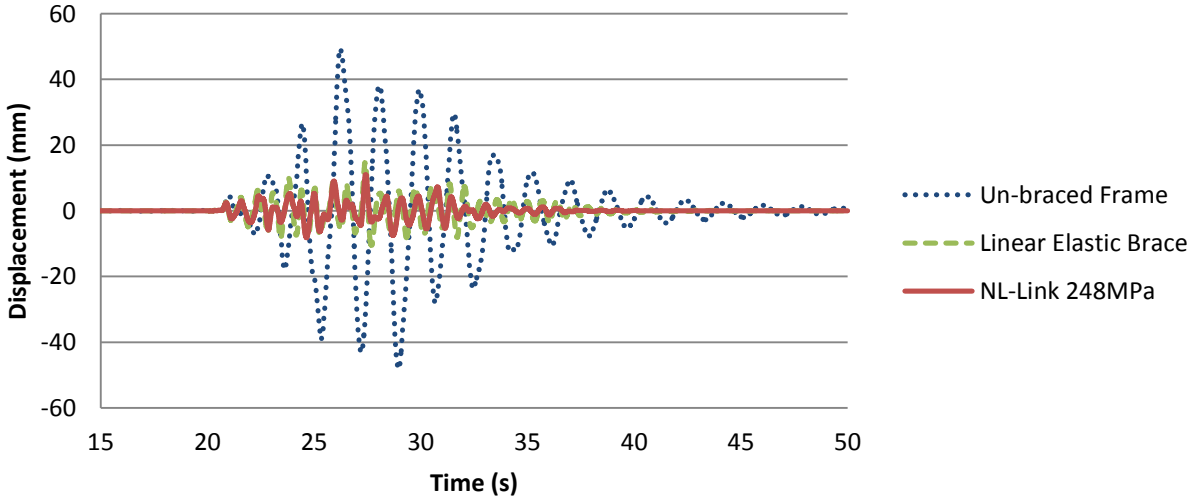

Figure 4.16 – Top storey displacement TH 5

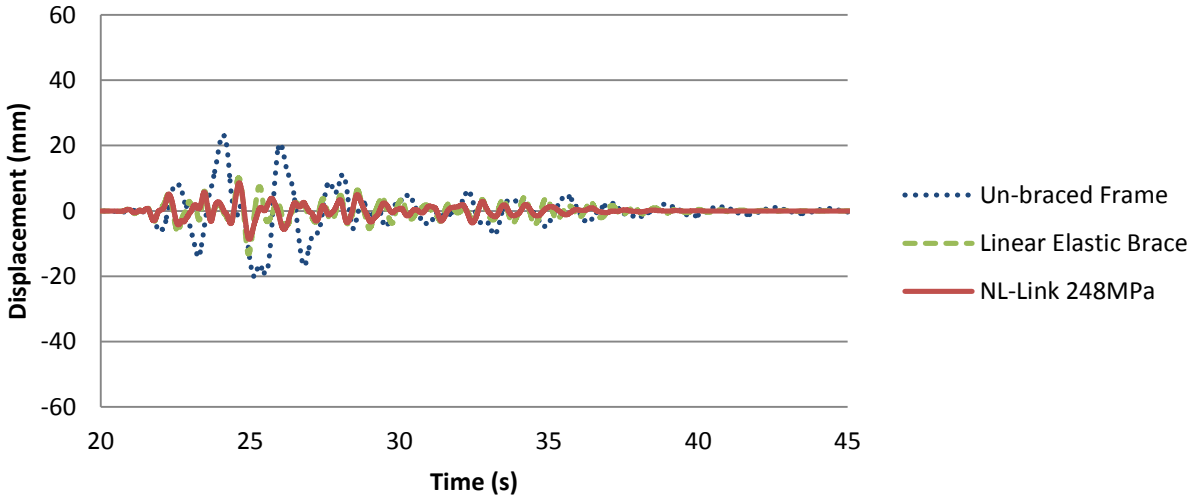

Figure 4.17 – Top storey displacement TH 10

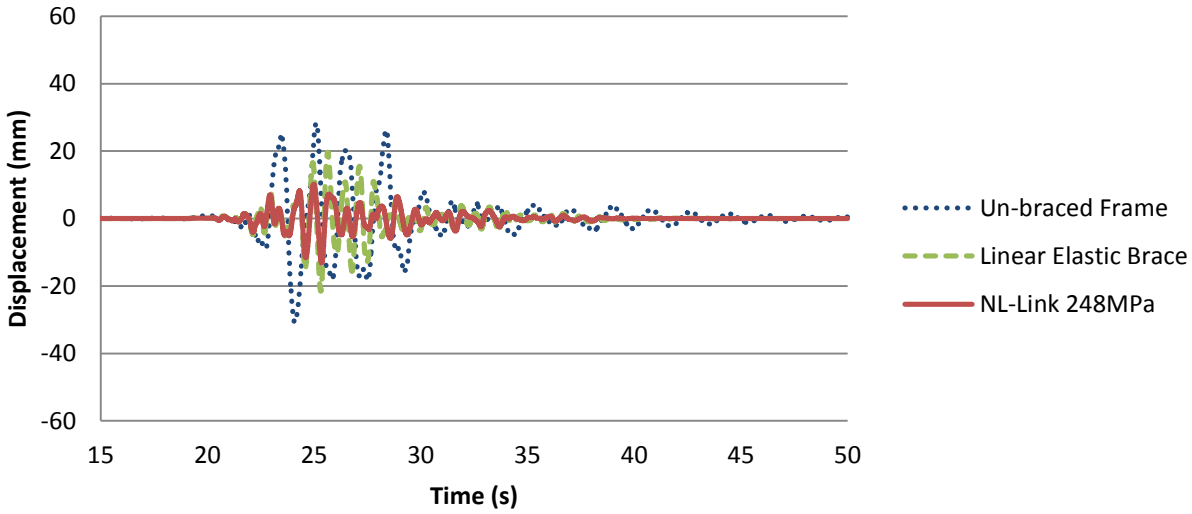

Figure 4.18 – Top storey displacement TH 11

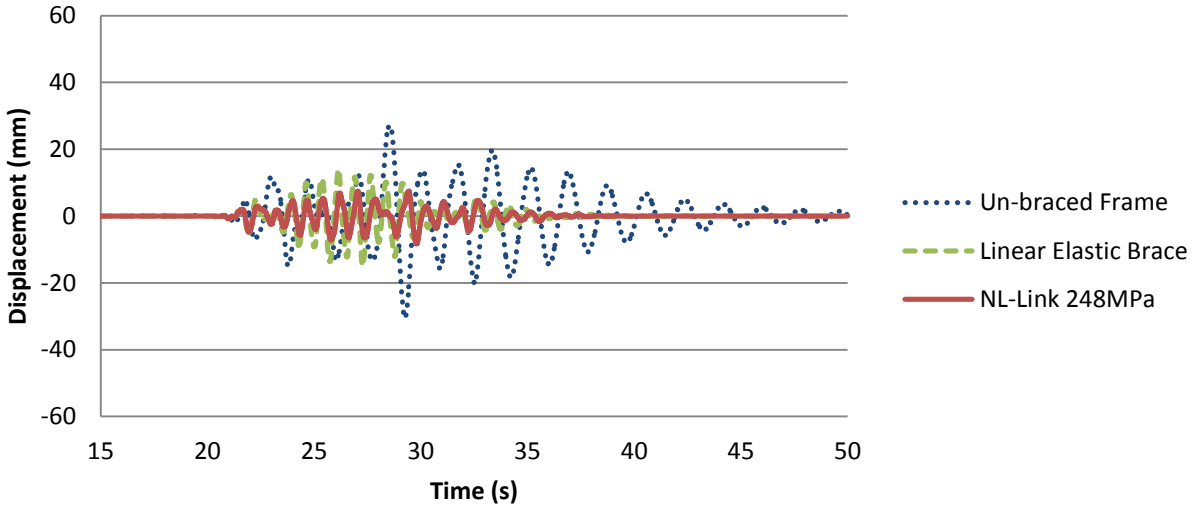

Figure 4.19 – Top storey displacement TH 16

The results of the top storey displacements emphasized the extremely conservative approach of the ESFP and the effectiveness of applying a minimum of five unique ground motions to obtain an overall representative dynamic structural response. For the braced models, the ESFP value is less than 10% larger than the greatest dynamic value; however, the ESFP displacement values for the un-braced model is over 30% larger than the greatest dynamic value. The greatest dynamic values from the FNA were generated by TH 5 for the un-braced frame and TH 11 for the BRBF. This variation is due to the decreased building period as a result of the installation of the lateral SFRS. The un-braced module has a fundamental period of 1 second, whereas for the braced frame it is 0.721 s. Recalling both PSA values for each TH in Figure 4.13, it can be seen that the TH 11 PSA values are the greatest at $T_a = 0.721$ s whereas the TH 5 PSA values are dominate at $T_a = 1$ s.

Regardless of the actual values, once the FEA values have been multiplied by the corresponding structures' R_d and R_o factors, the displacements are all very close in magnitude. When comparing the un-braced frame inter-storey drifts, the drift limits for this ground motion are all below 24 mm, these results are presented in Table 4.11 and graphically in Figure 4.20.

Table 4.11 – ESFP and FNA TH5 inter-storey drifts for an un-braced frame

Level	ESFP (R_d=1.5, R_o= 1.3)			FNA TH5 (R_d=1.5, R_o= 1.3)			Drift variance
	ETABS Storey Drift	Storey Drift x Rd R_o	Inter-storey Drift	ETABS Storey Drift	Storey Drift x R_d R_o	Inter-storey Drift	
	mm	mm	mm	mm	mm	mm	
roof	72	140.4	21.4	49.3	96.1	18.3	14%
5th	61	119	29.3	39.9	77.8	14.2	51%
4th	46	89.7	33.1	32.6	63.6	17.9	46%
3rd	29	56.6	33.2	23.4	45.6	24	28%
2nd	12	23.4	23.4	11.1	21.6	21.6	8%
Ground	0	0	0	0	0	0	0%

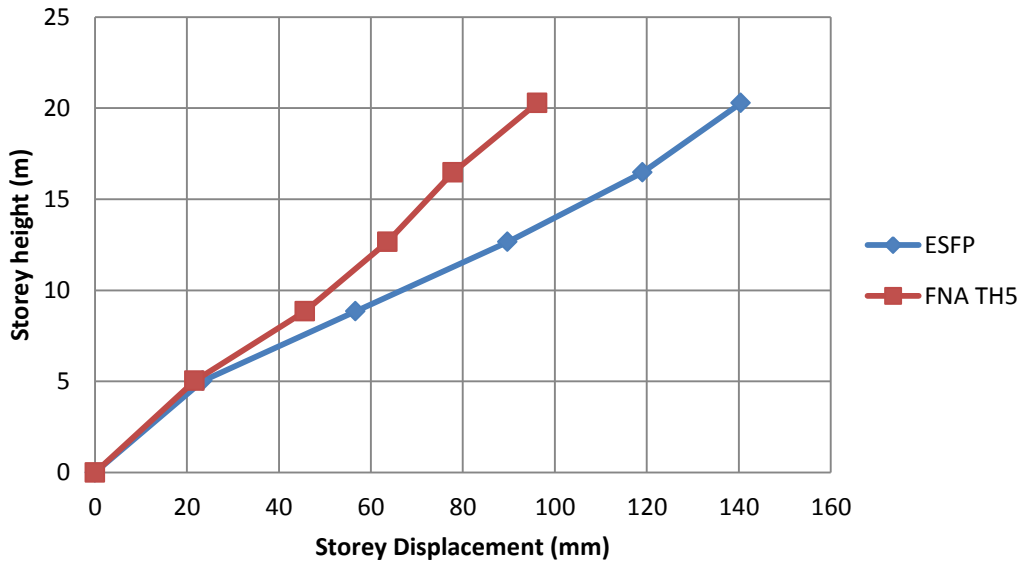

Figure 4.20 – FNA and ESFP Storey Drift

4.3.3.2 BRB Forces

The non-linear behaviour of the BRB link elements when subjected to a ground motion provides valuable insight into the design and performance of this SFRS. In order to assess the brace behaviour, the maximum axial force of each bracing element was analysed against the five ground motions via FNA and using the multi-linear kinematic plastic link elements with non-linear axial properties for the design steel, F_y=248MPa. The ESFP model with linear-elastic elements was also subjected to the same ground motions. Axial forces determined using the ESFP with a fully bonded composite brace are compiled below for a reference. These results are summarised in Table 4.12 with the maximum brace force highlighted to identify the dominate TH function for the dynamic analysis.

Table 4.12 – BRB Forces

Model	Brace	ESFP	TH3		TH5		TH10		TH11		TH16	
			Comp	Tens	Comp	Tens	Comp	Tens	Comp	Tens	Comp	Tens
		kN	**kN**	**kN**	**kN**	**kN**	**kN**	**kN**	**kN**	**kN**	**kN**	**kN**
FNA NL Link	BR 8	-	-190.4	209.1	-180.3	272.8	-175.4	165.3	-266.5	198.6	-152.2	166.5
	BR 7	-	-293.3	311.5	-256.3	376.6	-275.2	273.7	-401.4	306.8	-246.1	237.5
	BR 6	-	-404.3	437.3	-327.6	432.8	-366.8	367.6	-547.1	424	-355.7	313
	BR 5	-	-315.9	353.1	-261.8	293.4	-279.9	279.4	-431.1	338.8	-289.3	263.9
FNA Linear Elastic Brace	BR 8	-	-190.9	166.2	-251.7	218.7	-200.3	206.2	-241.4	243.5	-186.1	182
	BR 7	-	-260.5	217	-315.9	295.2	-184.6	247.8	-368.1	333	-307.1	263.7
	BR 6	-	-339.6	318.5	-414.4	382.3	-244	336.5	-496.6	456.9	-417	336.8
	BR 5	-	-240.6	246.9	-338.6	299.6	-227.1	219.2	-357.4	288.4	-298.5	251.3
ESFP	BR 8	157	-	-	-	-	-	-	-	-	-	-
Linear Elastic Brace	BR 7	259	-	-	-	-	-	-	-	-	-	-
	BR 6	327	-	-	-	-	-	-	-	-	-	-
	BR 5	285	-	-	-	-	-	-	-	-	-	-

4.3.3.3 Iterative Analysis

The brace forces from the ESFP are roughly 30-40% of the greatest dynamic results and even under the most severe design ground motion, none of the BRBs appear to be subjected to a brace force in the plastic range. The inability to exhibit any hysteretic dampening prompted an iterative analysis to determine the amplitude of ground motion that would activate plastic deformations in the BRBs and to examine strain hardening until ultimate capacity has been achieved. As previously determined in Section 4.3.3.1, the driving ground motion for the BRBF of this fundamental period was TH 11. The initial iterative analysis on the as-designed, 248 MPa link elements saw TH 11 scaled up through a series of increasing load cases to examine the plastic range of the brace. The time history or TH multiplier represents the number of times greater (rounded to the larger integer) a ground motion must be in order to bring the model to either yield or ultimate capacity.

It should be noted for this scaled analysis that the entire reinforce concrete moment frame model is linear with the exception of the link elements. When subjected to the deformations associated with the iterative analysis, it is expected that the concrete structure would neither remain linear nor survive these excessive ground motions required to achieve ultimate brace capacity. The function of iterative analysis is purely a tool to assess the approximate ultimate capacity of the BRBs so these may be applied to more effective capacity design. The point of yield of the brace was based purely on the braced dimensions and inner yield section geometry, while the tensile and compressive ultimate capacities are a determined by the friction and strain hardening factors: β and ω, that were derived as a part of the qualification testing, Following this initial iterative study, it was determined that the braces began to yield between 2 and 3 times TH 11 and continued to harden until braces started to fail between 19 and 20 times the design ground motion. These results of the initial iterative analysis are presented in Table 4.13 with a 20 times larger TH 11 ground motion presented in a link hysteresis for BR6 in Figure 4.21.

Table 4.13 – Brace NL response to TH 11

Brace	Factored Resistance Tr = Cr @ 248 MPa	TH 11 multiplier required to reach yield	Probable compressive ultimate resistance	Probable tensile ultimate resistance	TH 11 multiplier required to reach ultimate
	kN		kN	kN	
BR8	540	3	1,040	945	20
BR7	646	2	1,244	1,131	19
BR6	882	2	1,698	1,544	20
BR5	882	3	1,698	1,544	25

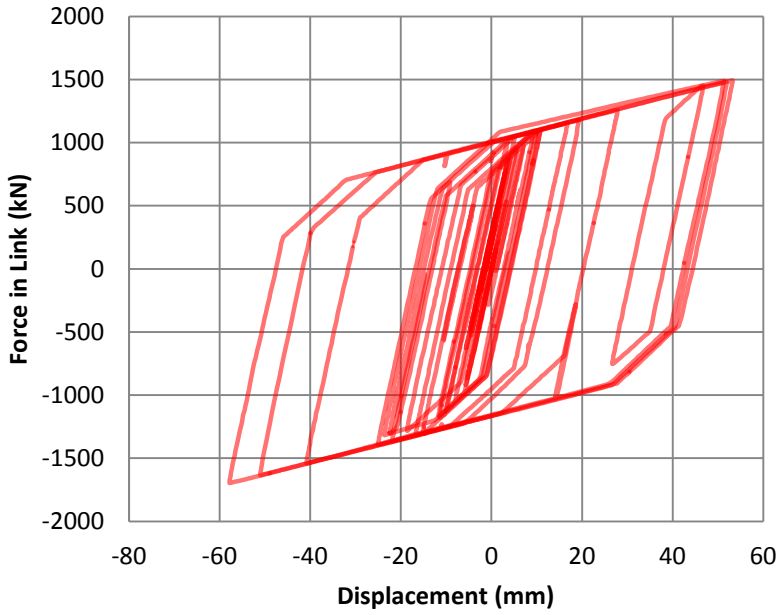

Figure 4.21 – BR6 20xTH11 Link Hysteresis

If the braces were constructed of 248 MPa steel they would perform elastically under a ground motion that is represented by the NBCC 2% probability of exceedance in a 50 year return period. The BRBF would not enter strain hardening until a seismic event of at least twice the intensity was experienced. As reported in Section 3.7, this research has confirmed that the design material was in fact not used in the construction of the Sawyer seismic upgrade. BRBs constructed out of either 350 or 450 MPa steel would not be expected to respond plastically until a seismic event of between three and five times greater than those prescribed by the NBCC return period. Table 4.14 presents the results of an iterative analysis using TH 11 for all steel grades including: 248, 350 and 450 MPa steel.

Table 4.14 – BRB iterative analyses for 248, 350 and 450 MPa steel

Brace	Inner yield material	Factored yield resistance	TH 11 multiplier required to reach yield	Probable compressive ultimate resistance	Probable tensile ultimate resistance	TH 11 multiplier required to reach ultimate
		kN		kN	kN	
BR8	248	540	3	-1,040	945	20
BR7	248	646	2	-1,244	1,131	19
BR6	248	882	2	-1,698	1,544	20
BR5	248	882	3	-1,698	1,544	25
BR8	350	762	4	-1,370	1,280	25
BR7	350	912	3	-1,640	1,532	24
BR6	350	1,245	3	-2,238	2,092	26
BR5	350	1,245	4	-2,238	2,092	32
BR8	450	980	5	-1,370	1,235	22
BR7	450	1,173	4	-1,640	1,478	22
BR6	450	1,601	4	-2,239	2,017	23
BR5	450	1,601	5	-2,239	2,017	32

This iterative analyses confirms that the BRBF, as built, will likely never perform plastically given the UHS for Kingston and are over strength to the point that they offer the structure a rigid bracing element, or ductility and over strength factors, $R_d = 1$ and $R_o = 1.3$. The CISC commentary to S16 addresses this very situation that in cases where the energy-dissipating elements have been oversized, a limit has been placed on the maximum forces that non-dissipating elements must resist by setting the maximum anticipated seismic load equal to that corresponding to R_d multiplied by $R_o = 1.3$. The SFRS for Sawyer Modules 1 and 2 were designed with $R_d = 3$ and $R_o = 1$ and now have an effective $R_d = 1$ and $R_o = 1.3$. This reduction in ductility is much better for the structure if displacements are to be controlled; however, if drift control was driving the design, a BRB would not be the most economical SFRS.

Another observation is related to the yield and failure envelopes for the different steel core materials. While the ultimate strengths of the 350 and 450 MPa steel braces are roughly the same, the larger yield envelope of the 350 MPa steel allows for further kinematic hardening and is able to withstand a ground motion two to three times greater than the 450 MPa brace. These results reinforce the requirements to specify and verify material properties throughout brace fabrication and the need for testing to ensure proper performance.

4.3.3.4 Bolted Connections

With a structure that is three times stiffer, the bolted connections were also reviewed to confirm the factored connection capacity. As previously discussed, this research does not examine the design and moment response of the connection system as it is a purely axial testing protocol and ignores the moments created at the end supports. The effects of different yield strengths have been discussed regarding the

performance of both BR6m and BR30m and a review of the bolted connection capacities was conducted. According to CSA S16 clause 27.8.4 [19] , the factored resistance of the brace shall be equal or greater than the probable tensile and compressive resistances, T_{ysc} and C_{ysc}, Equation 2.2 and Equation 2.3. Due to the additional friction factor applied to the compressive stroke, C_{ysc} governs the connection design. Taking into consideration the drastic increase in BRB capacity with the increase in steel yield strength, the capacities of the bolted connections were calculated using the guidelines set out in the 2009 CISC, Handbook of Steel Construction. The values highlighted in red in Table 4.15 correspond to connections that will yield before the inner yield section of the BRB enters strain hardening. The values in yellow correspond to the braces which have greater probable compressive resistance than the connection capacity, contrary to CSA S16 clause 27.8.4. These values are calculated using the results of the qualification testing and accounts for the friction and load sharing values associated with the compression stroke. Both friction and strain hardening factors are incorporated in the calculation of final connection capacity. These results are presented graphically for the six bolt connection and eight bolt connections in Figure 4.22 and Figure 4.23 respectively.

Table 4.15 – Bolted connection capacity

Brace	# Bolt Holes	A490 Double Shear[1]	Bolted Connection Capacity	Factored Resistance Tr=Cr @ 248 MPa	Probable Compressive Resistance Cysc[2]	Factored Resistance Tr=Cr @ 350 MPa	Probable Compressive Resistance Cysc	Factored Resistance Tr=Cr @ 450 MPa	Probable Compressive Resistance Cysc
		kN/Bolt	kN	kN	kN	kN	kN	kN	kN
BR1	8	284	2,272	882	1,703	1,245	2,238	1,601	2,239
BR2	8	284	2,272	882	1,703	1,245	2,238	1,601	2,239
BR3	6	284	1,704	646	1,247	912	1,640	1,173	1,640
BR4	6	284	1,704	540	1,042	762	1,370	980	1,370
BR5	8	284	2,272	882	1,703	1,245	2,238	1,601	2,239
BR6	8	284	2,272	882	1,703	1,245	2,238	1,601	2,239
BR7	6	284	1,704	646	1,247	912	1,640	1,173	1,640
BR8	6	284	1,704	540	1,042	762	1,370	980	1,370
BR9	8	284	2,272	1,726	3,332	2,436	4,380	3,132	4,381
BR10	8	284	2,272	1,726	3,332	2,436	4,380	3,132	4,381
BR11	6	284	1,704	1,439	2,777	2,030	3,650	2,610	3,651
BR12	6	284	1,704	1,439	2,777	2,030	3,650	2,610	3,651
BR13	8	284	2,272	992	1,915	1,400	2,517	1,800	2,518
BR14	8	284	2,272	992	1,915	1,400	2,517	1,800	2,518
BR15	6	284	1,704	646	1,247	912	1,640	1,173	1,640
BR16	6	284	1,704	646	1,247	912	1,640	1,173	1,640
BR17	8	284	2,272	1,260	2,432	1,778	3,197	2,286	3,198
BR18	8	284	2,272	1,260	2,432	1,778	3,197	2,286	3,198
BR19	6	284	1,704	1,260	2,432	1,778	3,197	2,286	3,198
BR20	6	284	1,704	1,260	2,432	1,778	3,197	2,286	3,198
BR21	8	284	2,272	1,726	3,332	2,436	4,380	3,132	4,381
BR22	8	284	2,272	1,439	2,777	1,778	3,650	2,610	3,651
BR23	6	284	1,704	1,008	1,945	1,423	2,557	1,829	2,558
BR24	6	284	1,704	1,260	2,432	1,778	3,197	2,286	3,198
BR25	8	284	2,272	1,726	3,332	2,436	4,380	3,132	4,381
BR26	8	284	2,272	1,726	3,332	2,436	4,380	3,132	4,381
BR27	8	284	2,272	1,726	3,332	2,436	4,380	3,132	4,381
BR28	8	284	2,272	1,726	3,332	2,436	4,380	3,132	4,381

Note [1] : Page 3-8, Table 3-4 CISC, 2010

Note [2] : Estimated β=1.1 and ω=1.75 based on typical results

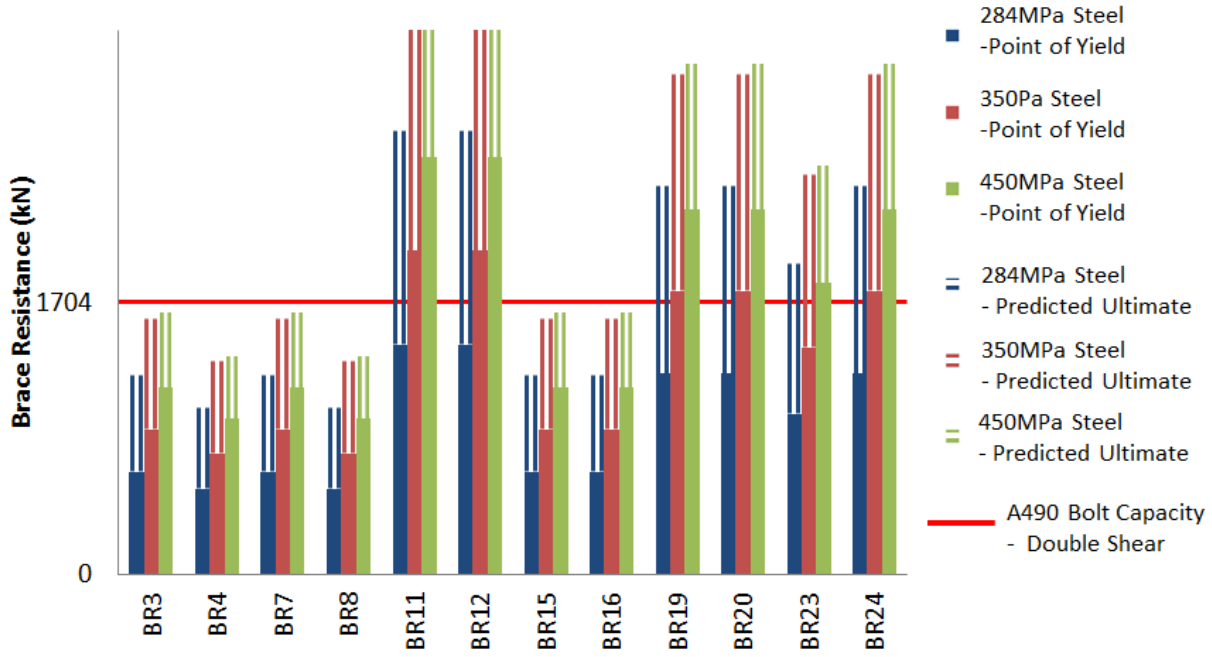

Figure 4.22 – 6 Bolt Connection Factored Resistance

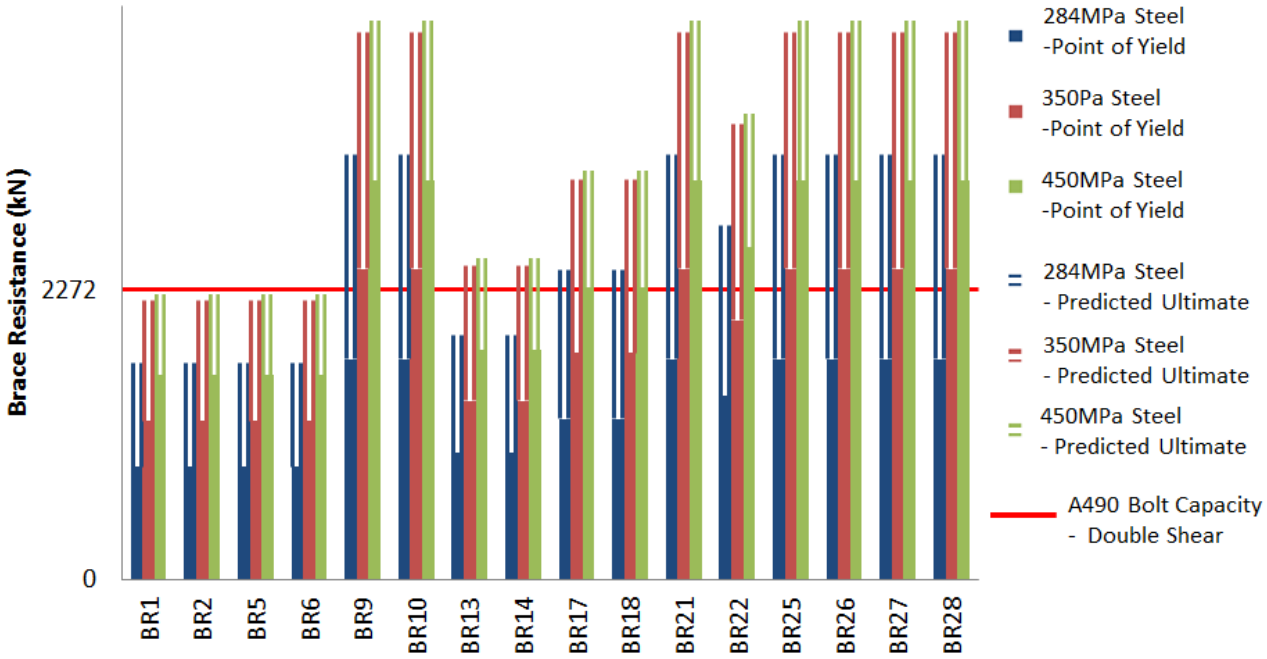

Figure 4.23 – 8 Bolt Connection Factored Resistance

The results of this connection capacity verification highlight a capacity deficit as the size of the brace and material yield strength increases. The connection capacity for the specified material cannot be strictly confirmed in this research. While there was no testing of the specified material, the similar construction along with the friction factor, β of both braces and the increased yield envelope of a typical

ASTM A32 specimen (Figure 3.26) provide sufficient information for reasonable estimates. The values for β and ω are estimated at 1.10 and 1.75 respectively. With these values, the probable compressive resistance for the specified ASTM A32 steel is estimated to be at least 1.93 times larger than the factored resistance. From this data, it is evident that the designed connections for this BRB system were never designed to incorporate the increased capacity due do friction or strain hardening, which is further compounded by the effects of load sharing. As previously discussed in the iterative analysis, the structure will likely never see a seismic event that would bring the BRBs to the point of yield and if it did, over half of the BRB connections would fail before the BRB would be able to perform plastically. This issue is only amplified with brace yield material that is higher than specified.

Another issue surrounding the connection detail is the presence of a capping plate at both ends of the brace with a13 mm allowance at either end of the BRB connections. This effectively allows for only 26 mm of compression stroke. In order to ensure maximum compression stroke, the capping plate was removed prior to testing. The profile of the actuator allowed it to run full un-encumbered cycles without engaging the outer steel casing in compression. The upper and lower design connections as seen in an excerpt from the structural drawings: Figure 4.24 and Figure 4.25 present the 26 mm compression allowance. The BRBs installed in modules 1 and 2 have the 13 mm top capping plates removed on all BRBs. This increases their effective compression stroke to 39mm. Figure 4.26 presents a clear image of a top connection missing the capping plate for BR6 in module 2, while Figure 4.27 presents an image of the bottom connection. The location and built up cladding surrounding the base connections make it difficult to get a clear view of the area; however, the lower capping plate is visible.

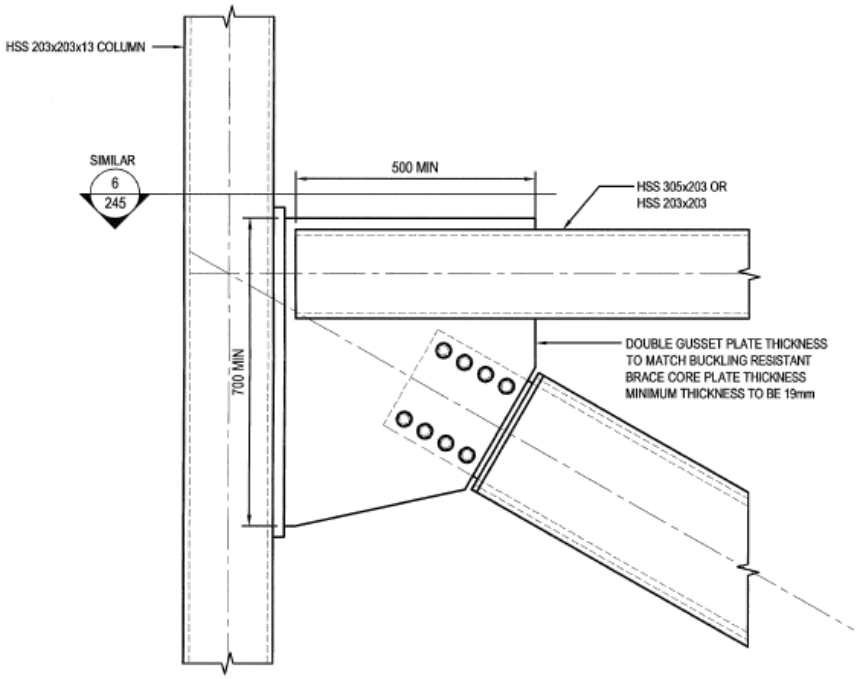

Figure 4.24 – Upper connection detail (Structural tender drawings, 2010)

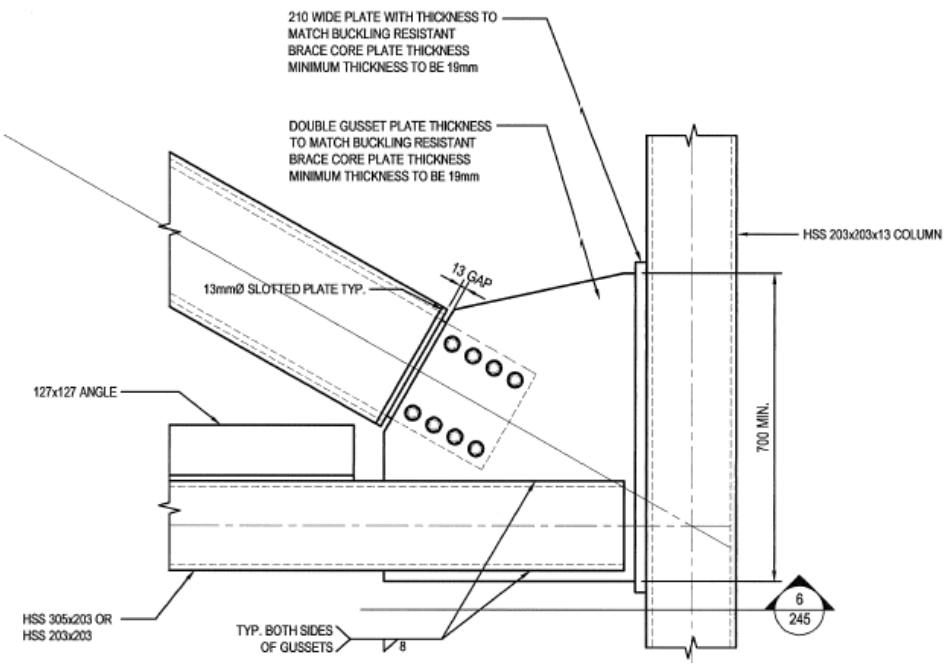

Figure 4.25 – Lower connection detail (Structural tender drawings, 2010)

Figure 4.26 – Upper connection installed

Figure 4.27 – Lower connection installed

If the connections were designed to survive a ground motion that excites the BRBs to the point of entering plastic strain hardening, the braces would not achieve the full range of the compression stroke due to the 39 mm compression stroke limit. Similar to the bolted connection, this compression limit affects a greater portion of the SFRS system and more of the structure as the yield capacity of the brace increases.

4.4. Summary of Modelling

The modelling outlined in this chapter reinforces the importance of qualification testing in order to determine the friction and strain hardening (ω and β respectively) and factors, which are critical to understanding the as-built brace performance. It also highlights the necessity of running a dynamic analysis to model the BRB hysteretic response, or lack thereof. While the NBCC allows for the EFSP to be used for this structure, the presence of a nonlinear SFRS requires a dynamic analysis in order to confirm the braces performance under an appropriate seismic ground motion time history.

From the results of both the static and dynamic analyses, it is clear that the as-built BRBs are in fact over strengthened to the point that they perform the function of a completely rigid SRFS. Using FNA, an iterative analysis was conducted to determine the seismic ground motion that would bring the BRBs into hysteretic dampening. It was determined that the range of braces, including those constructed using the specified 248 MPa steel would not start to yield until a seismic event of a least twice the specified amplitude of the NBCC UHS, which represents a 2% probability of exceedance in a 50 year return period. For braces constructed using 450 MPa steel, the ground motion would need to be five times larger. In addition to the effects of over strengthened braces, the bolted connections were identified as having capacity deficits once the ω and β factors were accounted for in the design. In the instance of the over strengthened braces, the bolted connections were designed for braces of much lower yield strength and would yield before many BRBs could begin to provide any hysteretic dampening, thus governing this SRFS as being rigid and elastic.

Although excessive over strengthening may not provide the most economical design for a ductile SFRS, the outcome, in this particular instance provides a completely safe and effective rigid SFRS. This unintentionally rigid SFRS greatly reduces inter-storey drifts by increasing the overall lateral stiffness of the entire structure.

Chapter 5: Conclusions

5.1 Summary

The research conducted on three BRBs as a part of the RMCC Sawyer Building seismic retrofit has provided valuable insight into the mechanics, design and testing of BRB systems. Further modelling using static and dynamic analyses of the un-braced structure, as-designed and as-built seismic force resisting systems provided valuable insight into the performance of the structure both pre and post-retrofit. While the first BRB (BR4) provided no useable strain hardening data, it did validate the effects of load sharing and re-emphasized the requirement for coupon testing. The inability to test BR4 within the limits of the 1,000 kN actuator reaffirmed the need to determine the exact material properties of each brace. Once a series of coupons were tested, both braces were trimmed to reach ultimate yield below 1,000 kN. The cyclic tests were conducted in accordance with the protocol outlined in the 2005 AISC seismic provisions for steel structures [2]. Following the cyclic testing, neither of the remaining two modified braces was able to achieve the required cumulative inelastic deformation of 200 times the yield deformation.

The results of the qualification testing produced two factors: strain hardening and friction factors (ω and β), which proved to be essential in modelling and analysis of the BRBs both statically and dynamically. The ω and β factors also played a role in understanding the effective tension and compression demands on the brace connections. The dynamic analysis used multi-linear kinematic plastic link elements with non-linear axial properties based on the data derived from the qualification testing. The dynamic analysis used five synthetic ground motions scaled to match the NBCC UHS.

It is assessed that the structure will remain linear and elastic, given the over-strengthened BRBs along with connection capacity and compressive cycle limits. In addition to the mechanical barriers that prohibit the braces from performing plastically, the forcing ground motion would have to be 2-5 times greater than prescribed by the NBCC UHS design. The design and construction of this seismic retrofit has effectively provided a rigid, non-ductile SRFS. This system inadvertently achieves a safe and effective method of providing a rigid and robust lateral support to this reinforced concrete moment frame.

5.2 Conclusions and Recommendations

5.2.1. Material Properties

Observation: The performance of a BRB is heavily dependent on the material properties, bonds and interfaces between all of the components of a BRB system. Proper coupon testing to confirm material properties is essential, in particular to verify the yield strength of the inner yield section. The inner yield section is the single most important design element of the BRB. The increased capacity of the brace as it enters plastic deformations is estimated by the guidelines for calculating the strain hardening and friction factors provided by the CISC steel code [19], which is determined from the testing protocol outlined in the AISC guidelines [2]. Since both BR6 and BR30 were constructed from material that exceeded the maximum allowable specification, they did not develop the required cumulative inelastic deformations required to satisfy the AISC guidelines.

Recommendation: Proper coupon testing of material properties must be conducted and a detailed account of material testing records must be kept prior to and during brace fabrication. In addition to specifying maximum yield strength, an ultimate strength should be prescribed in order to ensure proper development of a yield envelope, ensuring there exists adequate range for strain hardening.

5.2.2. Load Sharing

Observation: The effects of load sharing have proven to increase the overall capacity of the BRB, creating an overall brace capacity that is inflated by as much as 30%. Variation in the assembly and construction of BRBs can have a marked effect in the effects of load sharing with load sharing values of BR6m that are twice that of BR30m. If the qualification testing was performed on a single BRB where the assembly procedures minimized the effects of load sharing in a controlled environment, then the factors ω and β would underestimate the performance of further braces assembled in a less controlled environment. Further research into the causes of load sharing at these interfaces may help find mitigation techniques to reduce or eliminate the effects of excessive load sharing in the BRB system,

Recommendation: Develop standardized assembly techniques and inspection protocols in order to ensure similar fabrication and therefore, performance, across a series of BRB's. If the material properties and assembly techniques of BRBs are not verified, much of the engineering effort involved in specifying a BRB design may be negated by the marked increase in BRB capacity if the brace remains rigid and elastic.

5.2.3. Implementation of ω and β Factors

Observation: While the case may be rare where the implementation of a modern technology predates the adoption of relevant regulatory code, this scenario provides useful insight regarding the importance of qualification testing prior to installation. The results of the connection capacity verification highlight a capacity deficit as the size of the brace and material yield strength increases. Although the return period of a seismic event that would bring the BRBs to the point of yield is well outside the scope of concern from an NBCC perspective, over half of the BRB connections would fail before the BRB would be able to perform plastically.

Recommendation: Qualification must be conducted prior to final design and full brace production. The ω and β factors obtained from the qualification testing must be incorporated in to capacity design.

5.2.4. Connections

Observation: Although the moment resistance of the braces were not directly assessed as a part of this research, there were issues of localized buckling during the qualification testing. The design allows for 13 mm between the end of the connection and faces of the BRB capping plates, which will help limit the out of plane bending in the brace connections. The effects of brace moments can be all but eliminated if the connection plate was stiffened outside of the HSS outer steel casing. Another technique to reduce out of plane bending is to adapt perfectly pinned connections as detailed in the literature review. A second effect concerning the 13 mm clearance at each end of the BRB connection is the creation of a 26 mm limit on the compression stroke. This 26 mm limit, a function of the connection design, was increased to 39 mm with the removal of the upper 13 mm capping plate. If the connections were designed to survive a ground motion that excites the BRBs to the point of entering plastic strain hardening, the majority of as-built braces would not achieve the full range of the compression stroke due to the 39 mm compression stroke limit. Similar to the bolted connection, this compression limit affects more of the structure as the yield capacity of the brace increases.

Recommendation: BRB end connection should include out-of-plane stiffness and ensure adequate clearance for the compression cycle. Compression connection clearance must be able to accommodate full range of expected compression displacement in order to meet capacity design.

5.2.5. Ductility and Over strength

Observation: This research has confirmed that the SFRS system will likely never see a seismic ground motion of sufficient magnitude to force the BRBF to perform plastically. This is compounded by the extensive over strengthening of the BRBs to the point that they offer the structure a rigid bracing element, or an $R_d = 1$ and $R_o = 1.3$. The SFRS for Sawyer Modules One and Two were designed with $R_d = 3$ and $R_o = 1$ (it should be noted that NBCC 2009 uses $R_d = 4$ and $R_o = 1.2$ for BRBs) [20] and now have been reduced to $R_d = 1$ and $R_o = 1.3$. This reduction in ductility is in fact much better for the structure if displacements are to be controlled; however, if drift control was driving the design, a BRB may not have been the most appropriate SFRS as it requires drift to occur in order to commence strain-hardening. The over strengthening of the structure has highlighted the fact that a rigidly braced SFRS produces favourable results in limiting storey drifts and that even if a BRB system were to be implemented correctly, a rigid brace SFRS would be the more economical design for this particular application. The over strengthening of the BRBs in this upgrade has highlighted the fact that simpler, rigid lateral bracing would have also been effective at controlling inter-storey drifts.

Recommendation: More analysis should be conducted into modelling the performance of the un-braced structure to determine the best SFRS, if any, needed to be added to the moment resisting frame.

5.2.6. Analysis Options

Observation: FNA brings an essential level of fidelity in estimating a BRB's non-linear, hysteretic performance as well as confirming the overall structural response when hysteretic damping is involved. While the NBCC allows for the EFSP to be used for this structure, the presence of a non-linear SFRS and the use of the capacity design principles require an added level of analysis.

Recommendation: While it is not yet code mandated; a dynamic analysis should accompany any structural modeling where BRBs or any ductile, nonlinear SFRS are being implemented.

5.3. References

[1] Canadian Institute of Steel Construction, Handbook of Steel Construction, 2009.

[2] Ameriacn Institute of Steel Construction, Inc., Seismic Provisions for Structural Steel Buildings, 2005.

[3] M. Wakabayashi, T. Nakamura, A. Katagihara, H. Yogoyama and T. Morisono, "Experimental study on elastoplastastic behaviour of braces enclosed by precast concrete panels under horizontal cyclic loading," *Architectural Institute of Japan,* vol. 6, pp. 121-128, 1973.

[4] K. Kimura, K. Yoshizaki and T. Takeda, "Experimantal Study on braces encased by morter in filled steel tubes.," *Architectural Institute of Japan,* pp. 1623-1626, 1979.

[5] S. Mochizuki, Y. Murata, N. Andou and S. Takahashi, "Experimental study on unbonded braces under axial forces," *Architectural Institute of Japan,* pp. 1623-1626, 1979.

[6] G. Della Corte, M. D'Aniello, R. Landolfo and F. Mazzolani, "Review of Steel Buckling Restrained Braces," *Steel Construction,* vol. 4, no. 2, pp. 85-93, 2011.

[7] M. Iwata, T. Kato and A. Wada, "buckling-restrained braces as hysteretic dampers," *Proceeding of STESSA 2000,* pp. 33-38, 2000.

[8] I. D. Aiken, S. A. Mahin and P. Uriz, "Large-scale testing of buckling-restrained braced frames," in *Passive Controle Symposium; Tokyo Institute of Technology*, Japan, 2002.

[9] K. C. Tsai and P. C. Hsiao, "Pseudo-dynamic test of a full-scale CFT/BRB frame—Part II:," *Earthquake Engineering and Structural Dynamics,* vol. 37, pp. 1099-1115, 2008.

[10] L. A. Fahenstock, J. M. Ricles and R. Sause, "Experimental Evaluation of a large-scale buckling restrained brace frame," *American Society of Civil Engiineers, Journal of Structural Engineering,* vol. 133, pp. 1205-1214, 2007.

[11] R. Tremblay, "Testing and Design of Buckling Restrained Braces," *13th World Conference on Earthquake Engineering,* 2004.

[12] R. Tremblay, P. Bolduc, R. Neville and R. DeVall, "Seismic testing and performance of buckling-restrained bracing systems," *Canadian Journal of Civil Engineering,* vol. 33, no. 2, pp. 183-198, 2006.

[13] S. El-Baheya and M. Bruneau, "Buckling restrained braces as structural fuses for the seismic retrofit of reinforced concrete bridge bents," *Enginering Structures,* vol. 33, 2011.

[14] L. Di Sarno and G. Manfredi , "Seismic retrofitting with buckling restrained braces: Application to an existing non-ductile RC framed building," *Soil Dynamics and Earthquake Engineering,* vol. 30, 2010.

[15] K. Jinkoo and C. Hyunhoon , "Behavior and design of structures with buckling-restrained braces," *Engineering Structures,* vol. 26, 2004.

[16] L. Di Sarno and A. Elnashai, "Bracing systems for seismic retrofitting of steel frames," *Journal of Constructional Steel Research,* vol. 65, 2009.

[17] L. Di Sarno and G. Manfredi, "Bracing systems for seismic retrofitting of steel frames," *Journal of Constructional Steel Research,* vol. 65, 2009.

[18] Z. Junxian , W. Bin and O. Jinping, "A practical and unified global stability design method of buckling-restrained braces: Discussion on pinned connections," *Journal of Constructional Steel Research,* vol. 95, 2014.

[19] Canadian Institute of Steel Construction, Handbook of Steel Construction, Tenth Edition ed., 2012.

[20] *National Building Code of Canada,* 2010.

[21] G. Atkinson, "Earthquake Time Histories Compatible with the 2005 NBCC Uniform Hazard Spectrum," *Canadian Journal of Civil Engineering,* 25 Feb 2009.

[22] ASTM, *370-11a, Mechanical Testing of Steel Products.*, West Conshohocken, Pennsylvania.

[23] CSA, *G40.21, Welding and Structural Metals,* CSA, 1978.

[24] Chen, Hsiao, La and Liaw, "Application of low yield strength steel on controlled plastification ductile concentrically brace frames," *Canadian Journal of Civil Engineering,* vol. 28, pp. 823-836, 2001.

[25] R. Tremblay, D. G and B. J, "Seismic Rehabilitationof a four-story building with a stiffened bracing system.," in *8th Canadian Conference on Earthquake Engineering,* Vancouver, B.C., 1999.

[26] CSI America, "CSI Technical Knowledge Base," CSI, 31 March 2014. [Online]. Available: https://wiki.csiamerica.com/pages/viewpage.action?pageId=9536464. [Accessed 31 March 2014].

[27] Cement Association of Canada, *Concrete Design handbook,* 2008.

[28] Wilson, Yuan and Dickens, "Dynamic analysis by direct superposition of Ritz vectors," *Earthquake Engineering & Structural Dynamics,* vol. 10, no. 6, p. 813–821, 1982.

[29] E. L. Wilson, Static and Dynamic Analysis of Structures, Berkeley, CA, 2004.

[30] E. Bentz, "Response 2000," University of Toronto, 2010. [Online]. Available: http://www.ecf.utoronto.ca/~bentz/r2k.htm. [Accessed 10 Nov 2014].

Appendix A – Select Structural Drawings (c. 2008)

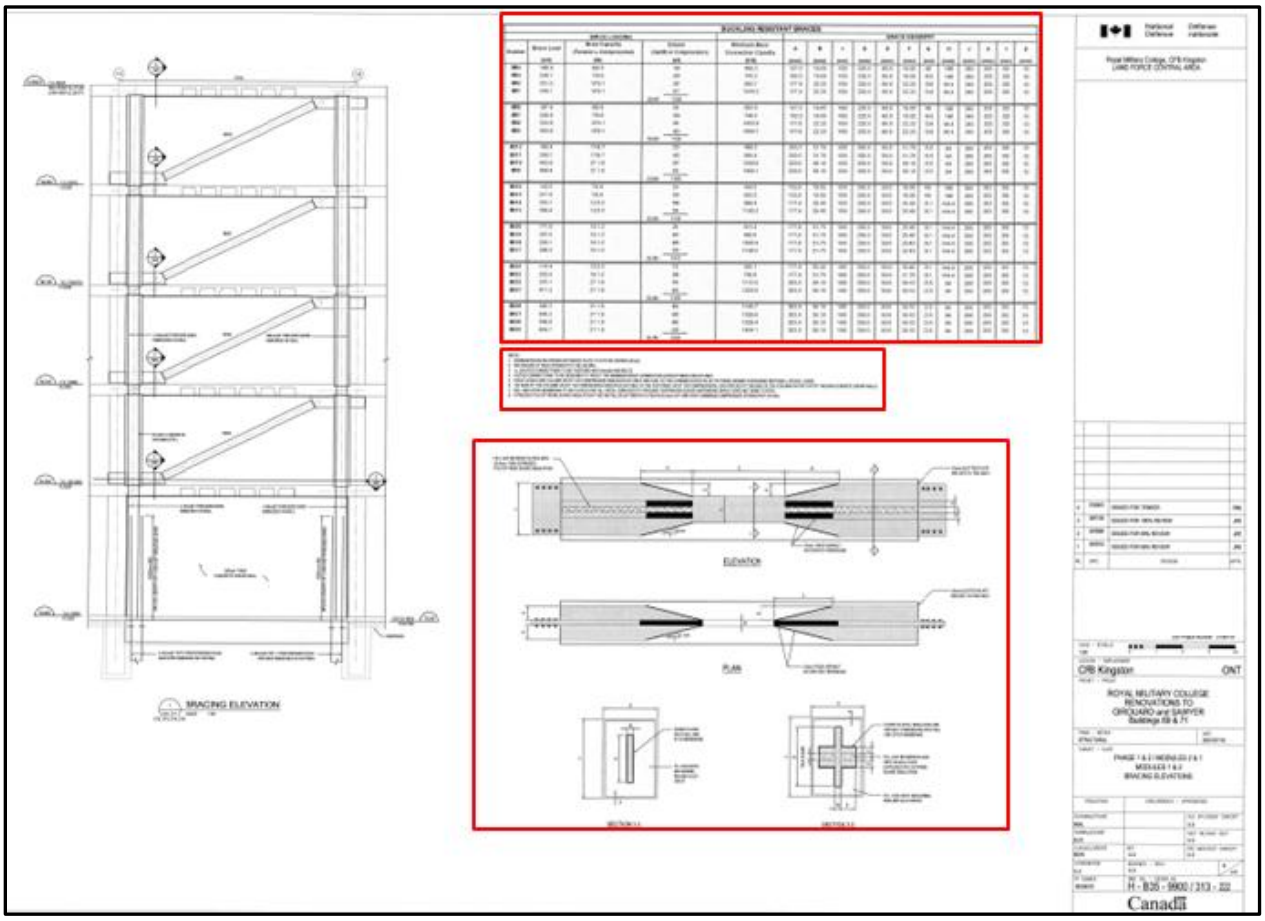

NOTES:
1. MAXIMUM BUCKLING RESISTANT BRACE PLATE YIELD TO BE 248 MPa (36 ksi).
2. HSS 305x203x13 YIELD STRENGTH TO BE 350 MPa.
3. ALL BOLTED CONNECTIONS TO BE FASTENED WITH 19mmØ A490 BOLTS.
4. BOLTED CONNECTIONS TO BE DESIGNED TO RESIST THE MINIMUM BRACE CONNECTION CAPACITY INDICATED IN TABLE.
5. BRACE LOADS AND COLUMN UPLIFT OR COMPRESSION INDICATED IN TABLE ARE DUE TO THE COMBINED EFFECTS OF FACTORED SEISMIC FORCES AND NOTIONAL LATERAL LOADS.
6. THE SUM OF THE COLUMN UPLIFT OR COMPRESSION INDICATED IN TABLE IS THE FACTORED UPLIFT OR COMPRESSION LOAD APPLIED AT THE BASE OF THE COLUMN ON THE TOP OF THE NEW CONCRETE SHEAR WALLS.
7. PEEL AND STICK MEMBRANE TO BE PLACED OVER ALL STEEL SURFACES TO PROVIDE CONTINUOUS SLEEVE AND ENSURE GROUT DOES NOT BOND TO STEEL.
8. EXTRUDED POLYSTYRENE BOARD INSULATION TO BE INSTALLED BETWEEN PLATES IN 50.8mm GAP AND HAVE A MINIMUM COMPRESSIVE STRENGTH OF 210 kPa.

BRACE LOADING					BRACE GEOMETRY											
Number	Brace Load (kN)	Brace Capacity (Tension & Compression) (kN)	Column (Uplift or Compression) (kN)	Minimum Brace Connection Capacity (KN)	A (mm)	B (mm)	C (mm)	D (mm)	E (mm)	F (mm)	G (mm)	H (mm)	J (mm)	X (mm)	Y (mm)	Z (mm)
BR4	166.4	660.5	199	499.2	127.0	19.05	1000	225.0	60.0	19.05	49	196	240	203	305	13
BR3	246.7	790.6	296	740.2	152.0	19.05	1000	225.0	60.0	19.05	36.5	146	240	203	305	13
BR2	331.2	1079.1	397	993.7	177.8	22.23	1000	225.0	60.0	22.23	23.6	94.4	240	203	305	13
BR1	348.1	1079.1	417	1044.2	177.8	22.23	1000	225.0	60.0	22.23	23.6	94.4	240	203	305	13
			SUM 1309													
BR8	167.5	660.5	201	502.5	127.0	19.05	1000	225.0	60.0	19.05	49	196	240	203	305	13
BR7	248.8	790.6	298	746.5	152.0	19.05	1000	225.0	60.0	19.05	36.5	146	240	203	305	13
BR6	334.6	1079.1	401	1003.9	177.8	22.23	1000	225.0	60.0	22.23	23.6	94.4	240	203	305	13
BR5	353.6	1079.1	424	1060.7	177.8	22.23	1000	225.0	60.0	22.23	23.6	94.4	240	203	305	13
			SUM 1324													
BR12	165.4	1759.7	232	496.2	203.0	31.75	1000	250.0	50.0	31.75	23.5	94	200	203	305	13
BR11	288.1	1759.7	403	864.4	203.0	31.75	1000	250.0	50.0	31.75	23.5	94	200	203	305	13
BR10	433.6	2111.6	607	1300.9	203.0	38.10	1000	250.0	50.0	38.10	23.5	94	200	203	305	13
BR9	486.4	2111.6	681	1459.1	203.0	38.10	1000	250.0	50.0	38.10	23.5	94	200	203	305	13
			SUM 1923													
BR16	143.5	790.6	201	430.5	152.0	19.05	1000	250.0	50.0	19.05	49	196	200	203	305	13
BR15	217.8	790.6	305	653.5	152.0	19.05	1000	250.0	50.0	19.05	49	196	200	203	305	13
BR14	333.1	1233.0	466	999.4	177.8	25.40	1000	250.0	50.0	25.40	36.1	144.4	200	203	305	13
BR13	388.4	1233.0	544	1165.3	177.8	25.40	1000	250.0	50.0	25.40	36.1	144.4	200	203	305	13
			SUM 1516													
BR20	171.8	1541.2	241	515.4	177.8	31.75	1000	250.0	50.0	25.40	36.1	144.4	200	203	305	13
BR19	287.5	1541.2	403	862.6	177.8	31.75	1000	250.0	50.0	25.40	36.1	144.4	200	203	305	13
BR18	335.1	1541.2	469	1005.4	177.8	31.75	1000	250.0	50.0	25.40	36.1	144.4	200	203	305	13
BR17	399.3	1541.2	559	1198.0	177.8	31.75	1000	250.0	50.0	25.40	36.1	144.4	200	203	305	13
			SUM 1672													
BR24	114.4	1233.0	137	343.1	177.8	25.40	1000	250.0	50.0	25.40	36.1	144.4	200	203	305	13
BR23	233.5	1541.2	280	700.6	177.8	31.75	1000	250.0	50.0	31.75	36.1	144.4	200	203	305	13
BR22	370.1	2111.6	444	1110.4	203.0	38.10	1000	250.0	50.0	38.10	23.5	94	200	203	305	13
BR21	411.3	2111.6	493	1233.9	203.0	38.10	1000	250.0	50.0	38.10	23.5	94	200	203	305	13
			SUM 1353													
BR28	380.2	2111.6	494	1140.7	203.0	38.10	1000	250.0	50.0	38.10	23.5	94	200	203	305	13
BR27	465.2	2111.6	605	1395.6	203.0	38.10	1000	250.0	50.0	38.10	23.5	94	200	203	305	13
BR26	509.8	2111.6	663	1529.4	203.0	38.10	1000	250.0	50.0	38.10	23.5	94	200	203	305	13
BR25	484.7	2111.6	630	1454.1	203.0	38.10	1000	250.0	50.0	38.10	23.5	94	200	203	305	13
			SUM 2392													

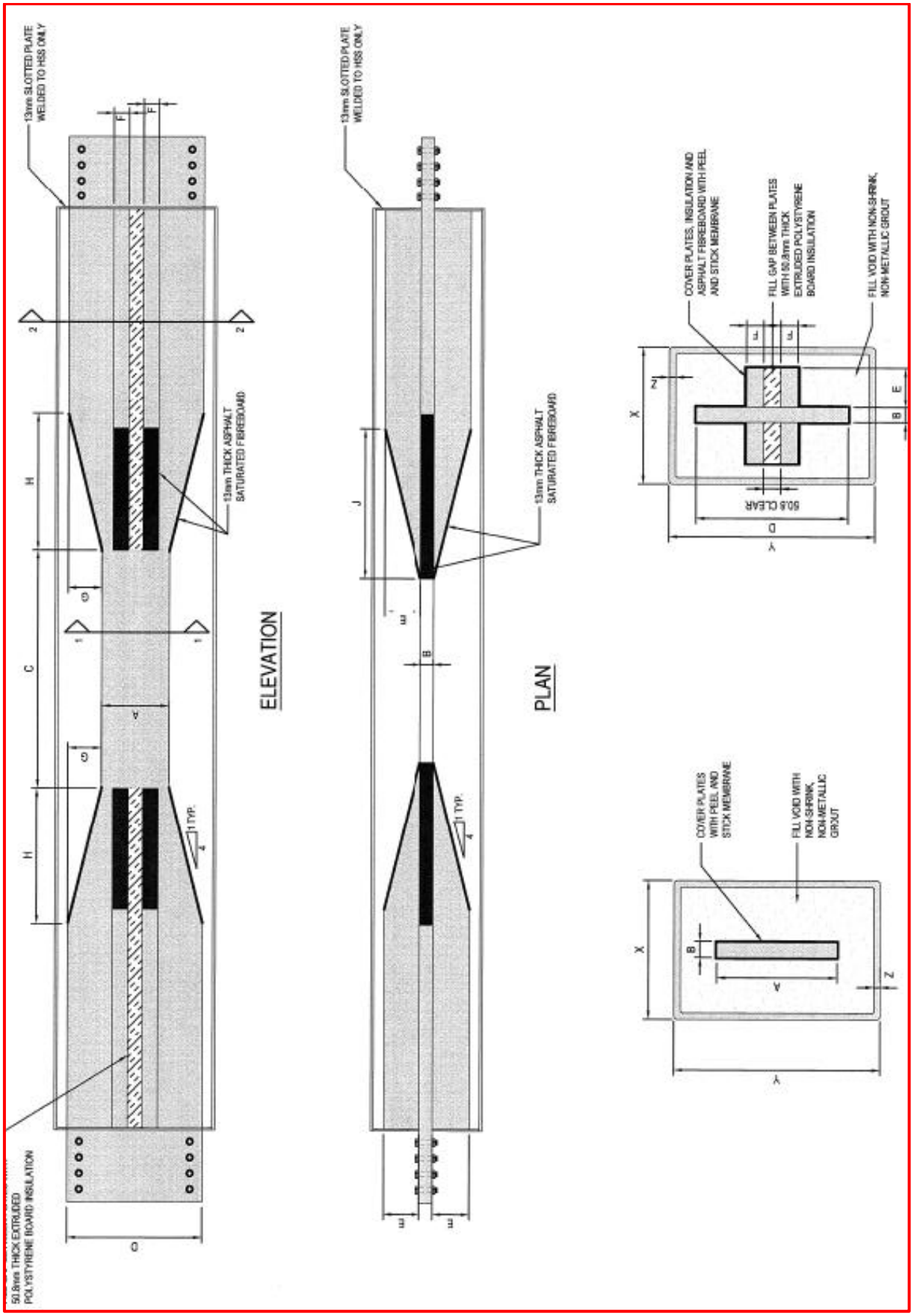
13mm SLOTTED PLATE WELDED TO HSS ONLY
13mm THICK ASPHALT SATURATED FIBREBOARD
50.8mm THICK EXTRUDED POLYSTYRENE BOARD INSULATION
ELEVATION
PLAN
COVER PLATES, INSULATION AND ASPHALT FIBREBOARD WITH PEEL AND STICK MEMBRANE
FILL GAP BETWEEN PLATES WITH 50.8mm THICK EXTRUDED POLYSTYRENE BOARD INSULATION
FILL VOID WITH NON-SHRINK, NON-METALLIC GROUT
50.8 CLEAR
COVER PLATES WITH PEEL AND STICK MEMBRANE
FILL VOID WITH NON-SHRINK, NON-METALLIC GROUT

Appendix B – Original Structural Drawings (c. 1972)

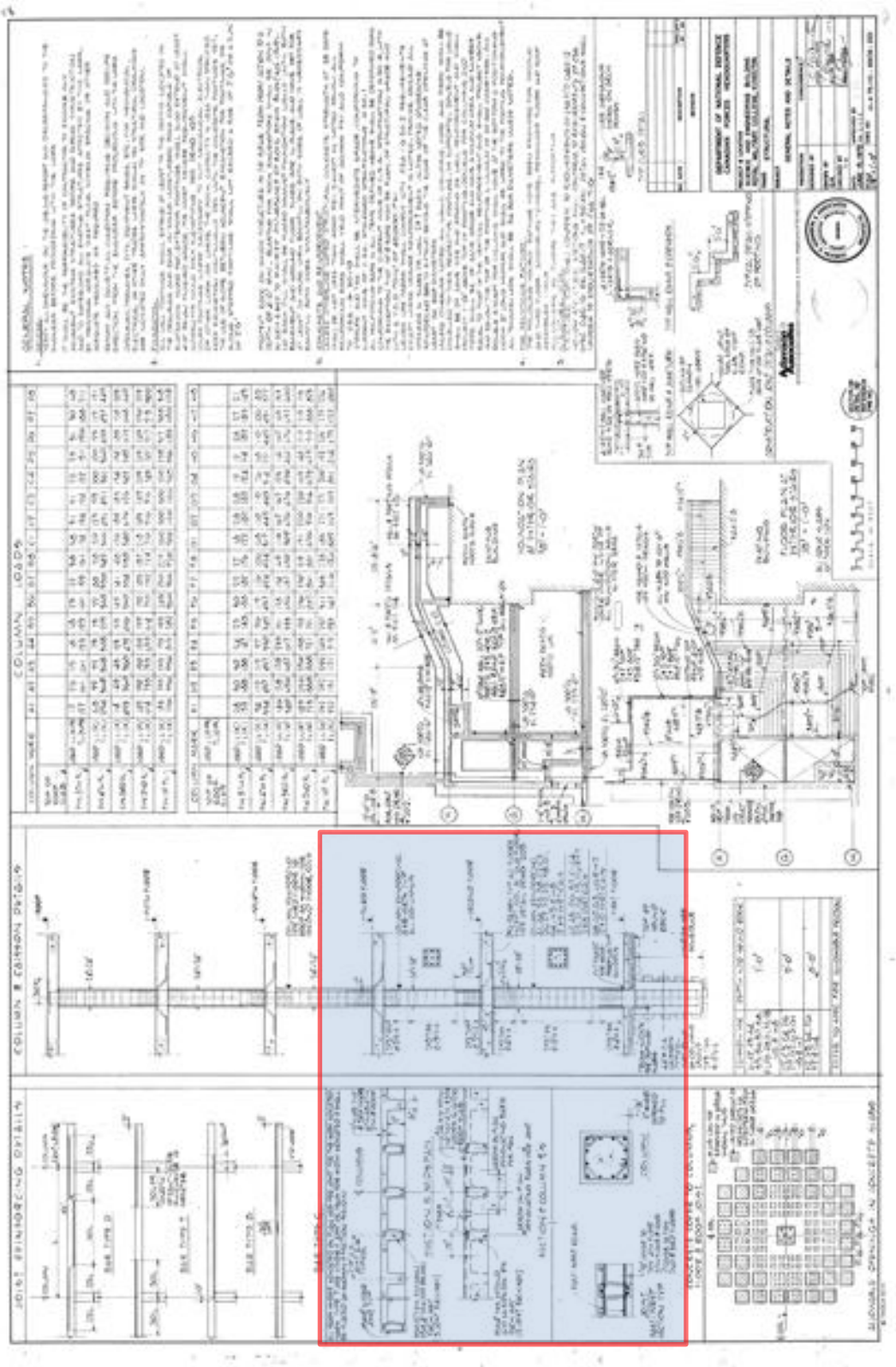

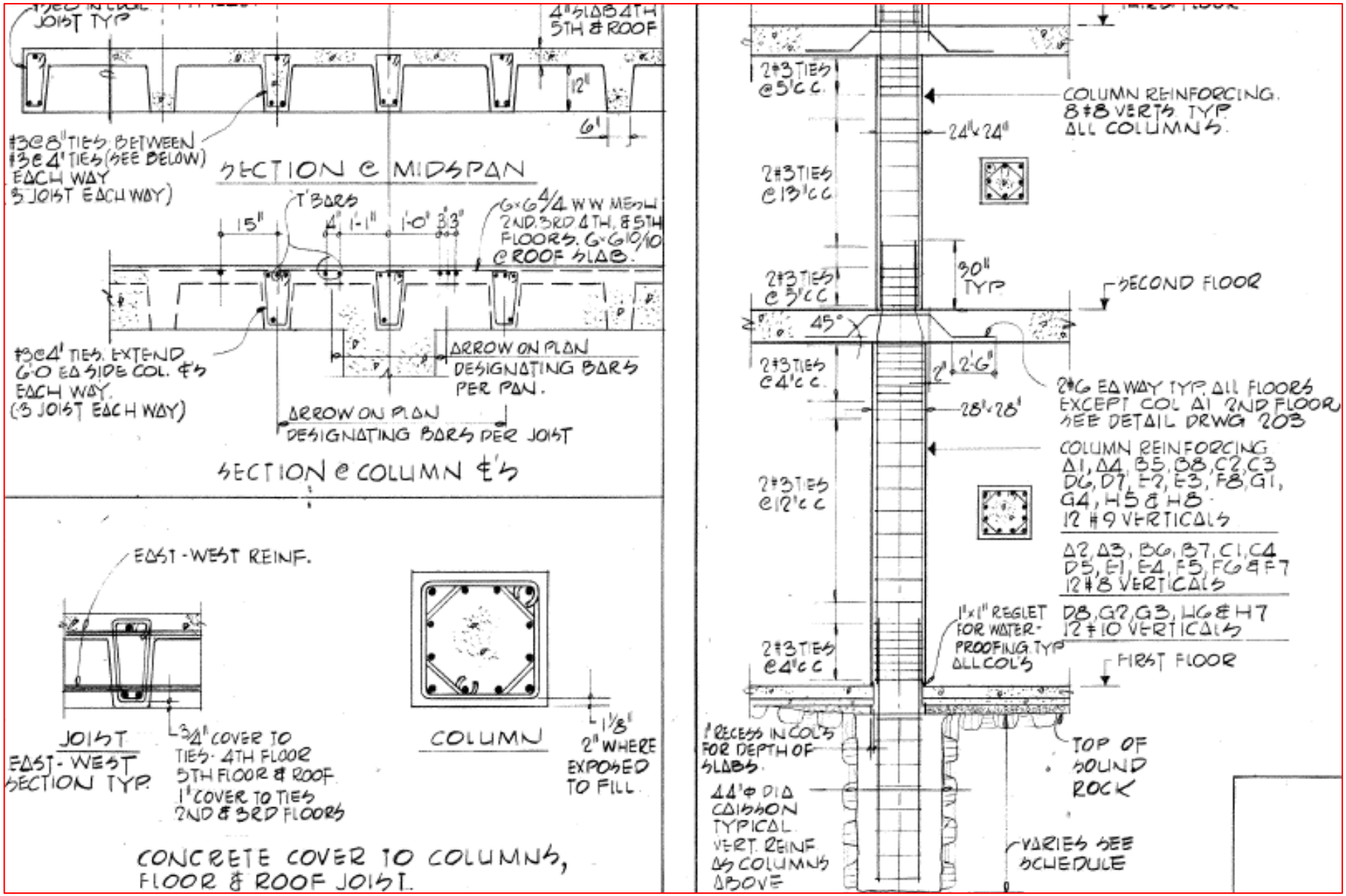
JOIST TYP
4" SLAB 4TH 5TH & ROOF
12"
6'
#3@8" TIES BETWEEN #3@4' TIES (SEE BELOW) EACH WAY (3 JOIST EACH WAY)
SECTION @ MIDSPAN
T BARS
15"
4"
1'-1"
1'-0"
3'3"
6x6 4/4 WW MESH 2ND, 3RD 4TH, & 5TH FLOORS. 6x6 10/10 @ ROOF SLAB.
#3@4' TIES. EXTEND 6'-0 EA SIDE COL. ℄s EACH WAY. (3 JOIST EACH WAY)
ARROW ON PLAN DESIGNATING BARS PER PAN.
ARROW ON PLAN DESIGNATING BARS PER JOIST
SECTION @ COLUMN ℄s
EAST-WEST REINF.
JOIST EAST-WEST SECTION TYP.
3/4" COVER TO TIES 4TH FLOOR 5TH FLOOR & ROOF
1" COVER TO TIES 2ND & 3RD FLOORS
COLUMN
1 1/8" 2" WHERE EXPOSED TO FILL
CONCRETE COVER TO COLUMNS, FLOOR & ROOF JOIST.
2#3 TIES @5' C.C.
2#3 TIES @13' C.C.
2#3 TIES @5' C.C.
2#3 TIES @4' C.C.
2#3 TIES @12' C.C.
2#3 TIES @4' C.C.
COLUMN REINFORCING. 8#8 VERTS. TYP ALL COLUMNS.
24"x24"
30" TYP
SECOND FLOOR
45°
2'-6"
2#6 EA WAY TYP. ALL FLOORS EXCEPT COL A1 2ND FLOOR SEE DETAIL DRWG 203
28"x28"
COLUMN REINFORCING
A1, A4, B5, B8, C2, C3 D6, D7, E2, E3, F8, G1, G4, H5 & H8 · 12 #9 VERTICALS
A2, A3, B6, B7, C1, C4 D5, E1, E4, F5, F6 & F7 12#8 VERTICALS
D8, G2, G3, H6 & H7 12#10 VERTICALS
1"x1" REGLET FOR WATER-PROOFING TYP ALL COLS
FIRST FLOOR
1' RECESS IN COLS FOR DEPTH OF SLABS.
44"Φ DIA CAISSON TYPICAL VERT. REINF AS COLUMNS ABOVE
TOP OF SOUND ROCK
VARIES SEE SCHEDULE

Appendix C – Colum Moment and Axial Force Resistance Check

In this particular structure, the governing column moments are generated by the lateral forces. For the un-braced module used in this analysis, a moment and axial load verification was conducted in order to assess the buildings un-braced response prior to the seismic upgrade. From the Buildings original structural drawings (Appendix B), the column reinforcement for the two column sizes are presented in Figure C.5.1 and Figure C.5.2. The moment resistances for the columns were calculated using the Response 2000 reinforced concrete analysis program [30].

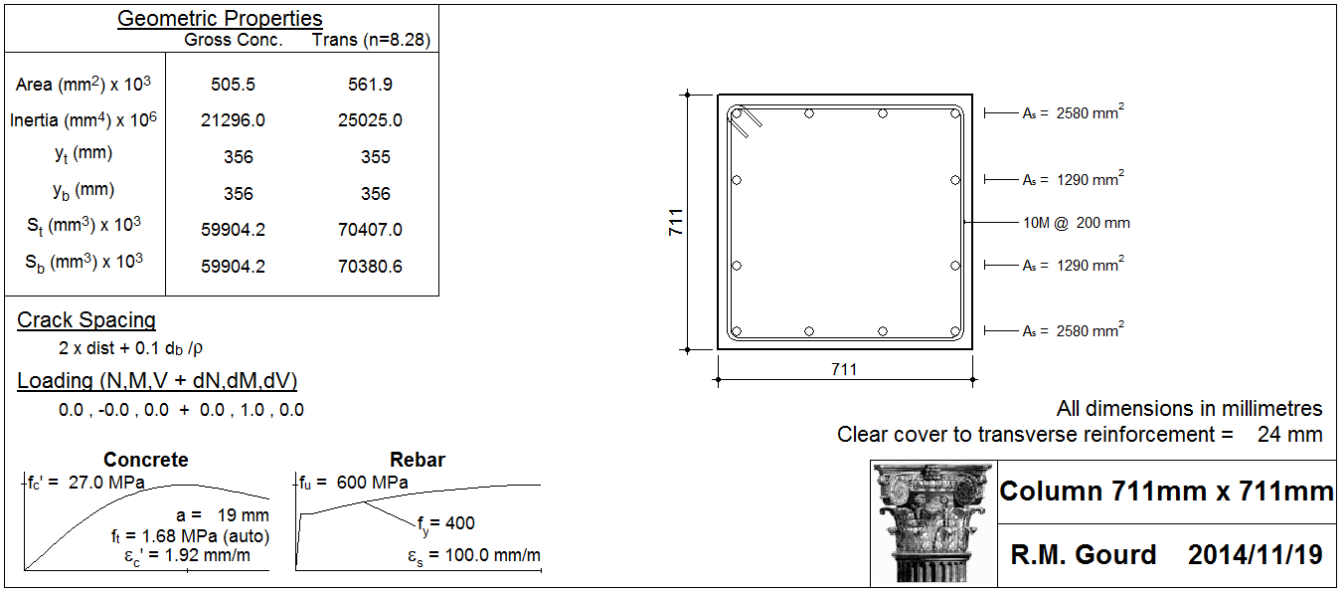

Figure C.5.1 – Column Detail (711m x 711mm)

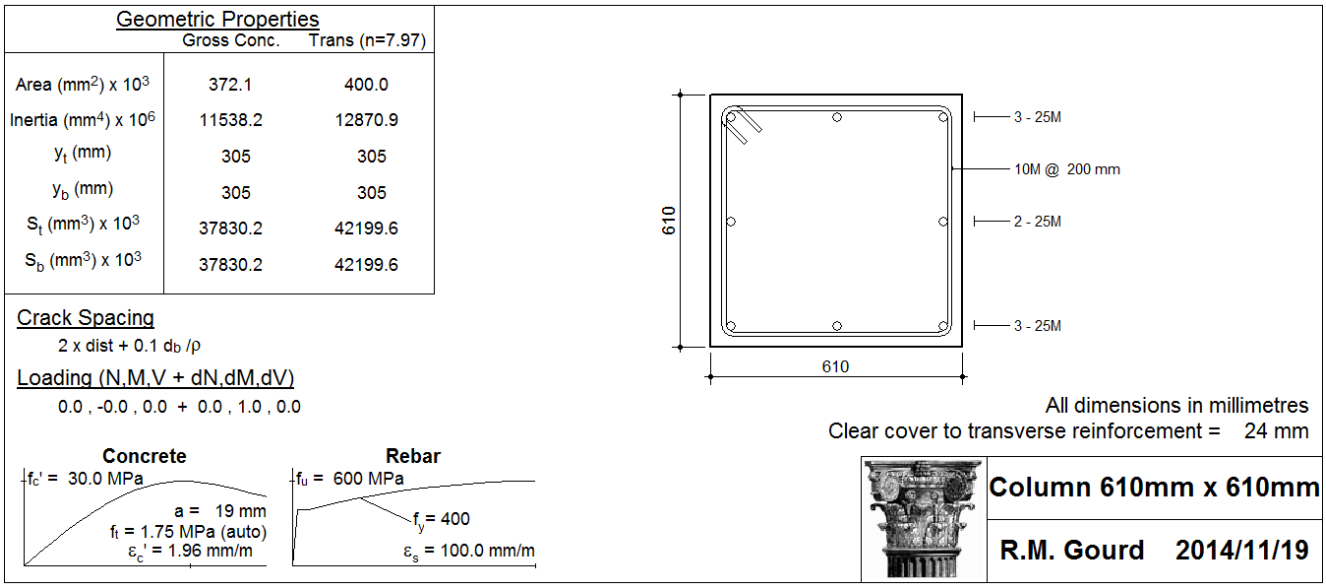

Figure C.5.2 – Column Detail (610m x 610mm)

After running the range of NBCC prescribed load cases in the FEA program, the dominating static load case for the column moments is that of the ESFP. This load case applies gravity loads including dead, superimposed dead, and 25% of the maximum snow load, along with the lateral loads derived from the ESFP in Appendix D. The bending moment diagram and axial force diagram for the columns are presented in Figure C.5.3.

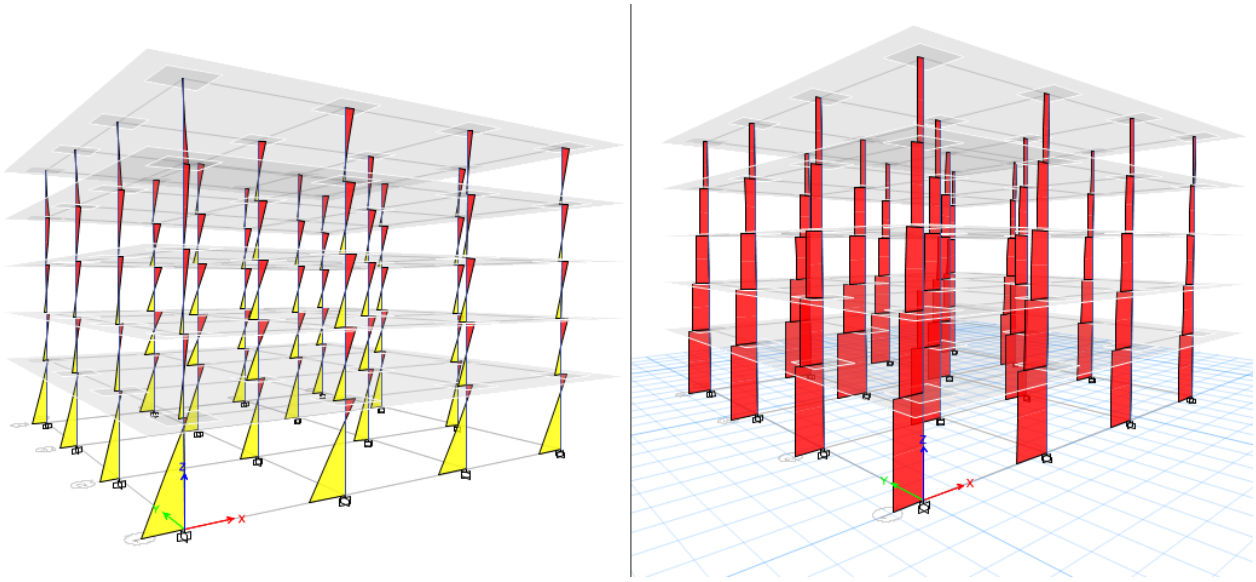

Figure C.5.3 – Factored column moment and axial load diagrams.

The maximum factored bending moments and axial loads for each column type were compared against the maximum moment and axial resistance. In addition to the moments generated by the lateral loads, the P-δ effects were also incorporated. These effects apply a moment generated by the eccentric axial loading caused by the lateral storey displacements. These resistance values were calculated using the Response 2000 program with a summary for both columns presented in Figure C.5.4 and Figure C.5.6. The results of the factored resistances and forces are presented in Table C.5.1. Moment interaction diagrams are presented in Figure C.5.5 Figure C.5.7

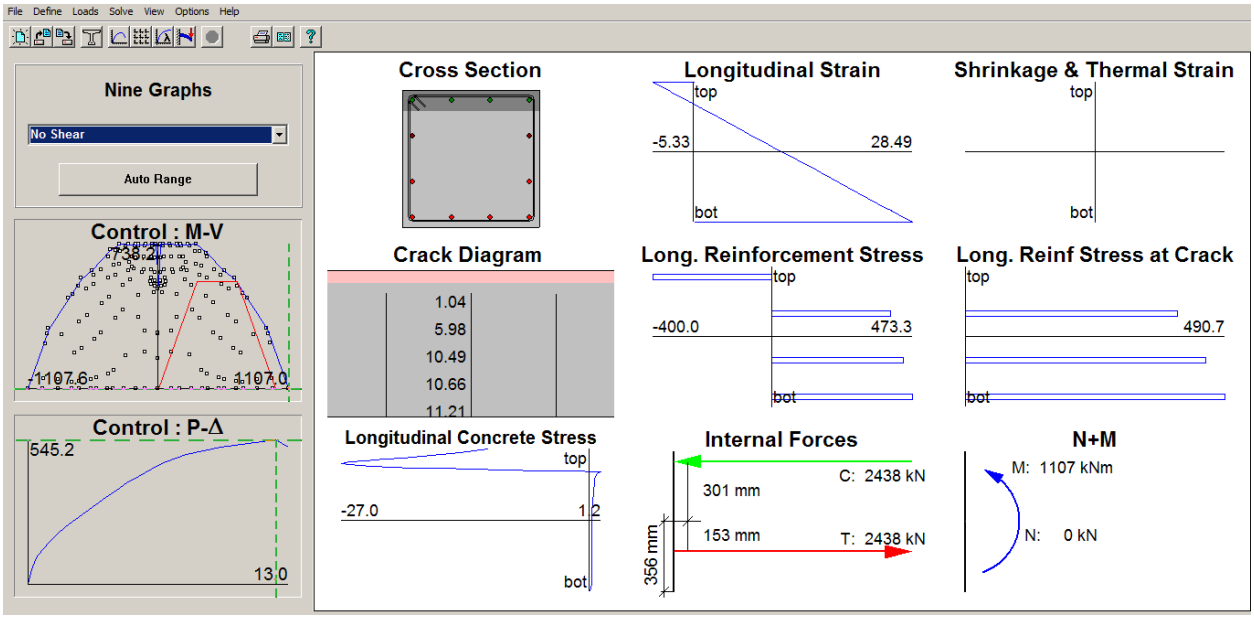

Figure C.5.4 – Moment Resistance Formulation (711 mm x 711 mm)

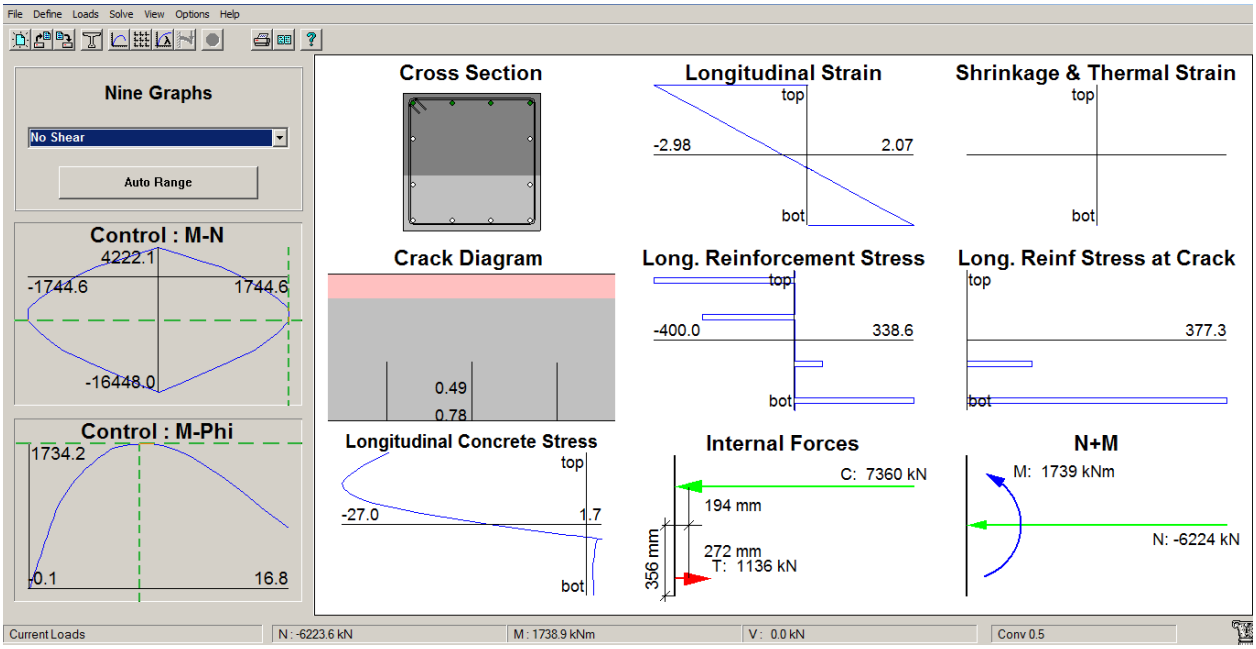

Figure C.5.5 – Moment axial load interaction (711 mm x 711 mm)

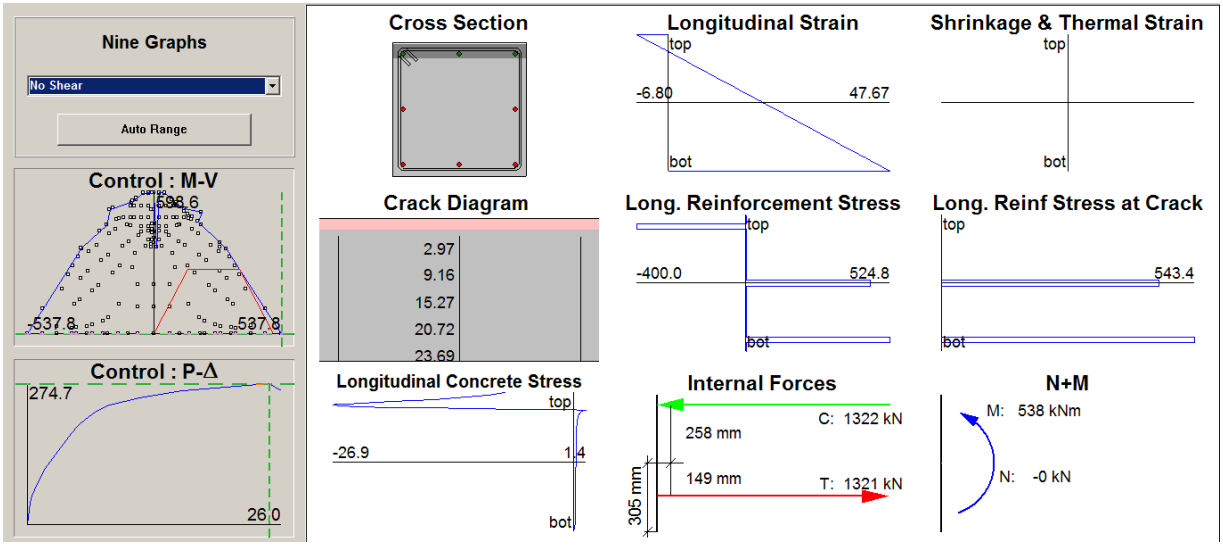

Figure C.5.6 – Moment Resistance Formulation (610 mm x 610 mm)

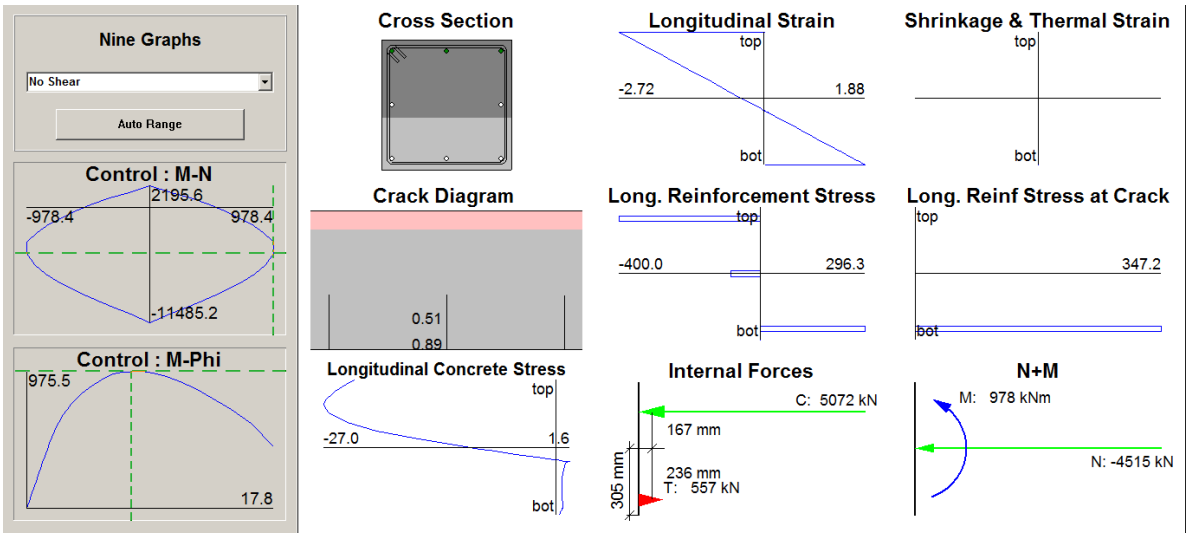

Figure C.5.7 – Moment axial load interaction (711 mm x 711 mm)

Table C.5.1 – Factored load and resistance for column moment and axial forces

Column dimensions	Mr	Mf	Mf (P-δ)	Pr_{max}	Pf
mm	kNm	kNm	kNm	kN	kN
711x711	1,107	758	804	13,158	2,965
610x610	537	293	302	9,188	2,881

Summary

The findings of this column verification determined that there is no axial or bending moment deficit due to seismic loads. Even when considering P-δ effects, the moment resistance is at its lowest point, 35% larger than the maximum factored bending moment created by the static application of the NBCC prescribed earthquake loads. In addition, the moment resistances were calculated based on the cross sectional properties of the RC section only. When the large gravity loads are applied to the columns as compressive forces, the moment resistance increases. The gravity loads applied by the dead and superimposed dead loads provides additional bending moment capacity to each column.

The moment interaction diagrams present a balanced nominal position, where the column achieves a maximum moment resistance at a specified axial load. These values are presented in Table C.5.2

Table C.5.2 – Moment-axial interaction balanced nominal values

Column Dimension	Moment-Axial Interaction	
	M	P
mm	kNm	kN
711x711	1,739	6,224
610x610	978	4,515

Appendix D – Equivalent Static Force Procedure

Design Spectra

The first step in the ESFP was to determine the soil classification for the building site as well as the spectral accelerations for the city of Kingston in accordance with the NBCC geographic seismic data. The five modules of the Sawyer building stretches across a divide in soil classifications. Modules 1 and 2 are sighted on original, undisturbed rock, while modules 3, 4, and 5 are sighted on reclaimed parts of Navy Bay. The soil in this particular location tends to be largely comprised of compacted fill, earning it the soil classification C. The design response spectrum for Kingston, Ontario is presented in Figure D.5.8. Given that acceleration based site coefficient, Fa is a function of soil classification and is set as 1.0 for soil class C and 0.7 for soil class B, the first condition of the ESFP mentioned in the modelling overview is met.

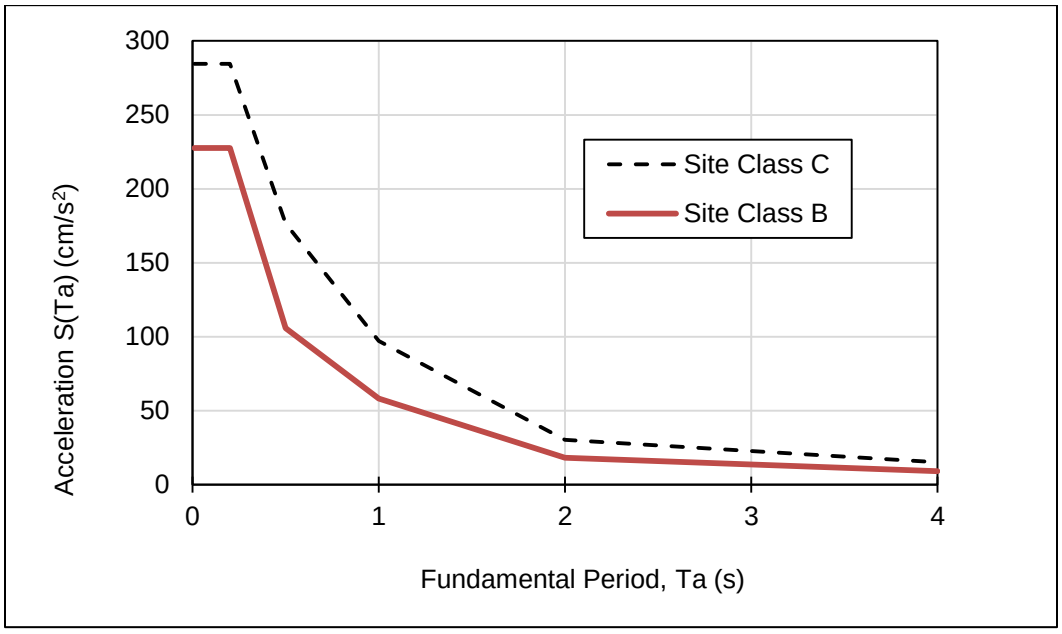

Figure D.5.8 – Kingston, On. Design Response Spectrum

Fundamental Period

In order to estimate the fundamental building period of a single module, a full 3D FE model was developed using frame and shell elements. The single module dimension and properties listed in Table D.5.3, with a fully extruded view of the waffle slab and column frame in Figure D.5.9.

Table D.5.3 – FE model details

Model Components	
Column 1st floor	0.711m x 0.711m
Column 2nd, 3rd ,4th and 5th floor	0.610 m × 0.610m
Storey height 1st floor	5.03 m
Storey height 2nd, 3rd ,4th and 5th floor	3.81 m
Column spacing	9.144 m in X and Y directions

Slab thickness 2nd and 3rd floor	0.102 m
Slab thickness 3rd, 4th and 5h floor	0.127 m
Slab dimension	32.8 m × 32.8m
Waffle dimension	0.305 m × 0.152 m
Waffle spacing	0.610 m in X and Y directions
Drop panel dimensions	2.58 m × 2.58 m
Drop panel depth 2nd and 3rd floor	0.406 m
Drop panel depth 3rd, 4th and 5h floor	0.433 m
Concrete unit weight (Including reinforcement)	24 kN/m³

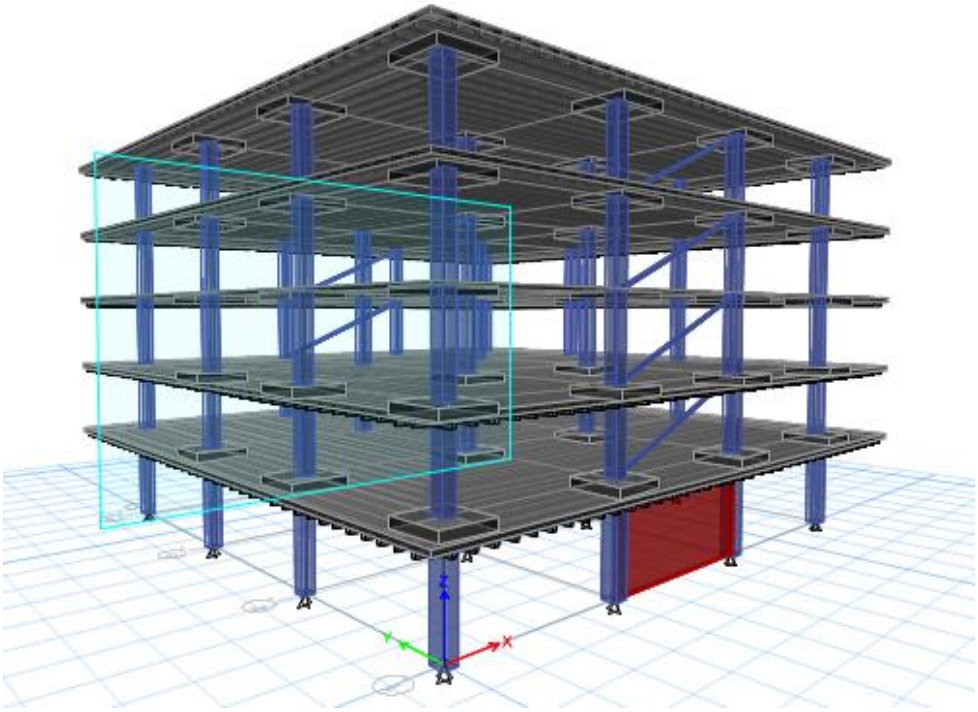

Figure D.5.9 – 3D FE model

Once the model was constructed, the FEA program generated the modal periods and frequencies for both directions. Due to symmetry within the model, the fundamental building period, T_a was found to be 0.721 s in both the East-West and North-South directions. According to NBCC 4.1.8.7(3) the rational method states that braced frames may not exceed 2.0 x T_a empirical, which is defined as 0.025 times the building height, in this case, 20.27 m; therefore, T_a of 0.721 s governs and the second condition of the ESFP is also met.

Seismic Weight and Base Shear

With the 3D model developed, the seismic weight can be easily calculated by storey. In addition to the dead weight of the building, the superimposed dead weight as well as 25% of the snow load must also be applied to the structure in order to capture an accurate seismic weight. Table D.5.4 presents all of the pertinent dead, superimposed dead and snow loads as found in the NBCC.

Table D.5.4 – Dead, superimposed dead and snow loads

Loads	
Dead Load	FEA program generated
Snow Load	2.1 kPa
Utilities / Mechanical	0.4 kPa
Building Partitions	1.0 kPa
Roofing and Insulation	0.5 kPa

With an accurate 3D model the storey heights and masses were summed in order to determine the total seismic weight of the building. The seismic weight included the dead load, superimposed dead load and a 25% snow load. This storey data is presented in Table D.5.5. The base shear, the ductility and over strength factors were selected in accordance with table 4.1.8.9 of the NBCC. It is important to note that when the BRBF system was designed, the 2005 NBCC presented R_d and R_o factors for Moderate Ductility Contently Braced Frames Tension-Compression Braces were respectively 3.0 and 1.3. In 2010 a provision for BRBF was added, citing R_d and R_o values respectively as 4.0 and 1.2. The higher mode effects, M_v, for periods less than 1 second are defined as 1.0 by the NBCC 4.1.8.11. [20]. The base shear equation is defined by the NBCC in Equation D.5.1.

$$V = \frac{S(T_a)M_v I_e W}{R_d R_o} \qquad \textbf{Equation D.5.1}$$

Table D.5.5 – Seismic weight by storey

Level, i	Height, h	Area	S Dead Loading	S Dead	Weight at Level i (kN)		
	m	m^2	kPa	kN	Floor	Columns	W_i
Roof	20.27	1077	0.5	538.5	6479	0	6479
5	16.46	1077	1.4	1507.8	6479	534	7013
4	12.65	1077	1.4	1507.8	6479	534	7013
3	8.84	1077	1.4	1507.8	7186	534	7721
2	5.03	1077	1.4	1507.8	7186	534	7721
Basement	0	0	0	0	0	706	706
					Total Seismic Weight (Dead Load):	36653	kN
					25% of Snow Load = 2.1kPa * 1077m^2 *0.25=	565	kN
					Total Superimposed Dead Load (SDL)	6570	kN
					Total Seismic Weight (DL + SDL + .25 SL):	43788	kN
					Total Base Shear V=	976	kN
					Higher mode effects Ft (kN)=	49	kN
					remaining Force Fx =(V-Ft)=	926	kN

The shear force is was multiplied by the storey height and storey weights in order to redistribute the base shear as a series of lateral point loads along the building's height.

Table D.5.6 presents the equivalent static lateral forces including the addition of higher mode effects on the top storey.

Table D.5.6 – Equivalent static force

Level	Wi	h	Wi*hi	$\underline{W_x h_x}$	F_x	Fxhx	Higher Mode	Equivalent Static Lateral Force
(i/x)	(kN)	(m)	(kN-m)	(ΣWihi)	(kN)	(kN-m)	kN	kN
Roof	6,479	20.27	131,323	0.297	275	5,572	68	**343**
5	7,013	16.46	115,437	0.261	242	3,978	0	**242**
4	7,013	12.65	88,717	0.200	186	2,349	0	**186**
3	7,721	8.84	68,253	0.154	143	1,263	0	**143**
2	7,721	5.03	38,836	0.088	81	409	0	**81**
Ground	705.6	0	0	0.000	0	0	0	**0**
	Sum:		**442566**	**1.000**	**926**	**13,571**		
					$F_t h_t$ (kN-m)=	1,384		
					Higher mode effects Ft (kN)=	68		
					Base Moment (kN-m)=	14,955		
					J for Ta=0.721	0.94		
					Reduced Base Moment (kN-m)=	14,058		